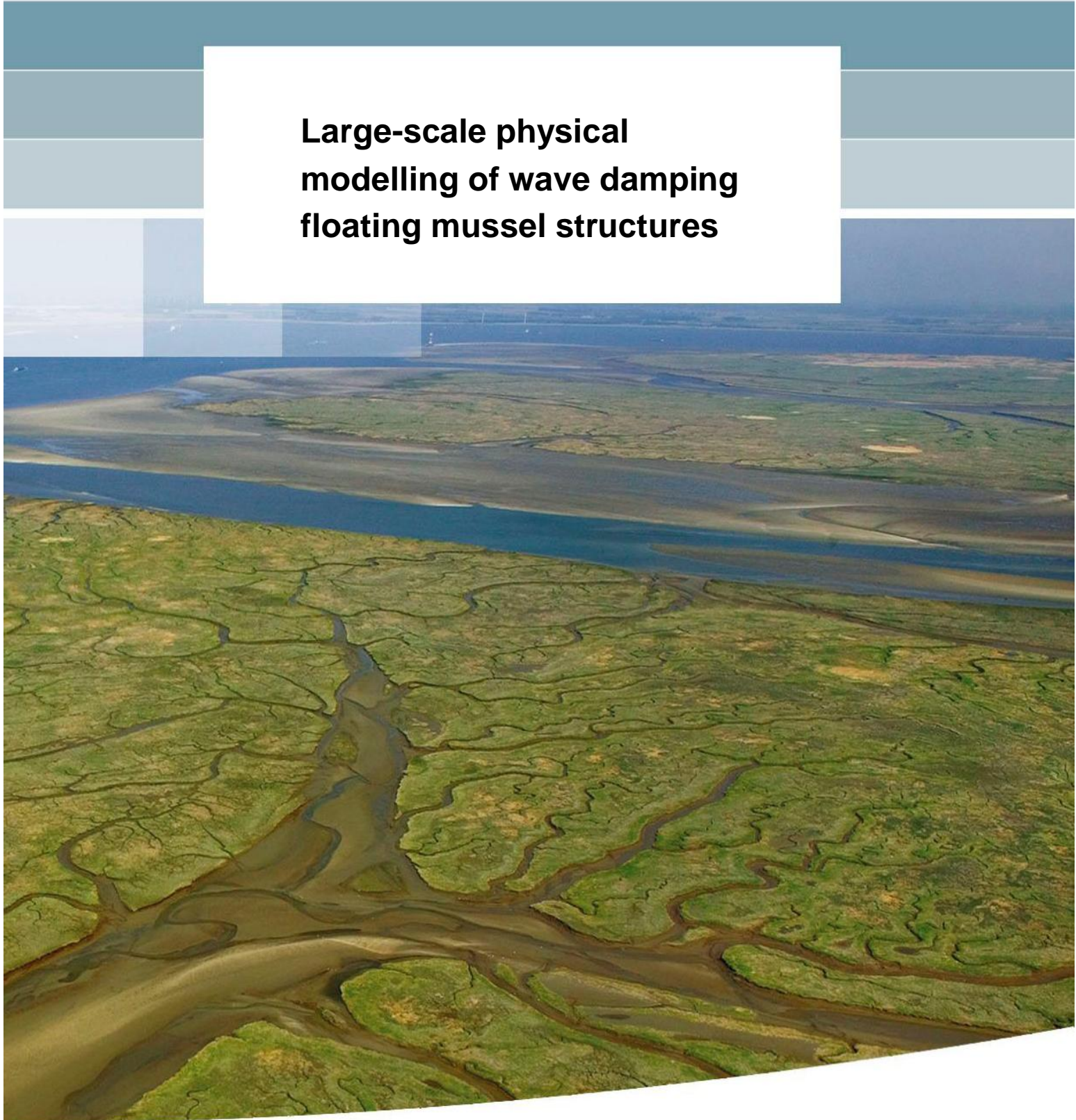


**Large-scale physical
modelling of wave damping
floating mussel structures**



Large-scale physical modelling of wave damping floating mussel structures

P. Steeg
B. K. Wesenbeeck

Title

Large-scale physical modelling of wave damping floating mussel structures

Client

Deltares MT

Pages

23 (excl. appendices)

Keywords

Floating breakwater, mussels, large-scale physical model, flume experiment, wave damping, transmission coefficient

Summary

To determine wave damping characteristics of floating mussel structures, large-scale physical modeling in the Deltares Delta Flume was performed. Mussel structures with a length of approximately 1.94 m and a depth of approximately $d = 1.50$ m have been tested in two test series:

- Series A: floating mussel structure in front of wave damping slope (transmission)
- Series B: floating mussel structure in front of a vertical wall (reflection)

Several test runs, consisting of approximately 1000 irregular waves with a significant wave height up to $H_s = 0.40$ m and a wave steepness of $s_p = 2\%$, 3% and 4% have been applied. Transmission, dissipation and reflection coefficients have been determined for each test and turns out to be a function of hydraulic parameters (water depth, local peak wave length) and structural parameters (depth of structure under water, length of structure). Based on measured data a prediction tool for wave transmission, reflection and dissipation is developed which is described in this report.

References

-

Version	Date	Author	Initials	Review	Initials	Approval	Initials
1.0	Nov. 2010	Ir. P. van Steeg		Dr. B. Hofland		Dr. M.R.A. van Gent	
		Dr. Bregje van Weesenbeeck					

State

final

Contents

List of Tables	i
List of Figures	iii
List of Photographs	v
List of Symbols	vii
1 Introduction	1
1.1 General	1
1.2 Background	1
1.3 Outline	2
2 Theoretical background	3
3 Physical model tests	5
3.1 Test set-up	5
3.1.1 Test facility	5
3.1.2 Coordination system	5
3.1.3 General test set-up	5
3.2 Materials	6
3.3 Instrumentation: wave measurements	7
3.4 Hydraulic conditions and test programme	8
3.5 Description and visual observation	9
3.6 Results: wave measurements	9
4 Analysis	13
4.1 Introduction	13
4.2 Vertical wave energy distribution	13
4.3 Analysis of results based on dimensionless parameter χ_{BLW}/L_p	14
4.4 Prediction of transmission, reflection and dissipation coefficients	15
4.4.1 Reflection coefficient	15
4.4.2 Dissipation coefficient	15
4.4.3 Transmission coefficient	15
4.5 Influence of frame	17
4.6 Summary prediction model	18
4.6.1 Case A: floating mussel structure without reflecting component behind structure	18
4.6.2 Case B: floating mussel structure with vertical wall behind structure	19
4.7 Restrictions of wave damping prediction model	19
5 Conclusions and recommendations	21
5.1 Conclusions	21
5.2 Recommendations	22
6 References	23

Appendices

A Tables

B Figures

C Photographs

D Exceedance curves and energy density spectra

E Theoretical background: determination of reflected, transmitted and dissipated wave energy

F Theoretical derivation of χ

G Theoretical determination of dissipation coefficient C_{diss}

H Calculation tool

List of Tables

In text

Table 3.1 Overview test series	5
Table 3.2 Overview of wave conditions (target values) for test series TS 400 (basic tests)	8
Table 3.3 Overview of wave conditions (target values) for test series TS 500 (reflecting wall)	8
Table 3.4 Overview of wave conditions (target values) for test series TS 700 (only frames) ...	8
Table 3.5 Overview of wave conditions (target values) for test series TS 600 (no structure) ...	8
Table 3.6 Overview test series	11
Table 4.1 Range of tested conditions	20
Table 4.2 Range of tested conditions (dimensionless)	20

In appendices

Table A.1 Measured wave conditions	
Table A.2 Reflection, transmission and dissipation coefficients	
Table A.3 Coordinates of all objects.....	
Table A.4 Mass of mussels ropes	
Table E.1 Overview determination incident, transmitted and reflected wave energy for an irregular wave field	

List of Figures

In text

Figure 2.1 Classification of floating structures (after PIANC, 1994)	3
Figure 3.1 Overview test set-up	6
Figure 3.2 Schematisation of determination of the wave energy components.....	8
Figure 3.3 Schematisation of interpretation of results of Test Series TS 500 (reflecting wall)..	9
Figure 4.1 Vertical energy distribution for shallow and deep water	13
Figure 4.2 Schematisation of object blocking a wave.....	13
Figure 4.3 Effect of wave and structure depth (derivation in Deltares, 2011).....	14
Figure 4.4 Reflection coefficient as function of $\chi_{BL}w/L_p$	15
Figure 4.5 Dissipation coefficient as function of $\chi_{BL}w/L_p$	15
Figure 4.6 Transmission coefficient as function of $\chi_{BL}w/L_p$	15
Figure 4.7 Schematisation of frame and mussels.....	17
Figure 4.8 Transmission coefficient for frame only	17
Figure 4.9 Measured transmission coefficient corrected for influence of frame	17
Figure 5.1 Summary test results and prediction.....	21

In appendices

Figure B.1 Overview of test set-up	
Figure B.2 Detail of mussel structure	
Figure B.3 Transmission, reflection and dissipation coefficient as function of significant wave height.....	
Figure B.4 Transmission, reflection and dissipation coefficient as function of relative structure length.....	
Figure B.5 Transmission, reflection and dissipation coefficient as function of vertical distribution of wave energy χ_{BL}	
Figure B.6 Transmission, reflection and dissipation coefficient as function of relative structure length and vertical distribution of wave energy $(w/L_p)\chi_{BL}$	
Figure B.7 Corrected transmission, reflection and dissipation coefficient as function of relative structure length and.....	
Figure D.1 Exceedance curve and energy density spectra for Test T414.....	
Figure D.2 Exceedance curve and energy density spectra for Test T413.....	
Figure D.3 Exceedance curve and energy density spectra for Test T406.....	
Figure D.4 Exceedance curve and energy density spectra for Test T408.....	

Figure D.5 Exceedance curve and energy density spectra for Test T401

Figure D.6 Exceedance curve and energy density spectra for Test T4011

Figure D.7 Exceedance curve and energy density spectra for Test T412

Figure D.8 Exceedance curve and energy density spectra for Test T405

Figure D.9 Exceedance curve and energy density spectra for Test T402

Figure D.10 Exceedance curve and energy density spectra for Test T514

Figure D.11 Exceedance curve and energy density spectra for Test T508

Figure D.12 Exceedance curve and energy density spectra for Test T501

Figure D.13 Exceedance curve and energy density spectra for Test T505

Figure D.14 Exceedance curve and energy density spectra for Test T502

Figure D.15 Exceedance curve and energy density spectra for Test T714

Figure D.16 Exceedance curve and energy density spectra for Test T713

Figure D.17 Exceedance curve and energy density spectra for Test T708

Figure E.1 Schematisation of the model set-up for an irregular wave field.....

Figure F.1 Schematisation of fixed structure blocking wave energy

Figure G.1 Dissipation of energy on a porous segment

Figure G.2 Graphical presentation of dissipation coefficient based on Eq. (6.9)

Figure H.1 Impression of calculation tool (page 1/2)

List of Photographs

In appendices

Photo C.1 Impression of mussel structure	
Photo C.2 Test without reflecting wall	
Photo C.3 Test with reflecting wall	
Photo C.4 Condition of mussels after testing (I).....	
Photo C.5 Condition of mussels after testing (II).....	
Photo C.6 Condition of mussels after testing (III).....	
Photo C.7 Testing without mussels (only frame).....	

List of Symbols

Symbol	Unit	Description
a	m	amplitude
C_{diss}	-	dissipation coefficient
C_r	-	reflection coefficient
C_t	-	transmission coefficient
d	m	depth of structure under water
D	m	height of structure
E_{BL}	N/m	blocked wave energy
E_{diss}	N/m	dissipated wave energy
E_i	N/m	incident wave energy
E_r	N/m	reflected wave energy
E_t	N/m	transmitted wave energy
f	Hz	frequency
f	-	coefficient
g	m/s ²	acceleration due to gravitational forces
h	m	water depth
H_s	m	significant wave height based on spectral wave period
k	rad/m	Wave number ($k = 2\pi/L$)
L_{op}	m	wave length at deep water based on T_p
L_p	m	local wave length based on T_p
m	kg	mass
n	-	number of individual mattresses
N	-	number of waves in a wave field
p	-	percentage of energy
t	s	time
T_p	s	peak wave period
u	m/s	velocity
w	m	length of floating structure in the direction of the waves
X	m	horizontal distance from the wave board in neutral position
Y	m	horizontal distance from the western flume wall
z	m	height of the mattress under water
α	-	ratio between the transmitted and reflected wave energy $\alpha = E_{\text{diss}}/E_r$
γ	-	peak enhancement factor of wave spectrum
χ_{BL}	-	ratio of energy which is influenced by structure
ω	rad/s	frequency

Commonly used indexes

Symbol	Description
A	index to relate the concerned parameter to waves travelling from the wave board to the wall
ARC	Active reflection compensation of the wave board
B	index to relate the concerned parameter to reflected waves travelling from the wall to the wave board
BL	blocking
bs	breaking on smooth concrete 1:4 slope
C	index to relate the parameter to re-reflected waves travelling from the floating structure to the wall
diss	dissipated
fl	flume
frame	part of structure at which mussels are attached
GHM	wave height meter at seaward side of floating mussel structure
hor	horizontal
i	incident
max	maximum
LL	lower limit
r	reflected
rr	re-reflected
structure	includes frame and mussels
t	transmitted
tot	total
u	upper limit
WHM	wave height meter at landward side of floating mussel structure
1	position: seaside of mattresses (or GHM 11,12, 13)
2	position: landward side of mattresses (or WHM 1, 2, 3)

1 Introduction

1.1 General

Harbors are often located in coastal areas and estuaries that were originally important habitats for numerous species. Many of these species have economical revenue, such as shrimp, fish and shellfish. It is argued that with simple adaptations that do not impede the primary function as a harbor, habitat for marine and diadromous species can be optimized. For example, harbor design is often oriented in 2D by having smooth concrete and steel walls and pillars. However, fish and crustaceans prefer 3D structures that increase the amount of available substrate and offer hiding places. Especially, juvenile fish tends to stay close to shore to avoid predators that forage in the open sea. This nursery function of coastal habitats applies to many harbor areas. It is illustrated by the main size of fish species present in the harbor of Rotterdam, most of these fishes are still relatively small.

In the Rijke Dijk program several pilot projects were executed that focused on optimization of artificial hard substrate habitat, such as pillars, peers, dams and dikes. One of these pilot project was executed in the harbor of Rotterdam. Here it was tested whether creation alternative substrate under water by constructing several structures with hanging ropes would increase biomass of filter feeding organisms, especially mussels. Hanging ropes were wrapped around steel pillars and fixed onto drifting platforms of pvc-pipes forming an under water forest from the surface down. Especially, these hanging under water forests (named pontoon hula's) rapidly gathered mussel biomass. These structures and the way they work shows parallels with rope cultures that are used for mussel farming.

In the Rotterdam harbor, each hanging rope contained up to 4 kilo's of mussels within less than half a year. Mussels are famous filter feeders, implying that they filter water as a feeding method, thereby removing small sediment and organic compounds from the water column. Therefore, besides forming refuge and foraging space for fish species, the hanging structures might be able to exert a positive influence on water quality. Next to this, hanging ropes or nets that naturally gather biomass of mussels or weeds may form cheap wave dampening units that can be applied in areas where there is little space. However, effects of hanging mussels on wave dampening were never properly quantified.

The current study focuses on collection of wave damping properties of hanging mussel structures. This is tested in a large-scale flume facility with a range of wave conditions. Experiments and analyses were set up to provide general relationships between wave damping characteristics and hydraulic (water depth, wave length) and structural conditions (depth of structure under water, length of structure). These experiments follow on previous tests of wave dampening of brushwood mattresses (Deltares, 2011). The hanging structures definitely allowed for more water moving through them than the brushwood mattresses. Obtaining more insight in parameters that determine wave attenuation will allow scaling up of results. This helps application of results to other situations.

1.2 Background

Within Deltares research Theme "Water safety" of Deltares Strategic Research program, several innovative concepts with respect to water retaining are studied. One of the aims of this research program is to explore wave damping aspects of ecological materials. In summer 2010, these explorations were started by exploring wave-dampening properties of brushwood

mattresses in large-scale flume facilities (Deltares, 2010). These first tests were followed by similar tests on the hanging mussel structures in September 2010.

This report describes in detail test set-up and execution of large-scale physical model tests in the Deltares Delta Flume and subsequent data analyses.

The physical model tests were performed in the Delta Flume of Deltares under supervision of ir. P. van Steeg¹ and Dr. B.K. van Wesenbeeck² with assistance of mr. A. Scheer, mr. P.A. Wiersma, mr. L. Tulp and mr. J.H. Ouderling. Dr. B. Hofland contributed significantly with respect to derivation of design formulas. This report is written by ir. P. van Steeg and Dr. B.K. van Wesenbeeck and is reviewed by Dr. B. Hofland.

1.3 Outline

Chapter 2 summarizes the theoretical background on wave damping by floating breakwaters. The model set-up is given in Chapter 3, followed by results, analysis of results and development of a prediction method in Chapter 4. Chapter 5 deals with main conclusions and recommendations on design of mussel structures, applications and knowledge gaps.

1. Deltares, paul.vansteeg@deltares.nl

2. Deltares, bregje.vanwesenbeeck@deltares.nl

2 Theoretical background

An analogy is made to existing literature of floating breakwaters. In PIANC (1994), floating breakwaters are schematically separated into two groups:

- Reflective structures (reflect the wave energy)
- Dissipative structures (dissipate the wave energy)

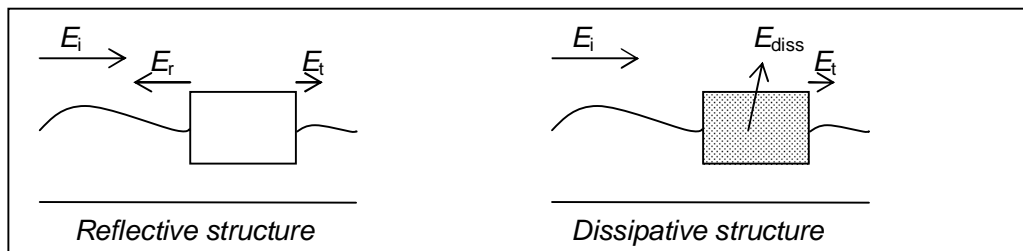


Figure 2.1 Classification of floating structures (after PIANC, 1994)

It should be realised that there is no floating structure which would only be reflective or only dissipative. The distinction is only made to understand the physics.

The main effect of reflective structures is to reflect incoming waves so that wave energy behind the structure is reduced (see also Figure 2.1). PIANC (1994) describes fixed structures and oscillating structures. Reflective structures can be divided in an infinitely thin screen (no width or $w = 0$) and a body with a certain width ($w > 0$). Examples of reflecting structures are pontoons or floating breakwaters.

Dissipative systems dissipate wave energy through viscous, or turbulent, effects. PIANC (1994) divides the dissipative systems in two types, surface systems and turbulence generators. The dissipative systems influence wave propagation in at least three ways:

- 1 Their mass and inertia induce a first attenuation, as reflective systems do;
- 2 They form a semi flexible sheet, which tend to follow fluctuation of the water surface. Provided wave lengths are short enough and the rigidity of the structure is high enough so that restoring forces may be important, this sheet will limit surface vertical displacements;
- 3 Their porosity generates drag forces, which contribute to energy losses.

Examples of surface systems are floating breakwaters made of car tyres (Volker et. al. 1979).

Besides wave damping aspects, mooring forces are considered as important parameters since forces on mooring systems and floating structure itself are large. Mooring forces are described in Van den Linden (1985) and PIANC (1994).

Floating mussel structures resemble both reflective systems and dissipating surface systems. This has implications to the type of modeling.

3 Physical model tests

3.1 Test set-up

3.1.1 Test facility

Physical model tests were carried out in the Delta Flume of Deltares. This flume has a width of 5.0 m, a height of 7.0 m and an overall length of 240 m. In this flume, waves can be generated, depending on several hydraulic conditions, up to a significant wave height (H_s) of 1.5 m.

3.1.2 Coordination system

In this report, a coordination system is used as follows:

X = distance from the wave board in neutral position (m)

Y = distance from the western flume wall (m)

3.1.3 General test set-up

The wave board is located at $X = 0.0$ m. A 1:4 smooth slope is located with the toe at $X = 180$ m. Four test series were performed. An overview is given in Table 3.1.

Table 3.1 Overview test series

	Specification of test series
Test Series 400	Mussel structure in front of wave damping slope
Test Series 500	Mussel structure in front of vertical reflecting wall
Test Series 700	Tests with frame but no mussels in front of wave damping slope
Test Series 600	Reference tests without structure in front of wave damping slope

Mussel structure of Test Series TS 400, which is described in Section 3.2, was placed at $X = 51.45$ m until $X = 55.75$ m while a 1:4 slope was located at $X = 180$ m. The mussel structure of Test Series TS 500, which is described in Section 3.2, was placed at $X = 63.45$ m until $X = 65.95$ m while a vertical reflecting wall was installed at $X = 67.55$ m. Photographs of mussel structures are given in Appendix C. During Test Series TS 400, Test Series TS 700 and Test Series TS 600, wave height meters, as described in Section 3.3, were placed in front ('seaward side') of the mussel structure (at $X_{\text{GHM11}} = 44.00$ m, $X_{\text{GHM12}} = 47.11$ m and $X_{\text{GHM13}} = 49.18$ m) and behind ('landward side') the mussel structure (at $X_{\text{WHM1}} = 85.00$ m, $X_{\text{WHM2}} = 87.00$ m and $X_{\text{WHM3}} = 88.00$ m). During Test Series TS 500, wave height meters were only placed in front of the structure (at the same location). Water level in all test series was $h = 4.00$ m. An overview of the test set-up is given in Figure 3.1, Figure B.1 and Figure B.2.

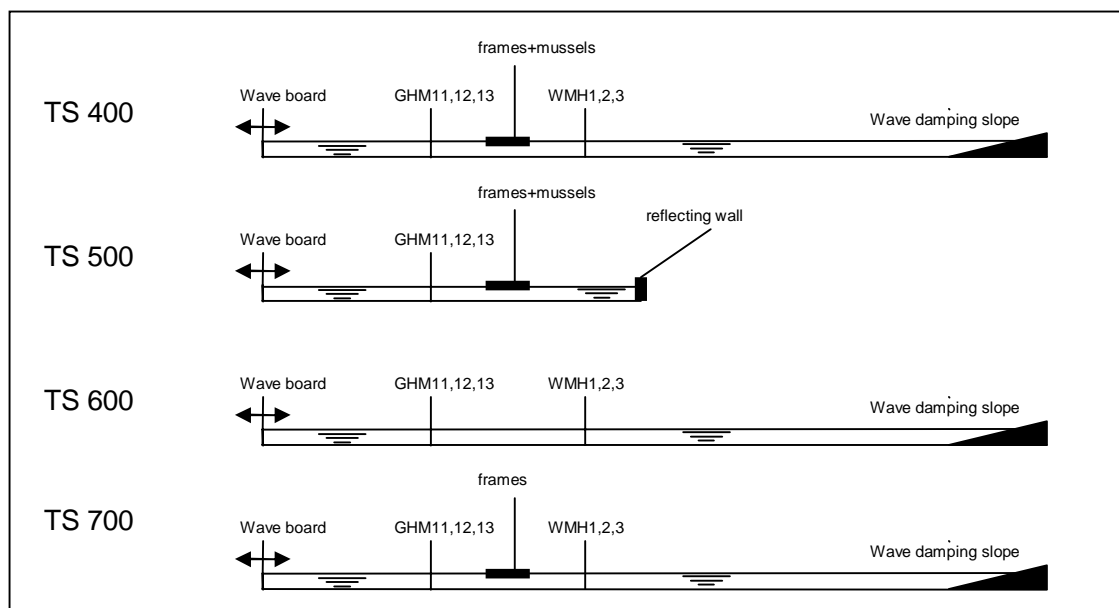


Figure 3.1 Overview test set-up

Waves, as described in Section 3.4, with incident wave energy E_i , are generated at the wave board. The waves travel towards the wave height meters in front of the structure (GHM11, GHM12 and GHM13), and reach the mussel structures. A part of the wave energy reflects directly ($E_{r,A}$). This reflected wave energy is travelling from the mussel structure back towards the wave board, which absorbs returning wave energy with the Active Reflection Compensation System. The remainder of the wave energy ($E_i - E_{r,A}$) is travelling through the mussel structure which dissipates a part of this wave energy ($E_{diss,A}$). Resulting wave energy behind the mussel structure is transmitted wave energy ($E_{t,A}$) which travels towards the wave height meters behind the mussel structure (WHM1, WHM2, WHM3) and towards the 1:4 smooth concrete slope. The slope reflects a part of this wave energy and resulting wave energy ($E_{r,B}$) travels back in the direction of the wave board and passes wave height meters WHM3, WHM2 and WHM1. Then, a part of this energy is re-reflected against the mussel structure ($E_{r,C}$) and a part of this energy is dissipated in the mussel structure ($E_{diss,B}$). The resulting transmitted wave energy $E_{t,B}$ passes the wave height meters GHM13, GHM12 and GHM11 and is absorbed by the wave board. In the analysis it was assumed that re-reflected energy component $E_{r,C}$ can be neglected. How the several energy components were determined is described in Section 3.3.

3.2 Materials

Four mussel structures were used simultaneously during the test-runs. The mussel structures were developed in the harbour of Rotterdam (salt water). A single mussel structure consisted of a polyester frame and a net on which the ropes with mussels were attached. On each intersection of the net, a rope with mussels was attached. Additional ropes with mussels were attached to the polyester frame itself. Average mass of a ropes including mussels was, after testing and based on measurements of six ropes, 3.3 kg per rope (with mussels). To improve buoyancy of structure, buoys were attached to the polyester frames.

A schematization of this set-up and the dimensions of the structure is given in Figure B.1 and Figure B.2. The length of a mussel rope was approximately 1.50 m. The net length of the whole structure (in the same direction of the waves) was approximately 1.94 m, the net width of the whole structure was approximately 4.50 m. Rope density was on average 69 ropes/m²

The four individual frames were attached to each other by using strong ropes. This is indicated with red lines in lower panel of Figure B.2. Seaward frames were also fixated to the flume wall by using thin steel cables.

3.3 Instrumentation: wave measurements

Wave characteristics were measured by means of three wave gauges in front of the mussel structure and three wave gauges behind the mussel structure. The location of the wave gauges is given in Table A.3. Wave gauges at the seaward side of the mussel structures (GHM11, GHM12 and GHM13) are so-called mechanical wave-followers and they measure surface elevation of water at a fixed location. Wave gauges at the landward side of the mussel structure (WHM1, WHM2 and WHM3) are a pair of vertical wires at a fixed location. They determine surface elevation by measuring electrical resistance between the wires which is a function of the water level. WHM1, WHM2 and WHM3 were not used at Test Series TS 500.

To separate incident and reflected waves a cross-correlation technique was used as described by Mansard and Funke (1980). The signals from a set of three wave gauges were used to determine the following wave characteristics:

$H_s = H_{m0}$	significant wave height based on spectral period (m)
T_p	peak wave period (s)
N	number of waves (-)
$s_{o,p}$	deepwater wave steepness $s_{o,p} = \frac{2\pi H_{s,i,1}}{gT_p^2}$ (-)
C_r	reflection coefficient (-)
C_t	transmission coefficient (-)
C_{diss}	dissipation coefficient (-)
α	ratio between the dissipated and transmitted energy
p	percentage of energy (%)

where the following indices are used:

1	location: at seaward side of the mussel structure (GHM 11, 12, 13)
2	location: at landward side of the mussel structure (WHM 1, 2, 3)
r	reflected wave
rr	re-reflected wave
i	incident wave
A	wave travelling from wave board through mussel structure towards slope
B	wave travelling from slope though mussel structure towards waveboard
C	wave re-reflected against landward side of mussel structure and travelling from mussel structure towards slope

Example: $H_{s,i,1}$ is the significant incident wave height at the seaward side of the mussel structure (GHM11, GHM12 and GHM13).

Energy of waves is partly reflected ($E_{r,A}$), partly dissipated ($E_{diss,A}$) and partly transmitted ($E_{t,A}$). How this is determined is described in Appendix E and summarized in Figure 3.2.

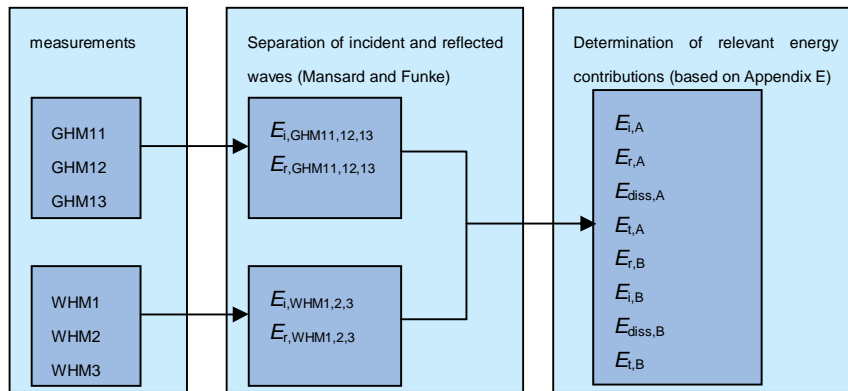


Figure 3.2 Schematisation of determination of the wave energy components

3.4 Hydraulic conditions and test programme

For all test-runs, irregular waves (JONSWAP spectrum with a peak enhancement factor of $\gamma = 3.3$) were used. A test-run consisted of approximately $N = 1000$ waves. Variations between test-runs were realised by changing significant wave height and / or wave steepness. The water depth was $h = 4.0$ m during all tests. An overview of target wave conditions is given in Table 3.2, Table 3.3, Table 3.4 and Table 3.5.

Table 3.2 Overview of wave conditions (target values) for test series TS 400 (basic tests)

	$s_{op} = 0.02$	$s_{op} = 0.03$	$s_{op} = 0.04$
$H_s = 0.10$ m	-	T414	T413
$H_s = 0.20$ m	T406	T408	T401 / T4011
$H_s = 0.30$ m	-	-	412
$H_s = 0.40$ m	-	405	402

Table 3.3 Overview of wave conditions (target values) for test series TS 500 (reflecting wall)

	$s_{op} = 0.02$	$s_{op} = 0.03$	$s_{op} = 0.04$
$H_s = 0.10$ m	-	T514	-
$H_s = 0.20$ m	-	T508	T501
$H_s = 0.30$ m	-	-	-
$H_s = 0.40$ m	-	T505	T502

Table 3.4 Overview of wave conditions (target values) for test series TS 700 (only frames)

	$s_{op} = 0.02$	$s_{op} = 0.03$	$s_{op} = 0.04$
$H_s = 0.10$ m	-	T714	T713
$H_s = 0.20$ m	-	T708	-
$H_s = 0.30$ m	-	-	-
$H_s = 0.40$ m	-	-	-

Table 3.5 Overview of wave conditions (target values) for test series TS 600 (no structure)

	$s_{op} = 0.02$	$s_{op} = 0.03$	$s_{op} = 0.04$
$H_s = 0.10$ m	-	-	-
$H_s = 0.20$ m	-	-	T601
$H_s = 0.30$ m	-	-	-
$H_s = 0.40$ m	-	-	-
$H_s = 0.60$ m	-	-	T603

Test program with measured wave conditions is given in Table A.1.

3.5 Description and visual observation

No damage to the mussel structures have been observed. To check whether possible damage (loss of biomass) led to a lower wave damping the first test-run (T401) was repeated at the end of Test Series TS 400 (Test-Run T4011). No significant difference between the transmission was measured which leads to the conclusion that there was no relevant damage to the structure that leads to different hydraulic behaviour.

It was clearly visible that individual sub structures could move almost independently from each other in a vertical direction (the mussel structures together cannot be considered as one ‘stiff’ element). No significant bending of a single structures was observed.

During the tests with steeper waves some wave breaking at the seaward side of the mussel structures was observed.

No significant turbulence or reflection at the mussel structure was visually observed. For tests with shorter waves, it could clearly be seen that the transmitted wave height was significantly lower than the incident wave height. The wave crest was clearly a straight line and perpendicular to the flume wall. No ‘side effects’ due to the open area between the mussel structure and the flume wall were visible. The transmitted waves broke as plunging waves on the 1:4 smooth concrete slope. No reflecting wave energy from the slope was visually observed.

3.6 Results: wave measurements

An overview of measured conditions is given in Table A.1. Derived transmission, dissipation and reflection coefficients as described in Appendix E are given in Table A.2. Wave height exceedance curves and energy density spectra are given in Appendix D.

Test Series TS 500 is considered as a special case. Although a reflecting wall was placed behind the structure, results of this test series can also be interpreted in a different way as illustrated in Figure 3.3.

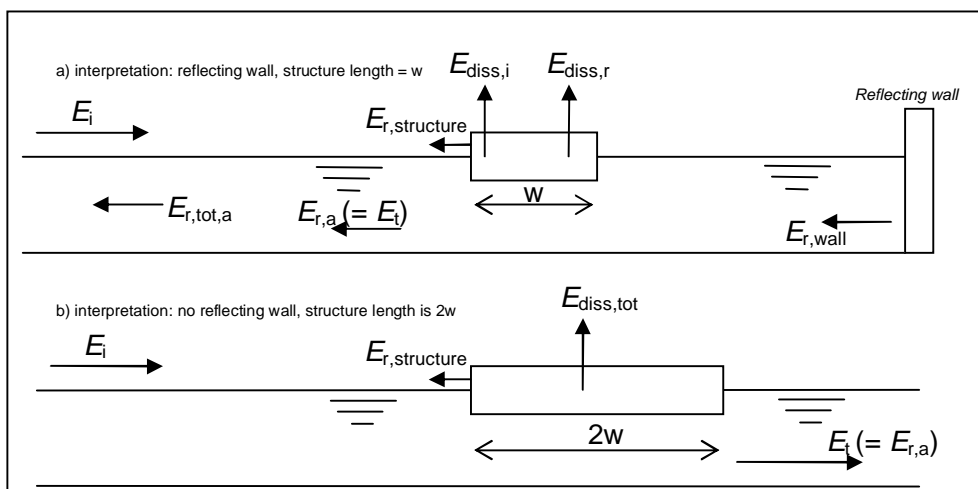


Figure 3.3 Schematisation of interpretation of results of Test Series TS 500 (reflecting wall)

In top panel of Figure 3.3, schematisation of Test Series TS 500 is same as tested situation. In this case, total reflected energy is defined as:

$$E_{r,tot,a} = E_{r,a} + E_{r,structure} \quad (3.1)$$

In lower panel of Figure 3.3, schematisation of Test Series TS 500 is different. Since wave energy travels twice through the mussel structure, the schematized structure is twice the length of the actual structure and there is no reflecting wall.

For Test Series TS 500, only total reflected wave energy $E_{r,tot,a}$ and incident wave energy E_i was measured giving only the possibility to determine corresponding reflection coefficient $C_{r,tot,a}$. This is good enough for determination of reflection coefficient C_r in schematisation of upper panel of Figure 3.3. However, to determine transmission coefficient C_t in lower panel of Figure 3.3, following set of equations is derived:

$$E_{r,a} = E_t \quad (3.2)$$

$$E_{r,tot,a} = E_t + E_{r,structure} \quad (3.3)$$

Rewriting Eq. (3.3) gives

$$E_t = E_{r,tot,a} - E_{r,structure} \quad (3.4)$$

or

$$C_t = \sqrt{C_{r,tot,a}^2 - C_{r,structure}^2} \quad (3.5)$$

Eq. (3.5) can now be used since $C_{r,tot,a}$ is determined based on tests results of Test Series TS 500 and $C_{r,structure}$ is measured for several parameters in Test Series TS 400.

Therefore, Test Series TS 500 is divided into two subsets:

- TS 500a: Results interpreted for a situation with reflecting wall (top panel of Figure 3.3).
- TS 500b: Results interpreted for a situation without reflecting wall but with a structure length twice the actual length of the structure (lower panel of Figure 3.3).

An overview of test series that is used for analysis is given in Table 3.6.

Table 3.6 Overview test series

Test Series	main goal	length w (m)	frame	mussel ropes	reflecting wall	dissipating slope
TS 400	transmission	1.94	v	v	-	v
TS 500a	reflection	1.94	v	v	v	-
TS 500b	transmission	3.88	v	v	-	v
TS 700	influence frame	1.94	v	-	-	v
TS 600	“zero” measurement	0	-	-	-	v

4 Analysis

4.1 Introduction

In Deltares 2010, influence of wave damping aspects of floating brushwood mattresses is studied. In this study it was concluded that transmission coefficient C_t is a function of structure length w , local peak wave length L_p , structure depth under water d and vertical wave energy distribution. This approach is followed and repeated in this report.

4.2 Vertical wave energy distribution

With relatively shallow water ($kh \ll 1$ where k is wave number ($k = 2\pi/L_p$)), wave energy is uniformly distributed over water depth. With relatively deep water ($kh > 1$), this is not the case, see Figure 4.1.

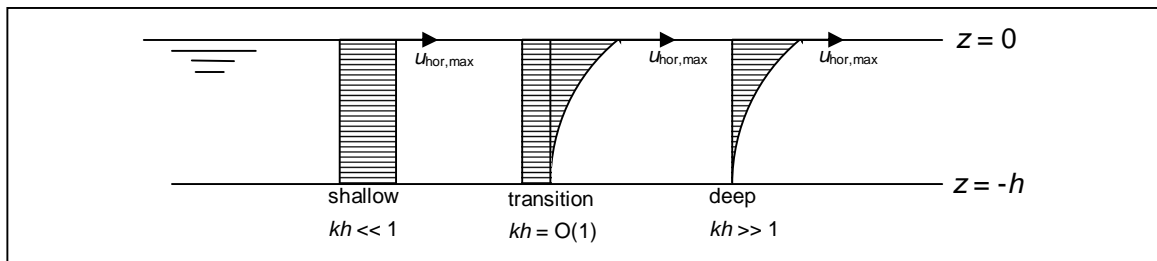


Figure 4.1 Vertical energy distribution for shallow and deep water

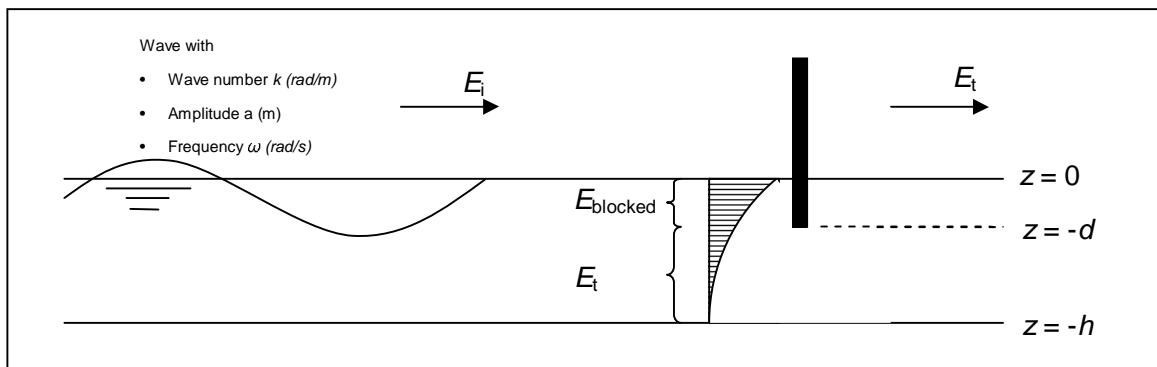


Figure 4.2 Schematisation of object blocking a wave

Attenuation of wave energy as function of ratio of water depth to wavelength h/L_p and ratio of water depth to protrusion depth of structure d/h is shown in the left panel of Figure 4.3. A theoretical derivation of this figure is given in Deltares, 2011. Ratio of blocked wave energy is noted with χ_{BL} , ratio of energy passing underneath the structure is noted with χ_t .

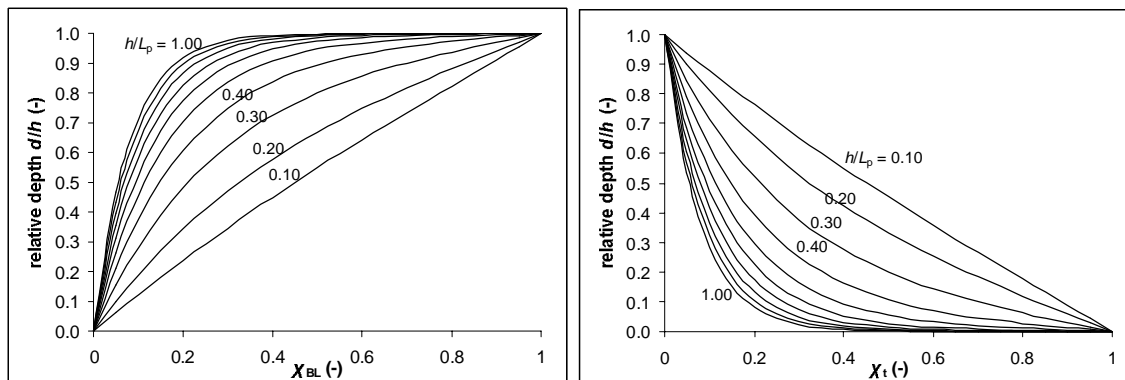


Figure 4.3 Effect of wave and structure depth (derivation in Deltares, 2011)

Ratio of blocked energy can be expressed by:

$$\chi_{BL} = \frac{\sinh 2kh - \sinh 2k(h-d) + 2kd}{\sinh 2kh + 2kh} \quad (4.1)$$

Where

k	=	wave number ($= 2\pi/L_p$)	[rad/m]
h	=	water depth at structure	[m]
d	=	protrusion depth of structure	[m]
χ_{BL}	=	ratio of blocked energy	[-]

Eq. (4.1) is derived in (Deltares, 2011). This schematization assumes no vertical movement of tested structures. Although this is not the case for this test set-up, it serves as a good first guess. Transmission coefficient C_t , dissipation coefficient C_{diss} and reflection coefficients C_r as function of dimensionless parameter χ_{BL} is shown in Figure B.5.

4.3 Analysis of results based on dimensionless parameter $\chi_{BL} w/L_p$

With Eq. (4.1), ratio of blocked energy χ_{BL} is determined for each individual test. Values of h/L_p , d/h and χ_{BL} for each test are given in Table A.1.

Now it is possible to plot transmission coefficient C_t , dissipation coefficient C_{diss} and reflection coefficients C_r as function of dimensionless parameter $\chi_{BL} w/L_p$, which is shown in Figure B.6. It can be seen that scatter of data is very low. For the sake of completeness and comparison of data, data obtained with brushwood mattresses as described in Deltares 2011 is given in this figure and remainder of this report. Transmission, reflection and dissipation coefficients as function of wave height H_s and as function of relative structure length w/L_p are given in Figure B.3 and Figure B.4 respectively.

4.4 Prediction of transmission, reflection and dissipation coefficients

Reflection, dissipation and transmission coefficients as function of dimensionless parameter $\chi_{BL}w/L_p$ are given in Figure 4.4, Figure 4.5, and Figure 4.6.

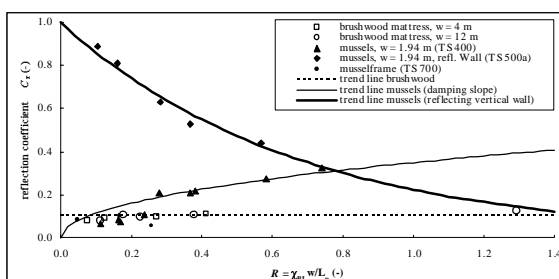


Figure 4.4 Reflection coefficient as function of $\chi_{BL}w/L_p$

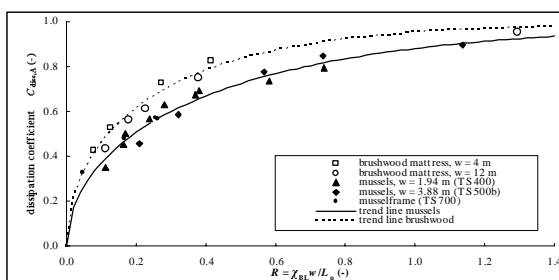


Figure 4.5 Dissipation coefficient as function of $\chi_{BL}w/L_p$

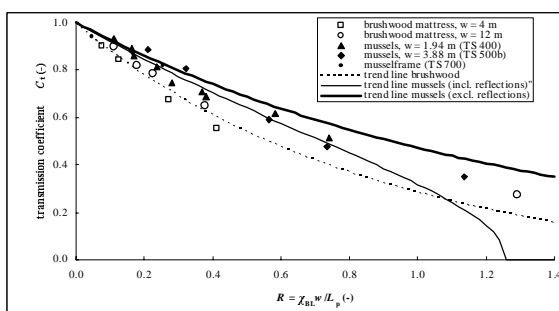


Figure 4.6 Transmission coefficient as function of $\chi_{BL}w/L_p$

4.4.1 Reflection coefficient

A trend line for reflection coefficient C_r is suggested by:

Damping slope:
$$C_r = \sqrt{1 - e^{-f_{r1} \chi_{BL} \frac{w}{L_p}}} \quad (4.2)$$

Reflecting wall
$$C_r = \sqrt{e^{-f_{r2} \chi_{BL} \frac{2w}{L_p}}} \quad (4.3)$$

with $f_{r1} = 0.13$ and $f_{r2} = 1.5$.

Eq. (4.2) and Eq. (4.3) are plotted in Figure 4.4. It is emphasized that reflection is not completely understood and that there is no physical basis for Eq. (4.2) and Eq. (4.3). Therefore, these equations should be used with caution.

4.4.2 Dissipation coefficient

Based on analysis given in Appendix G, Eq. (4.4) is used as a starting point for determination of a fitting line for dissipation coefficient C_{diss} :

$$C_{diss} = \sqrt{1 - e^{-f_{diss} x}} \quad (4.4)$$

with x chosen as:

$$x = \chi_{BL} \frac{w}{L_p} \quad (4.5)$$

gives

$$C_{diss} = \sqrt{1 - e^{-f_{diss} \chi_{BL} \frac{w}{L_p}}} \quad (4.6)$$

With $f_{diss} = 1.5$. Result of measured dissipation coefficient and trend line based on Eq. (4.6) is given in Figure 4.5. Since Eq. (4.6) is based on physical analysis (described in Appendix G) and a good fit with measured data is obtained, Eq. (4.6) is considered as reliable.

4.4.3 Transmission coefficient

Now transmission coefficient C_t can be derived by:

$$C_t = \sqrt{1 - C_{diss}^2 - C_r^2} \quad (4.7)$$

Combining Eq. (4.2), Eq. (4.6) and Eq. (4.7) gives:

$$C_t = \sqrt{e^{-f_{diss} \chi_{BL} \frac{w}{L_p}} + e^{-f_{r1} \chi_{BL} \frac{w}{L_p}} - 1} \quad (4.8)$$

Assuming no reflection at all ($C_r = 0$) Eq. (4.8) is rewritten as:

$$C_t = \sqrt{e^{-\int_{diss} \chi_{BL} \frac{w}{L_p}}} \quad (4.9)$$

Resulting trend line based on Eq. (4.8) and Eq. (4.9) is given in Figure 4.6. It can be seen that measured transmission coefficient C_t is in agreement with both derived trend lines (Eq. (4.8) and Eq. (4.9)) for lower values of $\chi_{BL}(w/L_p)$. For values of $\chi_{BL}(w/L_p) > 0.8$ there is only one measurement point (T514; $H_s = 0.10$ m, $T_p = 1.48$ s). This measurement point lies somewhere in between the two derived trend lines indicating that reflection coefficient prediction (Eq. (4.2)) is probably too high for higher values of $\chi_{BL}(w/L_p)$.

4.5 Influence of frame

To determine influence of the frame, measurements with only a frame were performed (Test Series TS 700). Definitions are given in Figure 4.7. Total structure ('tot') consists of a frame and mussels, each influencing a part of wave energy noted with $\chi_{BL,frame}$ and $\chi_{BL,mussels}$

Based on Test Series TS 700, influence of frame to transmission, dissipation, and reflection coefficient is determined. Results are shown in Figure 4.8.

Trend lines as function of $\chi_{BL,frame}$ are derived for transmission coefficient and dissipation coefficient and are given by:

$$C_{t,frame} = 1 - e^{-\left(\frac{\chi_{BL,frame} - a}{2b}\right)^2} \quad (4.10)$$

with $a = 1$, $b = 0.35$

$$C_{diss,frame} = \sqrt{1 - C_{t,frame}^2} \quad (4.11)$$

(Due to low values of reflection coefficient $C_{r,frame}$ this parameter is assumed to be zero).

Now it is possible to correct total transmission coefficient $C_{t,tot}$, total dissipation coefficient $C_{diss,tot}$ and energy blocking ratio $\chi_{BL,tot}$ for all test results as follows:

$$\chi_{BL,mussel} = \chi_{BL,tot} - \chi_{BL,frame} \quad (4.12)$$

$$C_{diss,mussel} = \sqrt{C_{diss,tot}^2 - C_{diss,frame}^2} \quad (4.13)$$

$$C_{t,mussel} = \sqrt{1 - C_{diss,mussel}^2 - C_{r,mussel}^2} \quad (4.14)$$

$$C_{r,mussel} = C_{r,tot} \quad (4.15)$$

Now, it is possible to plot $C_{t,mussel}$ as function of $\chi_{BL,mussel}(w/L_p)$. Results are given in red in Figure 4.9. It should be

noted that during the tests energy blocking ratio of the frame $\chi_{BL,frame}$ was never larger than 0.35 or:

$$0 < \chi_{BL,frame} < 0.35 \quad (4.16)$$

Indicating that the tail ($\chi_{BL,frame} > 0.35$) of Eq. (4.10), Eq. (4.11) and Figure 4.8 is not of interest. Original data ($C_{t,tot}$ as function of $\chi_{BL,tot}(w/L_p)$) is given in black.

In Figure 4.9 it can be seen that, although data points are influenced by presence of a frame, the trend lines as suggested in Section 4.4 is still valid and can therefore be used.

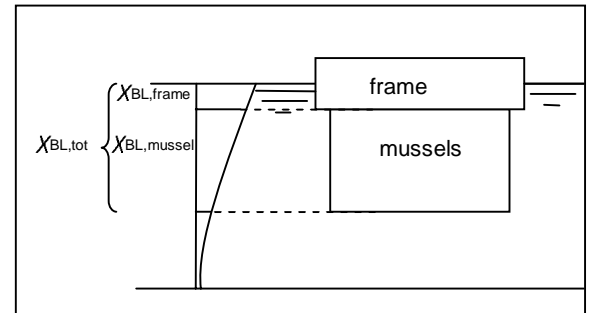


Figure 4.7 Schematisation of frame and mussels

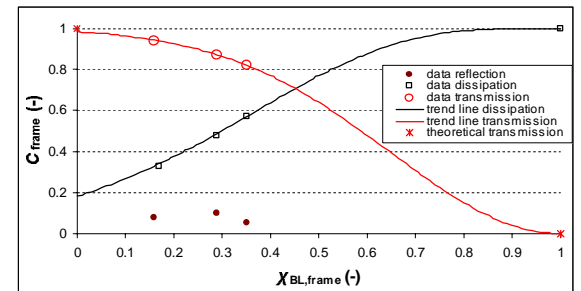


Figure 4.8 Transmission coefficient for frame only

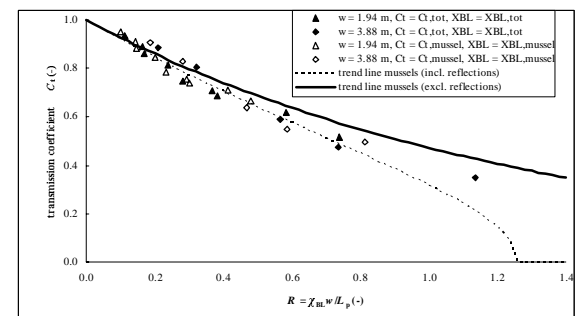


Figure 4.9 Measured transmission coefficient corrected for influence of frame

4.6 Summary prediction model

To predict wave transmission and reflection of floating mussel structures, two cases are distinguished:

- Case A: floating mussel structure without reflecting element behind structure
- Case B: floating mussel structure with vertical wall (100% reflection) behind structure

For both cases, following parameters are required:

$$\text{Wave number} \quad k = \frac{2\pi}{L_p} \quad (4.17)$$

$$\text{Blocked energy ratio} \quad \chi_{BL} = \frac{\sinh 2kh - \sinh 2k(h-d) + 2kd}{\sinh 2kh + 2kd} \quad (4.18)$$

where

d	=	depth of structure under water	[m]
h	=	water depth	[m]
k	=	wave number	[rad/m]
L_p	=	local peak wave length	[m]
χ_{BL}	=	wave energy blocking ratio	[-]

4.6.1 Case A: floating mussel structure without reflecting component behind structure

For case A following equations are suggested:

$$\text{Reflection coefficient} \quad C_r = \sqrt{1 - e^{-f_{r1} \chi_{BL} \frac{w}{L_p}}} \quad (4.19)$$

$$\text{Dissipation coefficient} \quad C_{diss} = \sqrt{1 - e^{-f_{diss} \chi_{BL} \frac{w}{L_p}}} \quad (4.20)$$

$$\text{Transmission coefficient (lower limit)} \quad C_{t,LL} = \sqrt{e^{-f_{diss} \chi_{BL} \frac{w}{L_p}} + e^{-f_{r1} \chi_{BL} \frac{w}{L_p}} - 1} \quad (4.21)$$

$$\text{Transmission coefficient (upper limit)} \quad C_{t,UL} = \sqrt{e^{-f_{diss} \chi_{BL} \frac{w}{L_p}}} \quad (4.22)$$

$$\text{Transmitted wave height} \quad H_{m0,t} = C_t H_{m0,i} \quad (4.23)$$

$$\text{Reflected wave height} \quad H_{m0,r} = C_r H_{m0,i} \quad (4.24)$$

With

C_{diss}	=	dissipation coefficient	[-]
C_r	=	reflection coefficient	[-]
$C_{t,LL}$	=	lower limit transmission coefficient	[-]
$C_{t,UL}$	=	upper limit transmission coefficient	[-]
f_{diss}	=	coefficient w.r.t. dissipation = 1.5	[-]

f_{r1}	=	coefficient w.r.t. reflection = 0.13	[-]
$H_{m0,i}$	=	incident significant wave height	[m]
$H_{m0,r}$	=	reflected significant wave height	[m]
$H_{m0,t}$	=	transmitted significant wave height	[m]
L_p	=	local peak wave length	[m]
w	=	length of structure	[m]
χ_{BL}	=	wave energy blocking ratio	[-]

4.6.2 Case B: floating mussel structure with vertical wall behind structure

For Case B following equations are suggested:

$$\text{Reflection coefficient} \quad C_r = \sqrt{e^{-f_{r2} \chi_{BL} \frac{2w}{L_p}}} \quad \text{with } f_{r2} = 1.5 \quad (4.25)$$

$$\text{Reflected wave height} \quad H_{m0,r} = C_r H_{m0,i} \quad (4.26)$$

C_r	=	reflection coefficient	[-]
f_{diss}	=	coefficient w.r.t. dissipation = 1.5	[-]
f_{r2}	=	coefficient w.r.t. reflection = 3	[-]
$H_{m0,i}$	=	incident significant wave height	[m]
$H_{m0,r}$	=	reflected significant wave height	[m]
L_p	=	local peak wave length	[m]
w	=	length of structure	[m]
χ_{BL}	=	wave energy blocking ratio	[-]

4.7 Restrictions of wave damping prediction model

In previous section a prediction method is given. When using this prediction model one should realize that the theoretical model as described is based on empirical data where:

1. The frame to which mussels were attached did not significantly influence test results. In case a different layout of this frame will be applied, this might influence transmission characteristics.
2. Anchoring / mooring did not play a significant role with respect to wave damping. If anchors will be applied, actual wave damping effect is assumed higher than the model predicts. Anchor forces, however, might also lead to more damage of mussel structures.
3. Porosity did not significantly change during test series. In actual situation porosity characteristics might change due to degradation or biological activity or porosity might be different compared to test set-up. It is not clear what influence of porosity is with respect to wave damping characteristics.
4. Data has a limited range. The range of tested parameters is given in Table 4.1. Relevant dimensionless parameters are given in Table 4.2.

Table 4.1 Range of tested conditions

Parameter	range
water depth	$h = 4.00 \text{ m}$
mussel depth under water	$d = 1.5 \text{ m}$
structure length	$1.94 \text{ m} \leq w \leq 3.88 \text{ m}$
wave length	$2.6 \text{ m} \leq L_p \leq 13.1 \text{ m}$
significant wave height	$0.068 \text{ m} \leq H_s \leq 0.41 \text{ m}$
rope density	$\Delta_{rope} = 69 \text{ ropes/m}^2$
average rope mass	$m_{rope} = 3.3 \text{ kg}$

Table 4.2 Range of tested conditions (dimensionless)

Parameter	range
ratio structure length and wave length	$0.15 \leq w/L_p \leq 1.14$
ratio structure depth and water depth	$d/h = 0.375$
ratio water depth and wave length	$0.31 \leq h/L_p \leq 1.53$
wave steepness based on deep water peak period	$0.021 \leq s_{o,p} \leq 0.041$
wave steepness based on local water peak period	$0.022 \leq s_p \leq 0.041$
ratio blocked wave energy	$0.71 \leq \chi_{BL} \leq 1.00$

5 Conclusions and recommendations

5.1 Conclusions

To obtain a first quantification of wave damping properties of floating mussel structures, a prediction tool based on large-scale flume experiments and based on a theoretical approach is developed. Structure characteristics (depth of structure under water d and structure length w) and hydraulic characteristics (water depth h and wavelength L_p) are identified as important parameters with respect to wave damping. Results are summarized in Figure 5.1 and Eq. (4.27) until Eq. (4.30).

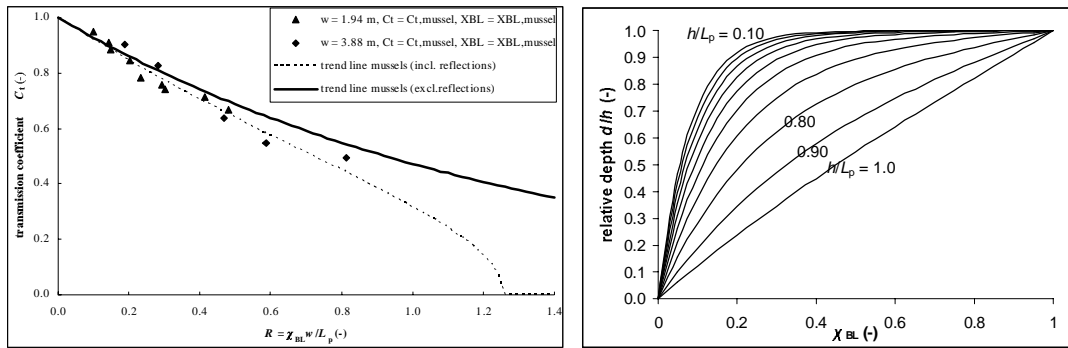


Figure 5.1 Summary test results and prediction

$$\text{Energy blocking ratio} \quad \chi_{BL} = \frac{\sinh 2kh - \sinh 2k(h-d) + 2kd}{\sinh 2kh + 2kh} \quad (4.27)$$

Transmission of floating mussel structure in front of damping slope:

$$\text{Transmission coefficient (lower limit)} \quad C_{t,LL} = \sqrt{e^{-f_{diss}\chi_{BL}\frac{w}{L_p}} + e^{-f_r\chi_{BL}\frac{w}{L_p}} - 1} \quad (4.28)$$

$$\text{Transmission coefficient (upper limit)} \quad C_{t,UL} = \sqrt{e^{-f_{diss}\chi_{BL}\frac{w}{L_p}}} \quad (4.29)$$

Reflection of a floating mussel structure located in front of vertical wall

$$\text{Reflection coefficient} \quad C_r = \sqrt{e^{-f_{r2}\chi_{BL}\frac{2w}{L_p}}} \quad (4.30)$$

Where $f_{diss} = 1.5$, $f_{r1} = 0.13$ and $f_{r2} = 1.5$ are derived empirically.

Measured transmission coefficient C_t varied between 0.51 and 0.93. Tested conditions are summarized in Table 4.1 and Table 4.2 and indicate the validation range of the prediction model.

Several theoretical wave-damping mechanisms, such as reflection, restoring forces due to stiffness of structure and turbulence are discussed. Although dissipation has largest contribution with respect to wave damping, reflection does have significant influence in some cases. It is very likely that wave-damping is less affected by restoring forces (no significant

bending of structure as a whole was possible due to type of connection of individual elements).

5.2 Recommendations

A first estimate of wave damping characteristics can be made based on results of this study. However, caution should be taken when up scaling results to field situations. It is strongly recommended to test a larger range (longer elements and larger waves, other water depths) in a large-scale flume before applying this in a prototype situation.

Focus of this study was primarily on the wave damping characteristics. It is recommended to perform a solid analysis (desk study / physical model) with respect to strength of the structures.

When applying floating breakwaters, anchorage requires special attention. Anchorage is relevant with respect to wave damping. It is very likely that this will improve wave damping characteristics but might also give severe damage to floating structures. It is recommended to study this aspect (desk study / physical model) before applying floating mussel structures on large scales in the field.

6 References

- Deltares, 2011 *Large-scale physical modeling of brushwood mattresses*. Deltares report, 1202393, July 2011.
- Lochner, R. Faber, O. and Penny, W., *The Civil Engineer in War, Vol. 2, Docks and harbours*, The institution of Civil engineers, London, England, 1948, pp, 256-290
- Mansard, E.P.D. and Funke, E.R., 1980, *The measurement of incident waves and reflected spectra using a least square method*, 17th Int. Conf. of Coastal Engineering, Sydney.
- PIANC, 1994, *Floating Breakwaters, A practical Guide for design and construction*", report of working group no. 13 of the permanent Technical Committee II, supplement to bulletin No. 85 (1994), ISBN 2-87223-052-1
- Van der Linden, M., 1985, *Golfdempende constructies (in Dutch)*, Delftse Universitaire Pers, ISBN 90-6275-263-2 SISO 699.2 UDC 627-235
- Volker, W., Harms, M. 1979, *Design criteria for floating tire breakwaters*, Journal of the waterway port coastal and ocean division, proceedings of the American Society of Civil Engineers, Vol. 105, No. WW2, May 1979

A Tables

Table A.1 Measured wave conditions

Table A.2 Reflection, transmission and dissipation coefficients

Table A.3 Coordinates of all objects

Table A.4 Dimensionless parameters based on vertical distribution of wave energy

Table A.1a Measured wave conditions (Test Series T400)

Test	structural parameters			WHM's seaward side of structure (GHM 11, 12, 13)								WHM's landward side of structure (WHM 1, 2, 3)					dimensionless parameters					
	water depth	structural length	structural depth	incident wave height	incident wave period	deep water wave length	wave length	wave number	incident wave steepness	nr. of incident waves	reflected wave height	incident wave height	incident wave period	incident wave steepness	nr. of incident waves	reflected wave height	dim. width	dim. water depth	relative depth of structure	energy blocking ratio	energy transmission ratio	dimensionless parameter
	h (m)	w (m)	d (m)	$H_{s,i,1}$ (m)	$T_{p,i,1}$ (s)	$L_{o,p,i}$ (m)	$L_{p,i}$ (m)	k (m)	$s_{o,i,1}$ (-)	$N_{i,1}$ (-)	$H_{s,r,1}$ (m)	$H_{s,i,2}$ (m)	$T_{p,i,2}$ (s)	$s_{o,i,2}$ (-)	$N_{i,2}$ (-)	$H_{s,r,2}$ (m)	$w/L_{p,i}$ (-)	$L_{p,i}/h$ (-)	d/h (-)	X_{BL} (-)	X_{TR} (-)	$X_{BL}(w/L_{p,i})$ (-)
T401	4.00	1.94	1.5	0.202	1.78	4.97	4.96	1.27	0.041	914	0.048	0.139	1.79	0.028	876	0.027	0.39	0.8	0.4	0.98	0.02	0.38
T406	4.00	1.94	1.5	0.208	2.49	9.70	9.58	0.66	0.021	1129	0.026	0.179	2.49	0.018	1077	0.024	0.20	0.4	0.4	0.83	0.17	0.17
T408	4.00	1.94	1.5	0.207	2.04	6.50	6.49	0.97	0.032	1093	0.045	0.155	2.05	0.024	1035	0.019	0.30	0.6	0.4	0.94	0.06	0.28
T402	4.00	1.94	1.5	0.403	2.52	9.91	9.78	0.64	0.041	1114	0.049	0.358	2.52	0.036	1047	0.040	0.20	0.4	0.4	0.83	0.17	0.16
T413	4.00	1.94	1.5	0.068	1.30	2.62	2.62	2.40	0.026	927	0.023	0.035	1.37	0.012	883	0.013	0.74	1.5	0.4	1.00	0.00	0.74
T414	4.00	1.94	1.5	0.102	1.46	3.32	3.32	1.89	0.031	984	0.030	0.063	1.43	0.020	973	0.018	0.58	1.2	0.4	1.00	0.00	0.58
T405	4.00	1.94	1.5	0.411	2.89	13.06	12.57	0.50	0.031	1153	0.051	0.384	2.90	0.029	1104	0.047	0.15	0.3	0.4	0.73	0.27	0.11
T412	4.00	1.94	1.5	0.302	2.18	7.45	7.42	0.85	0.041	1111	0.039	0.246	2.24	0.031	1062	0.027	0.26	0.5	0.4	0.91	0.09	0.24
T4011	4.00	1.94	1.5	0.199	1.81	5.13	5.13	1.22	0.039	1016	0.046	0.141	1.79	0.028	982	0.028	0.38	0.8	0.4	0.97	0.03	0.37

Table A.1b Measured wave conditions (Test Series T500)

Test	structural parameters			waves GHM11, GHM12, GHM13								WHM's landward side of structure (WHM 1, 2, 3)					dimensionless parameters					
	water depth	structural length	structural depth	incident wave height	incident wave period	deep water wave length	wave length	wave number	incident wave steepness	nr. of incident waves	reflected wave height	incident wave height	incident wave period	incident wave steepness	nr. of incident waves	reflected wave height	dim. width	dim. water depth	relative depth of structure	energy blocking ratio	energy transmission ratio	dimensionless parameter
	h (m)	w (m)	d (m)	$H_{s,i,1}$ (m)	$T_{p,i,1}$ (s)	$L_{o,p,i}$ (m)	$L_{p,i}$ (m)	k (m)	$s_{o,i,1}$ (-)	$N_{i,1}$ (-)	$H_{s,r,1}$ (m)	$H_{s,i,2}$ (m)	$T_{p,i,2}$ (s)	$s_{o,i,2}$ (-)	$N_{i,2}$ (-)	$H_{s,r,2}$ (m)	$w/L_{p,i}$ (-)	$L_{p,i}/h$ (-)	d/h (-)	X_{BL} (-)	X_{TR} (-)	$X_{BL}(w/L_{p,i})$ (-)
T514	4.00	3.88	1.5	0.1	1.48	3.40	3.4	1.85	0.030	981	0.05	-	-	-	-	-	1.14	1.2	0.4	1.00	0.00	1.14
T501	4.00	3.88	1.5	0.2	1.82	5.15	5.1	1.22	0.038	1007	0.10	-	-	-	-	-	0.75	0.8	0.4	0.97	0.03	0.74
T508	4.00	3.88	1.5	0.2	2.04	6.47	6.5	0.97	0.032	1095	0.13	-	-	-	-	-	0.60	0.6	0.4	0.94	0.06	0.57
T502	4.00	3.88	1.5	0.4	2.52	9.92	9.9	0.63	0.041	1114	0.33	-	-	-	-	-	0.39	0.4	0.4	0.82	0.18	0.32
T505	4.00	3.88	1.5	0.4	2.90	13.11	13.1	0.48	0.031	1167	0.36	-	-	-	-	-	0.30	0.3	0.4	0.71	0.29	0.21

Table A.1c Measured wave conditions (Test Series T700)

Test	WHM's seaward side of structure (GHM 11, 12, 13)			WHM's seaward side of structure (GHM 11, 12, 13)								WHM's landward side of structure (WHM 1, 2, 3)					dimensionless parameters					
	water depth	structural length	structural depth	incident wave height	incident wave period	deep water wave length	wave length	wave number	incident wave steepness	nr. of incident waves	reflected wave height	incident wave height	incident wave period	incident wave steepness	nr. of incident waves	reflected wave height	dim. width	dim. water depth	relative depth of structure	energy blocking ratio	energy transmission ratio	dimensionless parameter
	h	w	d	$H_{s,i,1}$	$T_{p,i,1}$	$L_{o,p,i}$	$L_{p,i}$	k	$s_{o,i,1}$	$N_{i,1}$	$H_{s,r,1}$	$H_{s,i,2}$	$T_{p,i,2}$	$s_{o,i,2}$	$N_{i,2}$	$H_{s,r,2}$	$w/L_{p,i}$	$L_{p,i}/h$	d/h	X_{BL}	X_{TR}	$X_{BL}(w/L_{p,i})$
T714	4.00	1.94	0.09	0.101	1.47	3.35	3.35	1.88	0.030	961	0.014	0.088	1.46	0.026	953	0.011	0.58	1.2	0.1	0.53	0.47	0.31
T708	4.00	1.94	0.09	0.202	2.05	6.56	6.54	0.96	0.031	1069	0.025	0.190	2.05	0.029	1060	0.020	0.30	0.6	0.1	0.32	0.68	0.09
T713	4.00	1.94	0.09	0.066	1.30	2.65	2.64	2.38	0.025	902	0.009	0.054	1.28	0.021	899	0.010	0.73	1.5	0.1	0.61	0.39	0.45

Table A.1d: Measured wave conditions (Test Series T600)

Test	WHM's seaward side of structure (GHM 11, 12, 13)			WHM's seaward side of structure (GHM 11, 12, 13)								WHM's landward side of structure (WHM 1, 2, 3)					dimensionless parameters					
	water depth	structural length	structural depth	incident wave height	incident wave period	deep water wave length	wave length	wave number	incident wave steepness	nr. of incident waves	reflected wave height	incident wave height	incident wave period	incident wave steepness	nr. of incident waves	reflected wave height	dim. width	dim. water depth	relative depth of structure	energy blocking ratio	energy transmission ratio	dimensionless parameter
	h	w	d	$H_{s,i,1}$	$T_{p,i,1}$	$L_{o,p,i}$	$L_{p,i}$	k	$s_{o,i,1}$	$N_{i,1}$	$H_{s,r,1}$	$H_{s,i,2}$	$T_{p,i,2}$	$s_{o,i,2}$	$N_{i,2}$	$H_{s,r,2}$	$w/L_{p,i}$	$L_{p,i}/h$	d/h	X_{BL}	X_{TR}	$X_{BL}(w/L_{p,i})$
T601	4.00	0.0	0.0	0.196	1.790	5.00	5.00	1.26	0.039	986	0.024	0.189	1.79	0.038	987	0.020	0.00	0.8	0.0	0.00	1.00	0.00
T603	4.00	0.0	0.0	0.601	3.090	14.91	14.08	0.45	0.040	1148	0.095	0.604	3.08	0.041	1128	0.085	0.00	0.3	0.0	0.00	1.00	0.00

Table A.3: Coordinates of all objects

Object	Test Series T400 (basic tests)		Test Series T500 (reflecting wall)		Test Series T700 (only frames)		Test Series T600 (No structure)	
	X (m)	Y (m)	X (m)	Y (m)	X (m)	Y (m)	X (m)	Y (m)
wave board	0	0 - 5	0	0 - 5	0	0 - 5	0	0 - 5
GHM11	44.00	2.50	44.00	2.50	44.00	2.50	44.00	2.50
GHM12	47.11	2.50	47.11	2.50	47.11	2.50	47.11	2.50
GHM13	49.18	2.50	49.18	2.50	49.18	2.50	49.18	2.50
anchors	51.45	0 / 5	59.80	0 / 5	51.45	0 / 5	-	-
front of structure	55.75	0 - 5	63.45	0 - 5	55.75	0 - 5	-	-
back of structure	58.25	0 - 5	65.95	0 - 5	58.25	0 - 5	-	-
WHM1	85.00	0.05	-	-	85.00	0.05	85.00	0.05
WHM2	87.00	0.05	-	-	87.00	0.05	87.00	0.05
WHM3	88.00	0.05	-	-	88.00	0.05	88.00	0.05
slope	180.0	0 - 5	-	-	180.0	0 - 5	180	0 - 5
reflecting wall	-	-	67.55	0 - 5	-	-	-	-

Table A.4 Mass of mussel ropes

rope nr	mass (kg)
1	3.7
2	2.6
3	4.2
4	2.3
5	3.5
6	3.2
average	3.3

B Figures

Figure B.1 Overview of test set-up

Figure B.2 Detail of mussel structure

Figure B.3 Transmission, reflection and dissipation coefficient as function of significant wave height
 H_{m0}

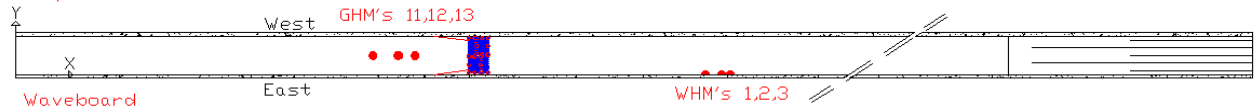
Figure B.4 Transmission, reflection and dissipation coefficient as function of relative structure length
 w/L_p

Figure B.5 Transmission, reflection and dissipation coefficient as function of vertical distribution of wave energy χ_{BL}

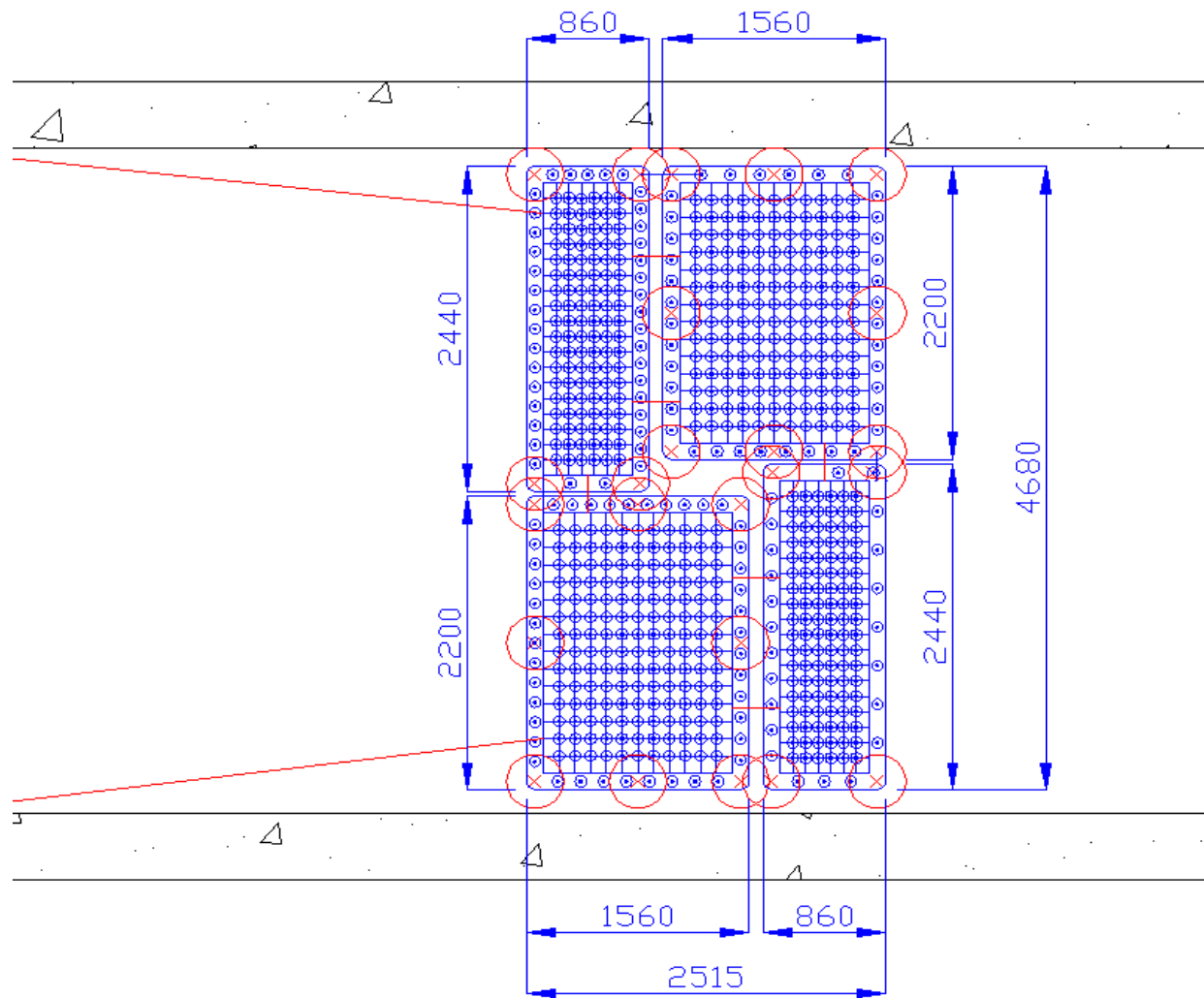
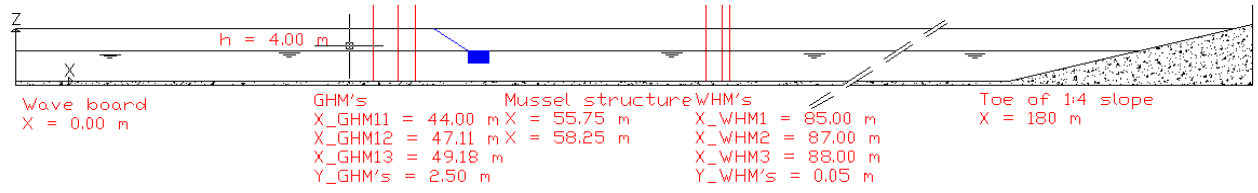
Figure B.6 Transmission, reflection and dissipation coefficient as function of relative structure length and vertical distribution of wave energy $(w/L_p)\chi_{BL}$

Figure B.7 Corrected transmission, reflection and dissipation coefficient as function of relative structure length and vertical distribution of wave energy $(w/L_p)\chi_{BL}$

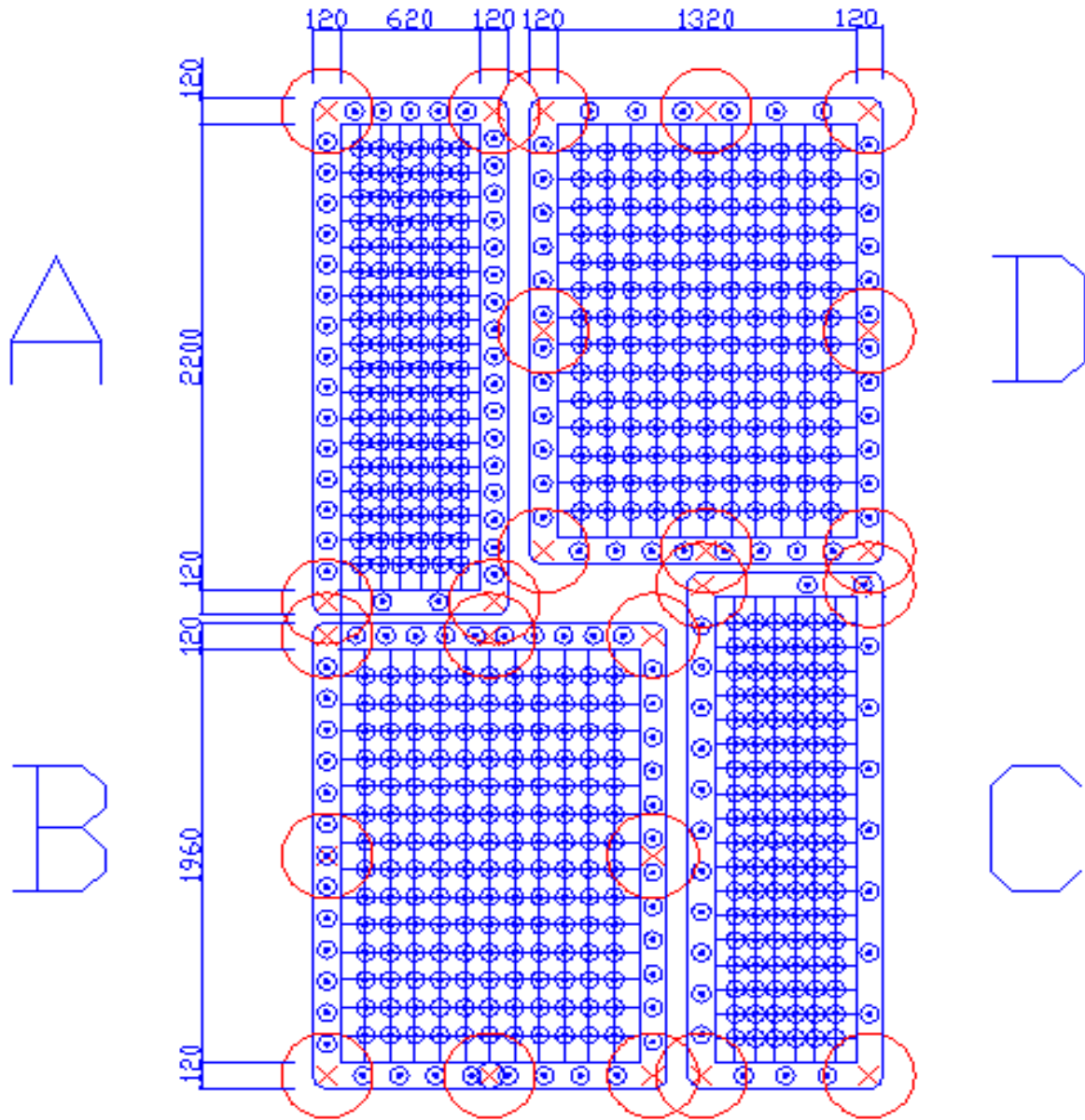
Top view



Side view



Overview of test set-up

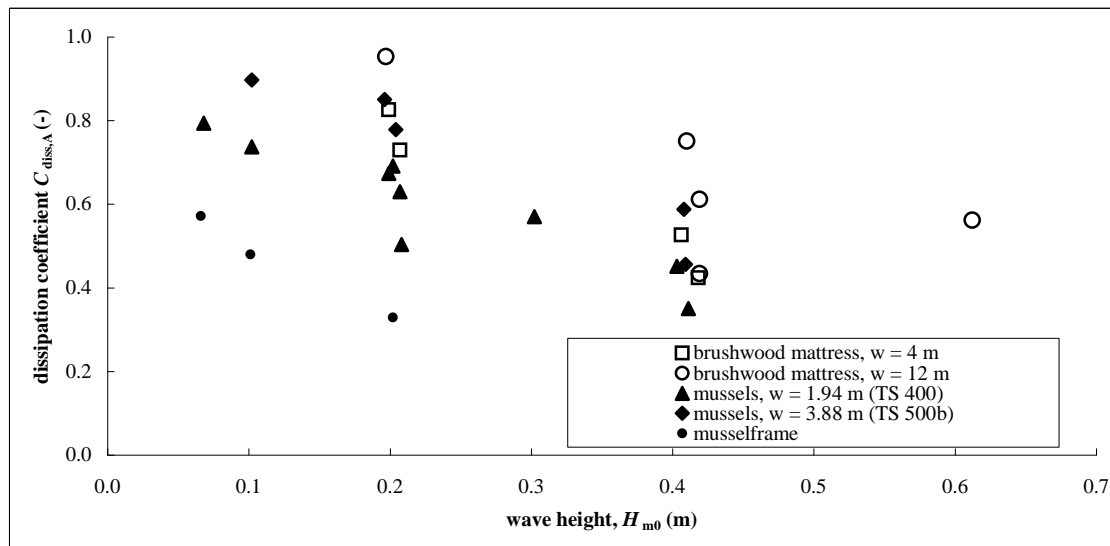
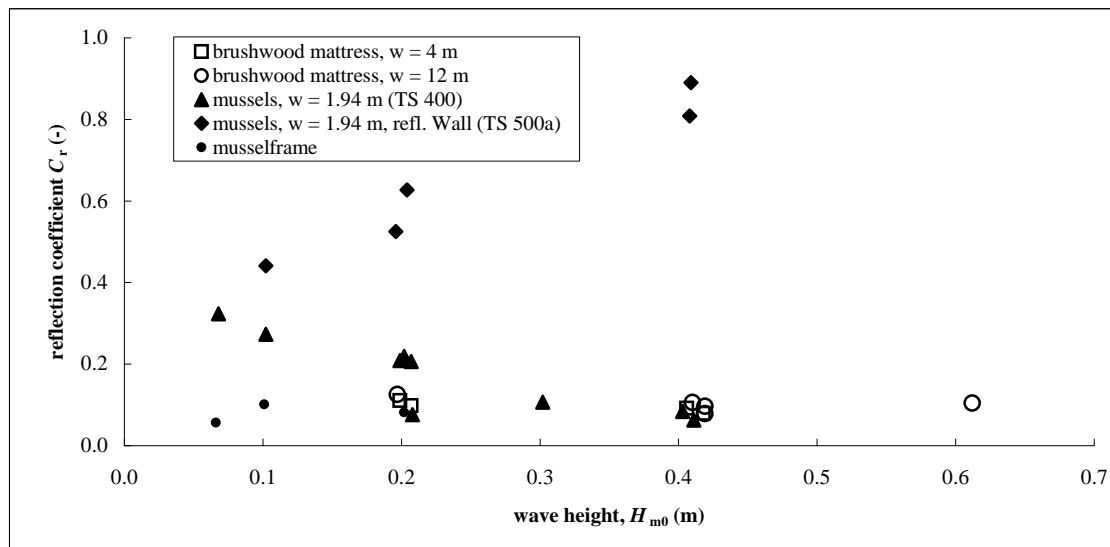
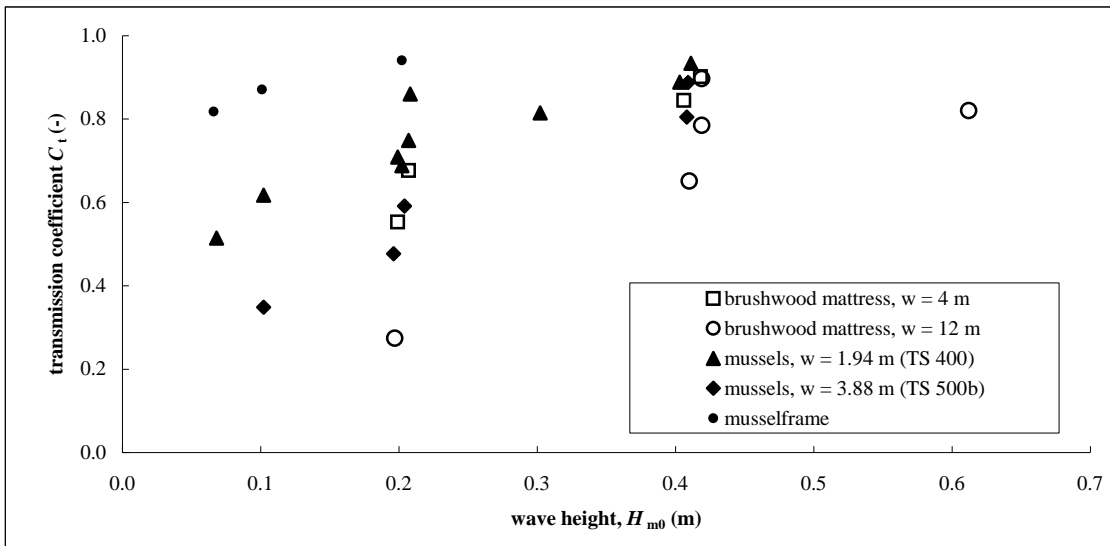


- A: $18 \times 6 + 7 + 3 + 11 + 2 = 131$ ropes
- B: $14 \times 11 + 12 + 8 + 12 + 7 = 193$ ropes
- C: $18 \times 6 + 17 + 2 + 15 + 5 = 147$ ropes
- D: $14 \times 11 + 12 + 8 + 13 + 10 = 197$ ropes

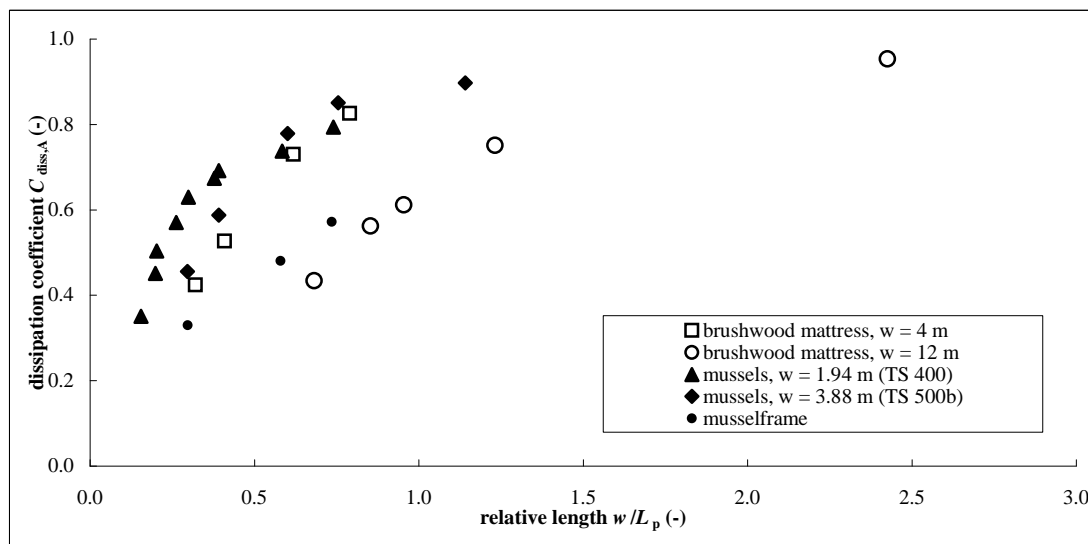
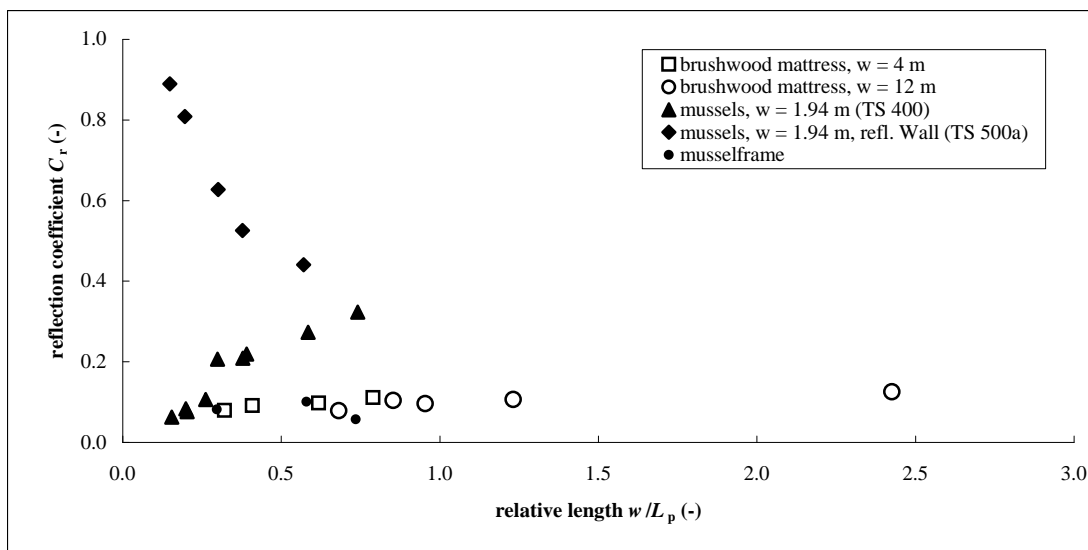
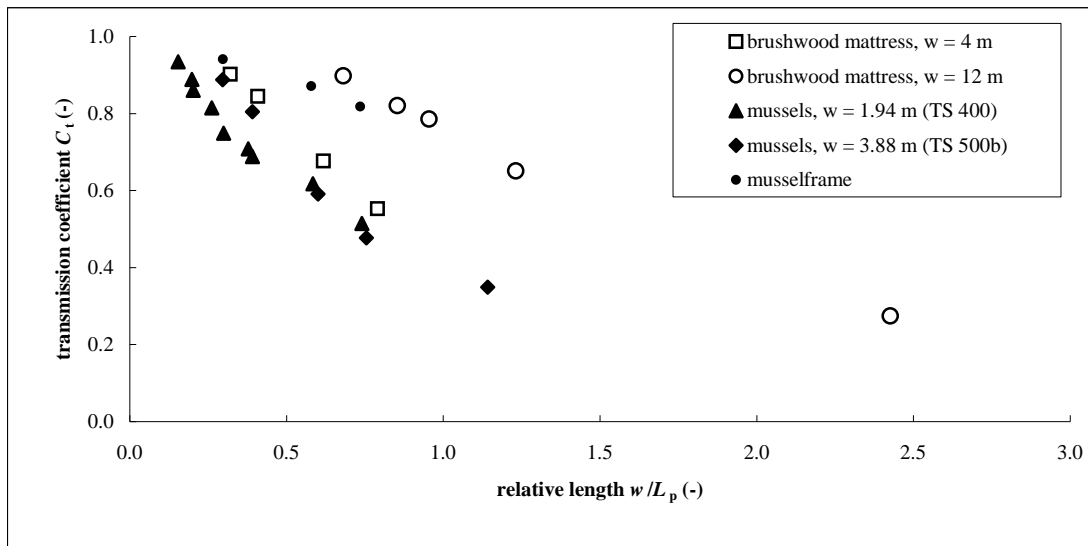
◉ rope with mussels

⊗ buoy

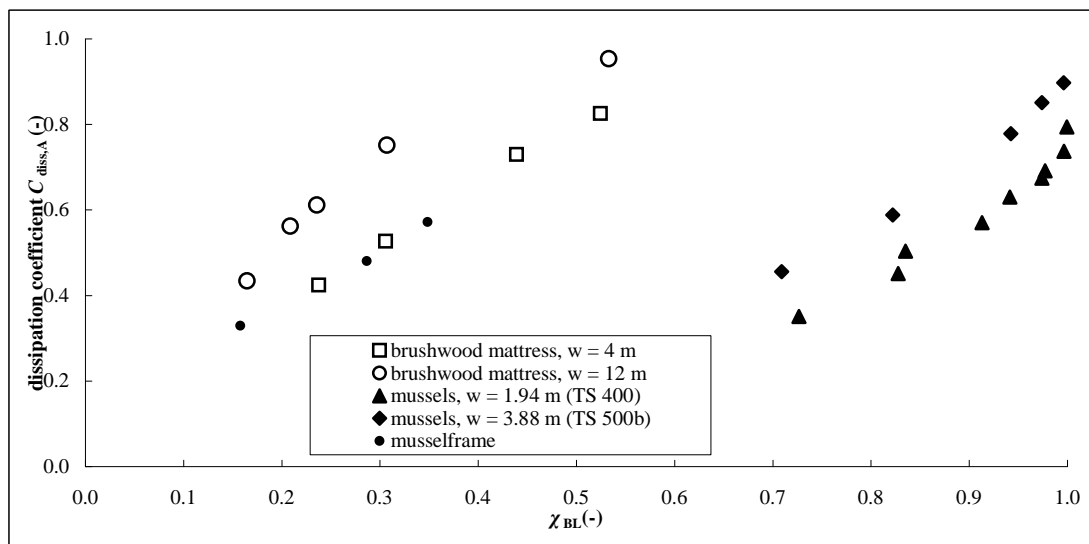
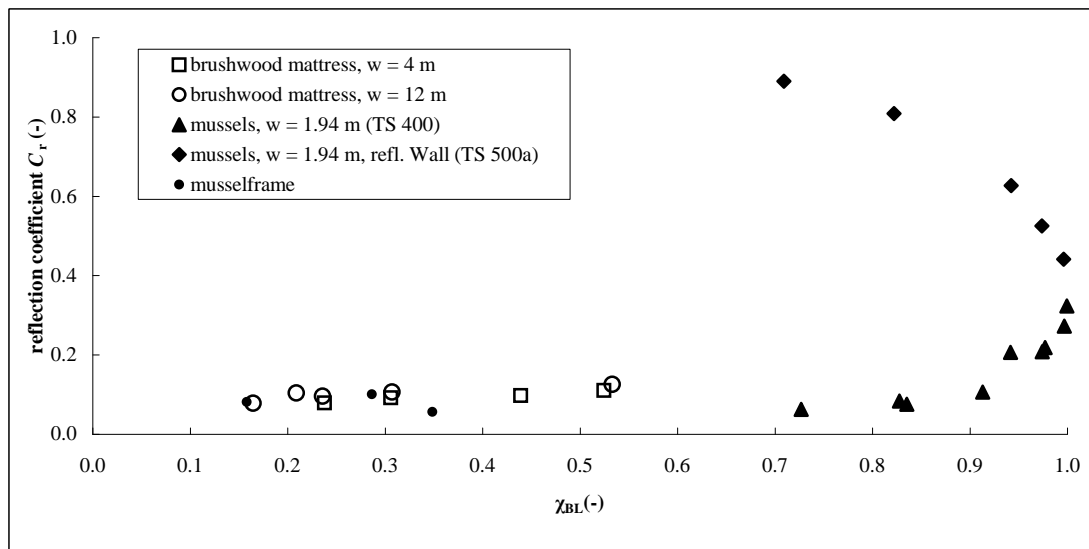
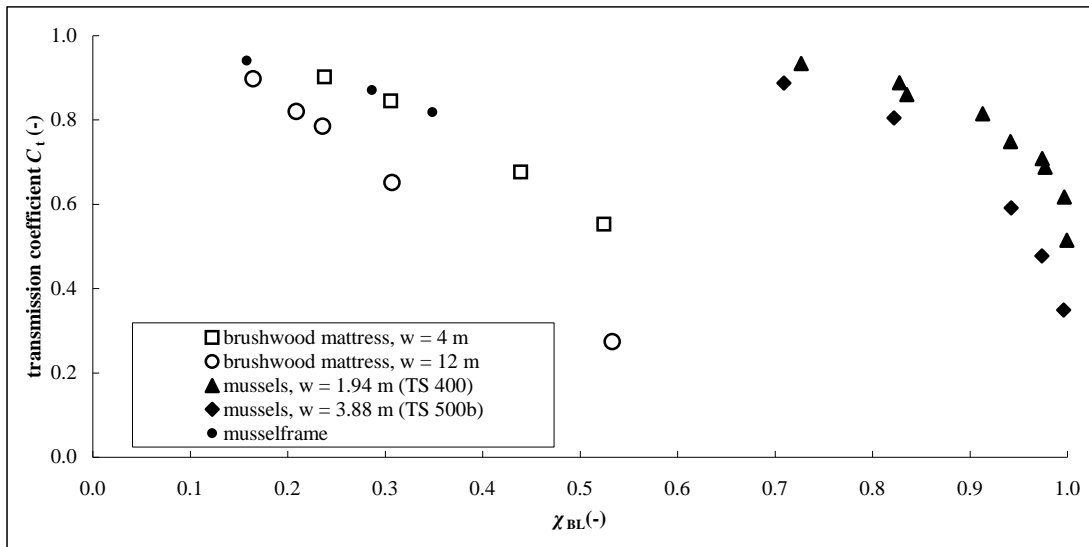
Detail of mussel structure



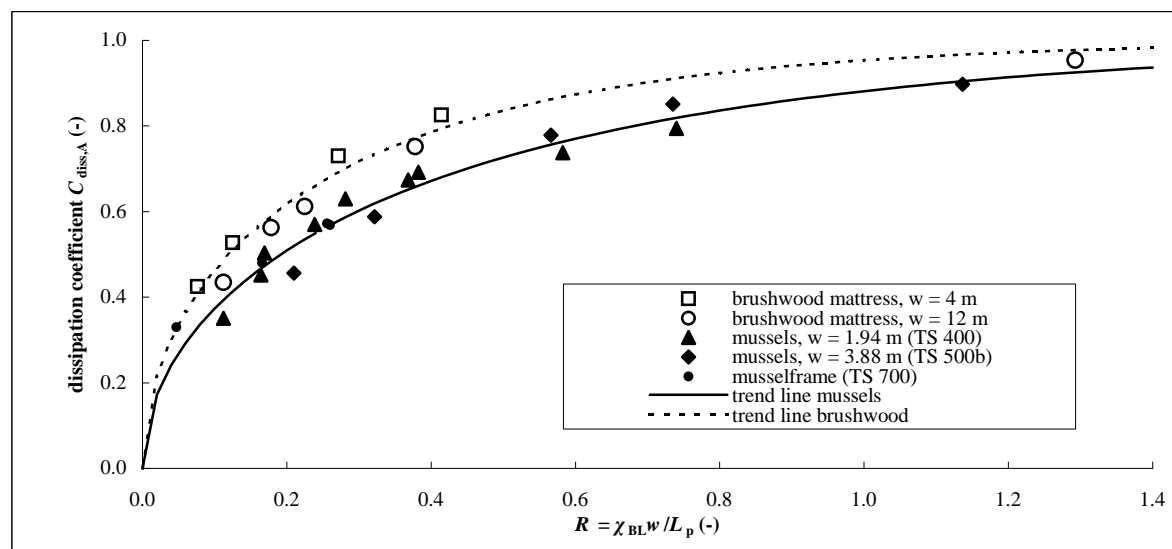
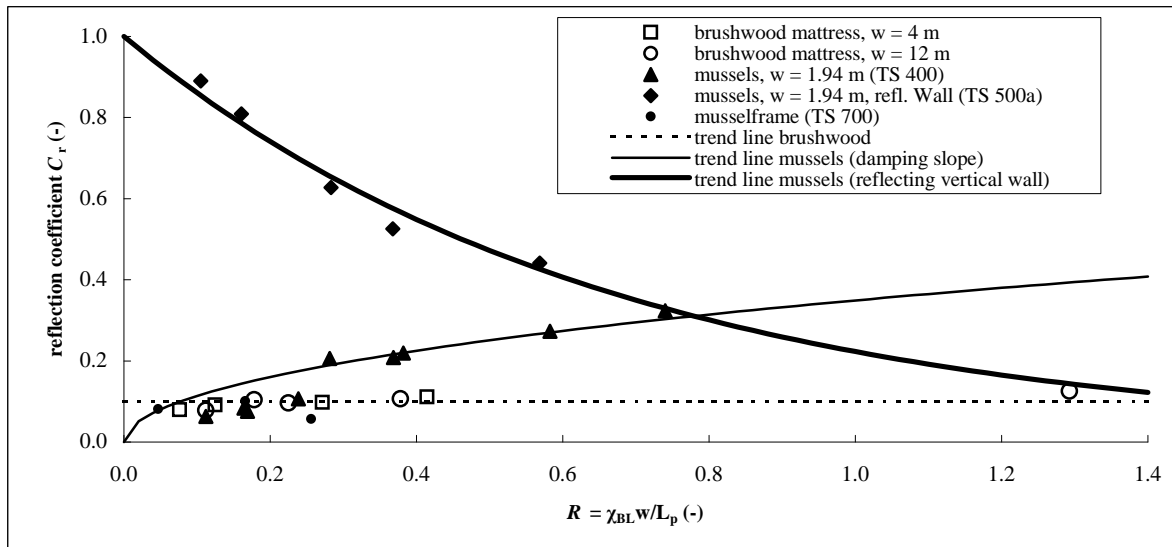
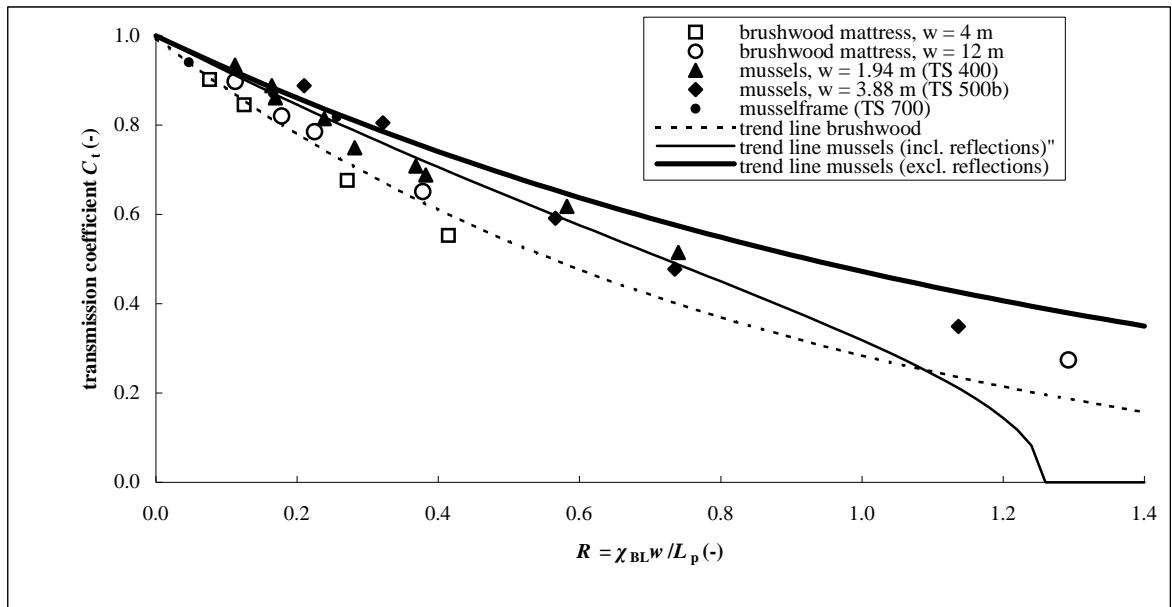
Transmission, reflection and dissipation coefficient as function of the significant wave height H_{m0}		
Deltares	1200193-005	Fig. B.3



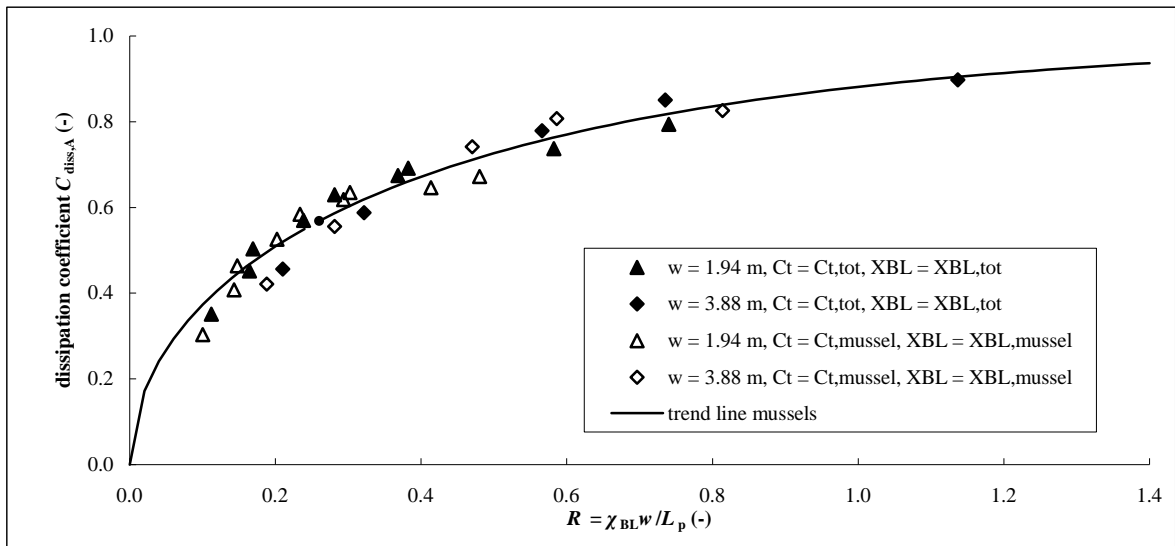
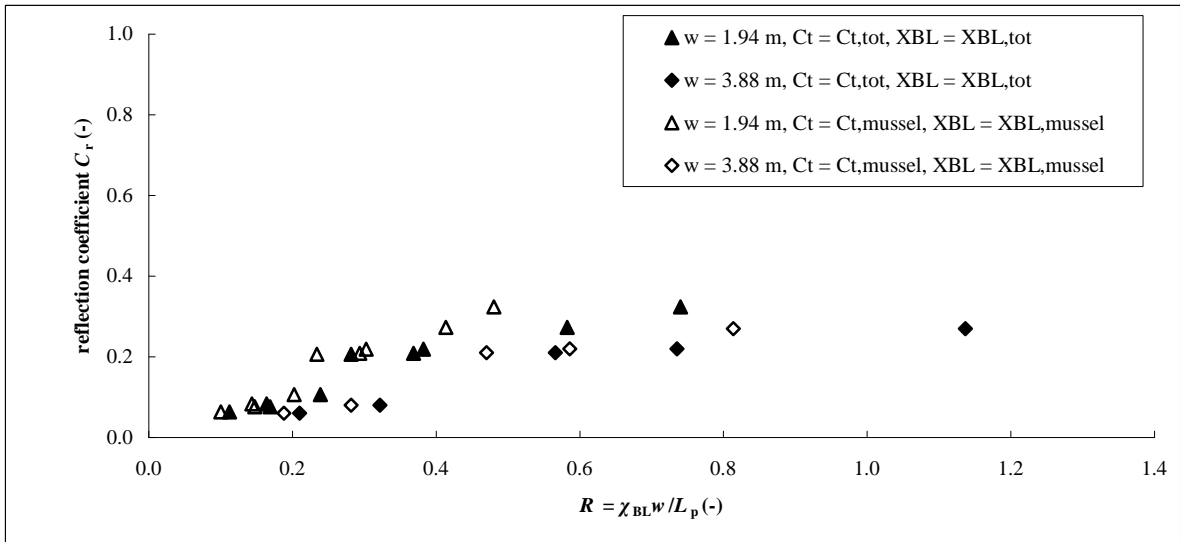
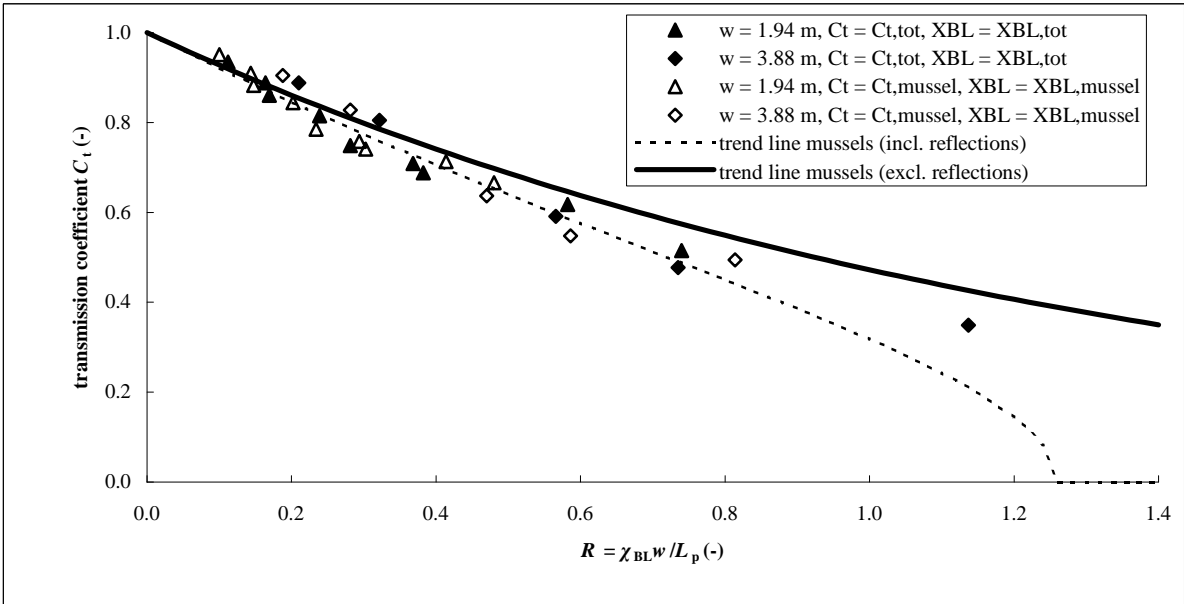
Transmission, reflection and dissipation coefficient as function of the relative structure length w/L_p



Transmission, reflection and dissipation coefficient as function of vertical distribution of wave energy χ_{BL}



Transmission, reflection and dissipation coefficient as function of the relative structure length and vertical distribution of wave energy $(w/L_p)\chi_{BL}$



Corrected Transmission, reflection and dissipation coefficient as function of $\chi_{BL} w/L_p$

C Photographs

<i>Photo C.1</i>	<i>Impression of mussel structure</i>
<i>Photo C.2</i>	<i>Test without reflecting wall</i>
<i>Photo C.3</i>	<i>Test with reflecting wall</i>
<i>Photo C.4</i>	<i>Condition of mussels after testing (I)</i>
<i>Photo C.5</i>	<i>Condition of mussels after testing (II)</i>
<i>Photo C.6</i>	<i>Condition of mussels after testing (III)</i>
<i>Photo C.7</i>	<i>Testing without mussels (only frame)</i>



Impression of mussel structure



Test without reflecting wall



Test with reflecting wall

Deltares

1200193-005

Fig. C.3



Condition of mussels after testing (I)



Condition of mussels after testing (II)



Condition of mussels after testing (III)



Testing without mussels (only frame)

D Exceedance curves and energy density spectra

Figure D.1 Exceedance curve and energy density spectra for Test T414

Figure D.2 Exceedance curve and energy density spectra for Test T413

Figure D.3 Exceedance curve and energy density spectra for Test T406

Figure D.4 Exceedance curve and energy density spectra for Test T408

Figure D.5 Exceedance curve and energy density spectra for Test T401

Figure D.6 Exceedance curve and energy density spectra for Test T4011

Figure D.7 Exceedance curve and energy density spectra for Test T412

Figure D.8 Exceedance curve and energy density spectra for Test T405

Figure D.9 Exceedance curve and energy density spectra for Test T402

Figure D.10 Exceedance curve and energy density spectra for Test T514

Figure D.11 Exceedance curve and energy density spectra for Test T508

Figure D.12 Exceedance curve and energy density spectra for Test T501

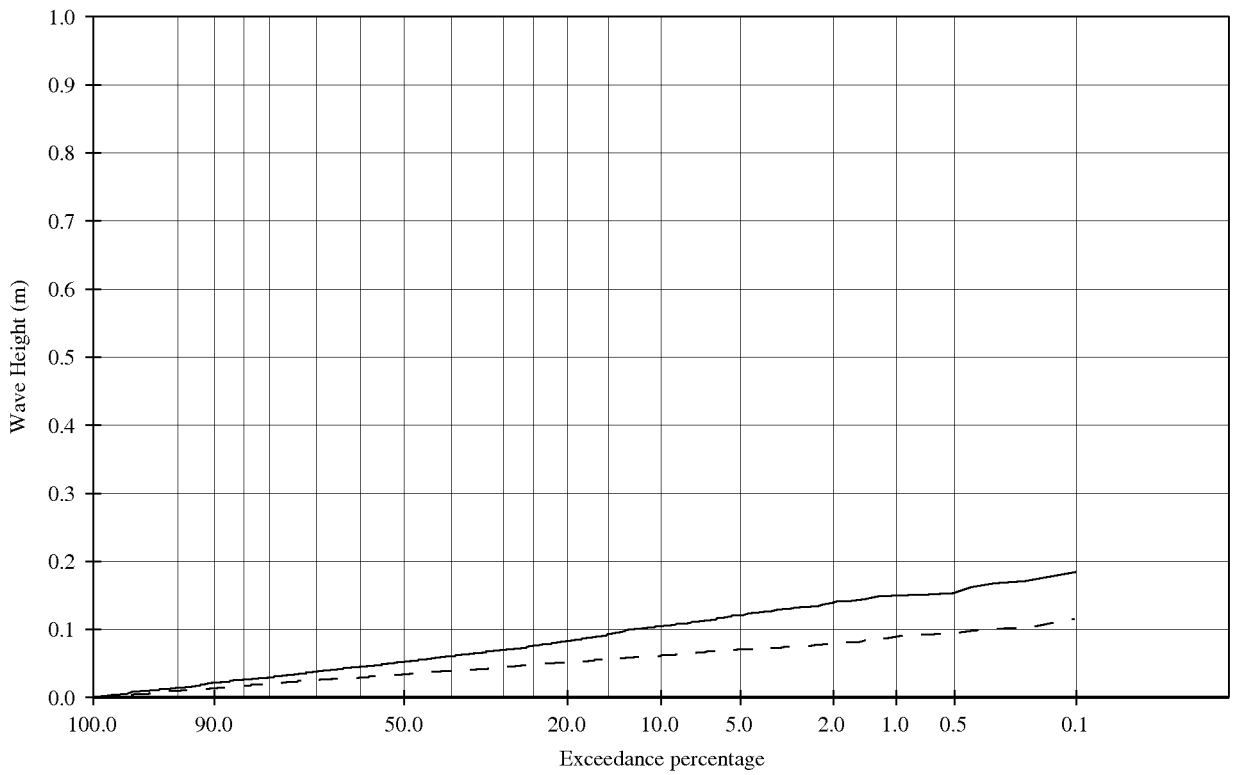
Figure D.13 Exceedance curve and energy density spectra for Test T505

Figure D.14 Exceedance curve and energy density spectra for Test T502

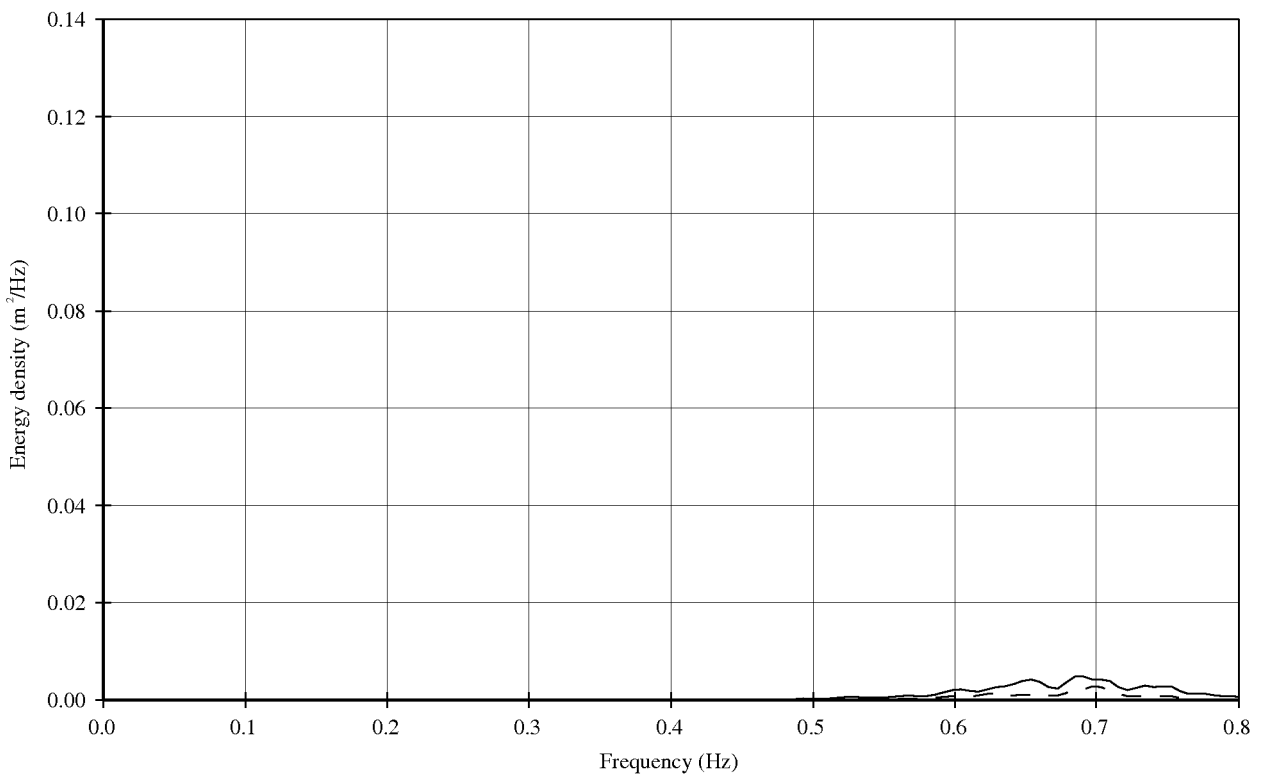
Figure D.15 Exceedance curve and energy density spectra for Test T714

Figure D.16 Exceedance curve and energy density spectra for Test T713

Figure D.17 Exceedance curve and energy density spectra for Test T708



— Incoming GHM 11;12;13 (Seaside of mussels)
 - - - Incoming WHM 1;2;3 (Landside of mussels)



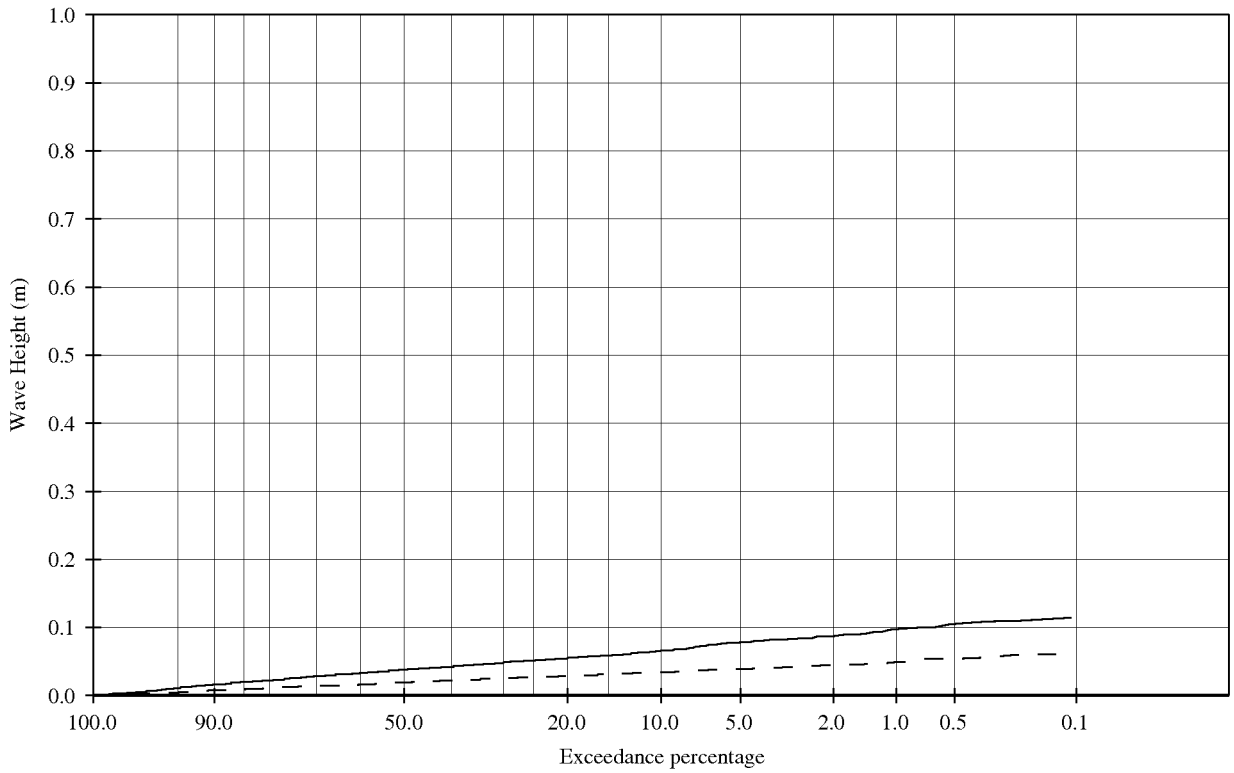
Wave height exceedance curves and
 energy spectra.

t414

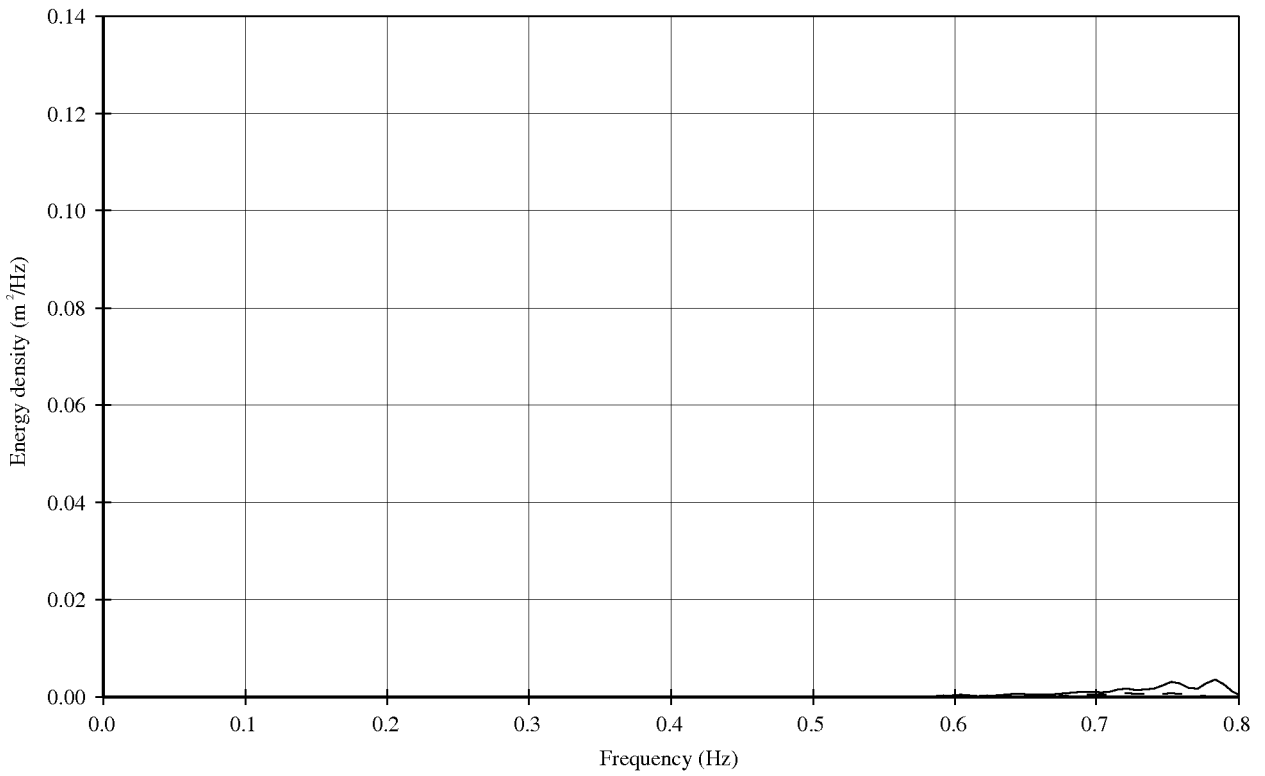
Deltares

1202393.005

FIG. D.1



— Incoming GHM 11;12;13 (Seaside of mussels)
 - - - Incoming WHM 1;2;3 (Landside of mussels)



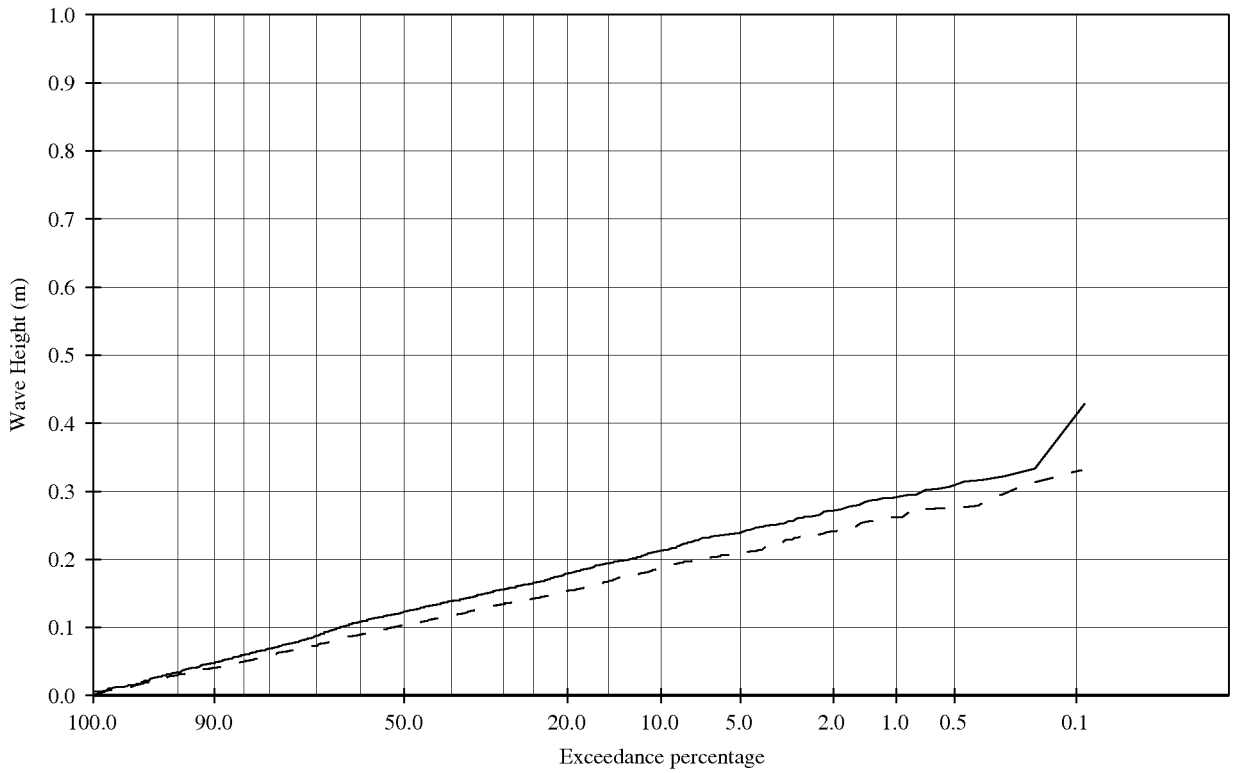
Wave height exceedance curves and
 energy spectra.

t413

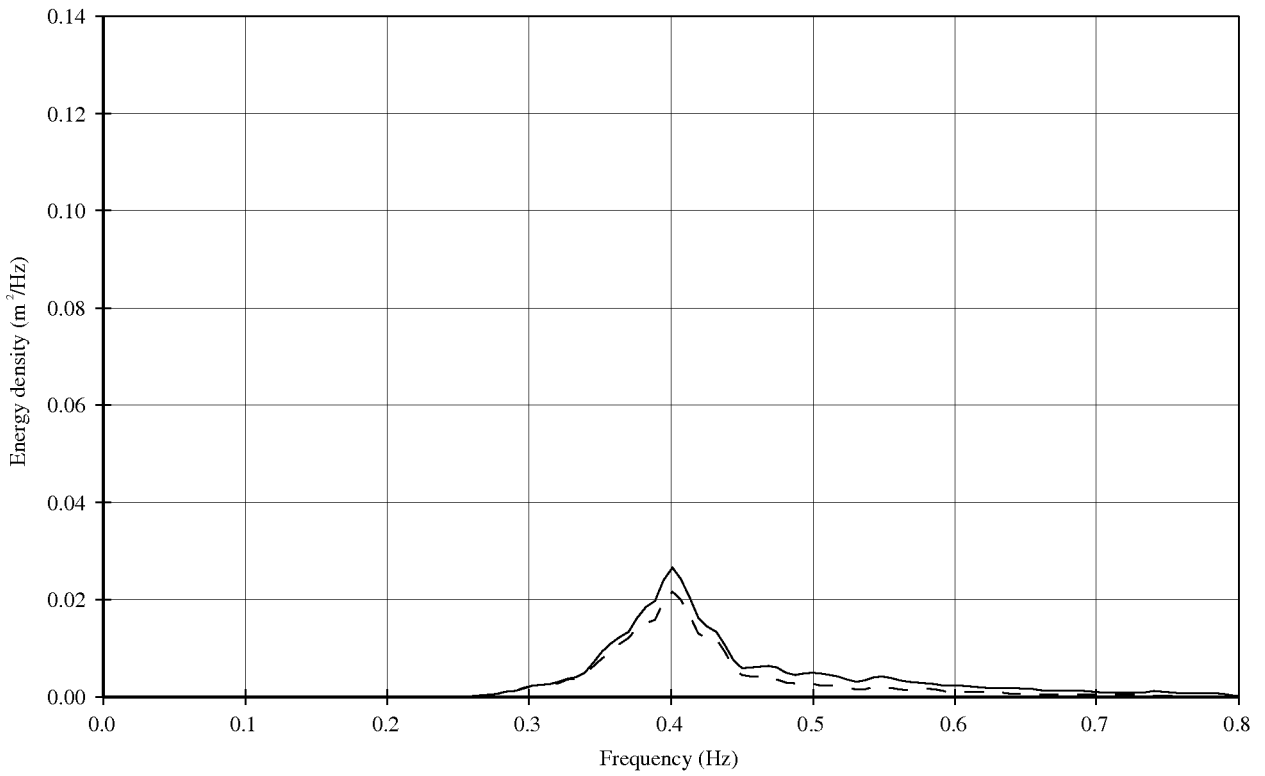
Deltares

1202393.005

FIG. D.2



———— Incoming GHM 11;12;13 (Seaside of mussels)
 - - - - Incoming WHM 1;2;3 (Landside of mussels)



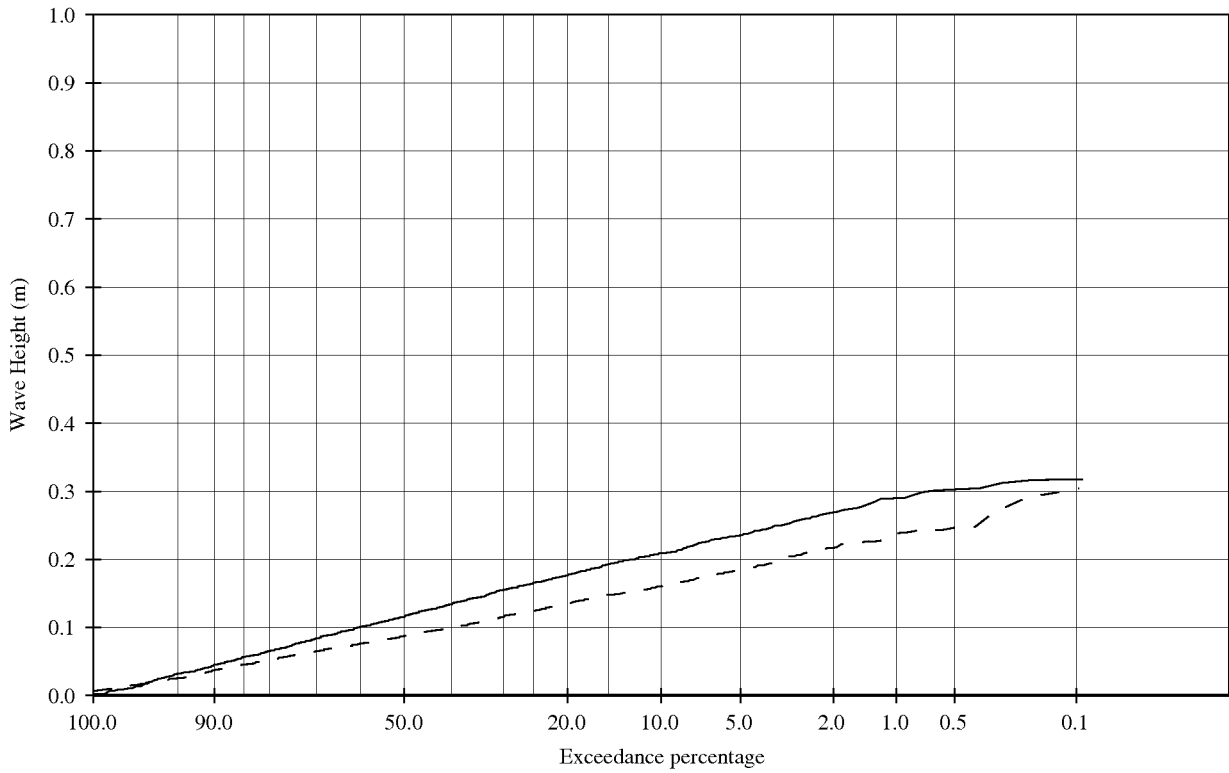
Wave height exceedance curves and
 energy spectra.

t406

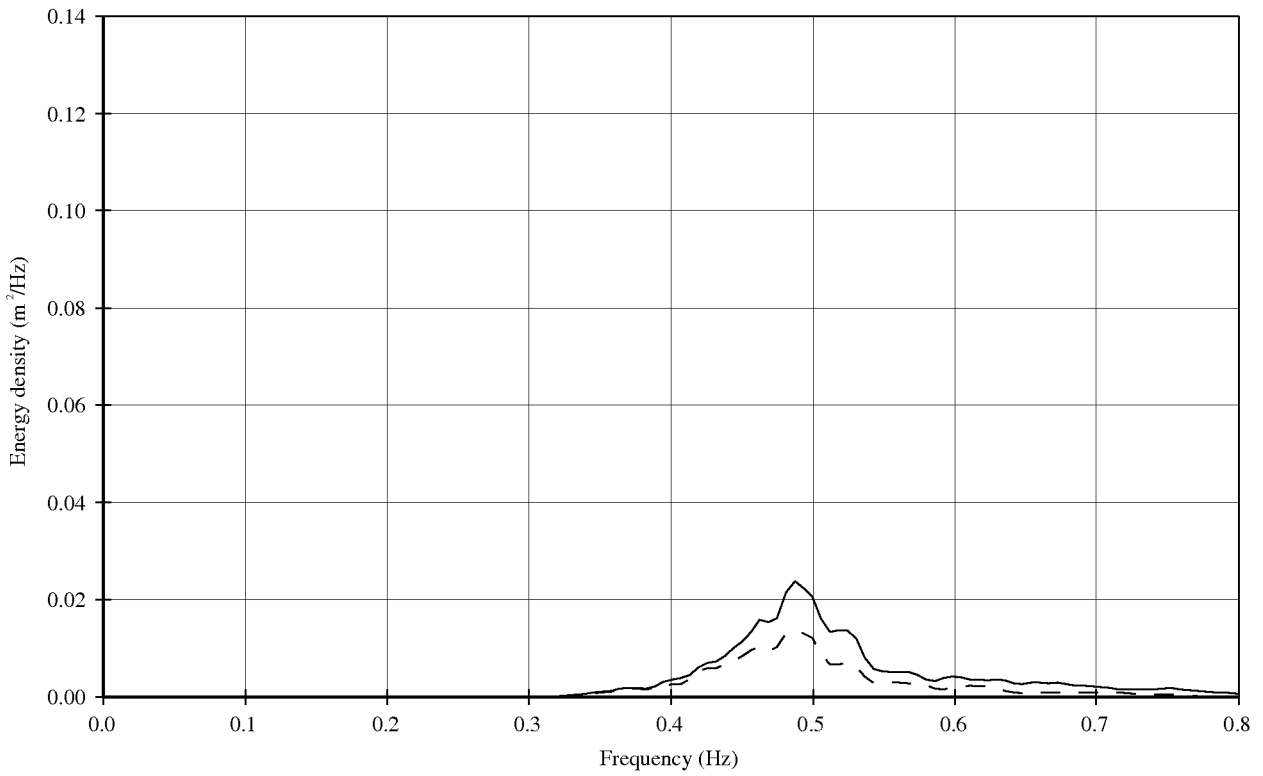
Deltares

1202393.005

FIG. D.3



———— Incoming GHM 11;12;13 (Seaside of mussels)
 - - - - Incoming WHM 1;2;3 (Landside of mussels)



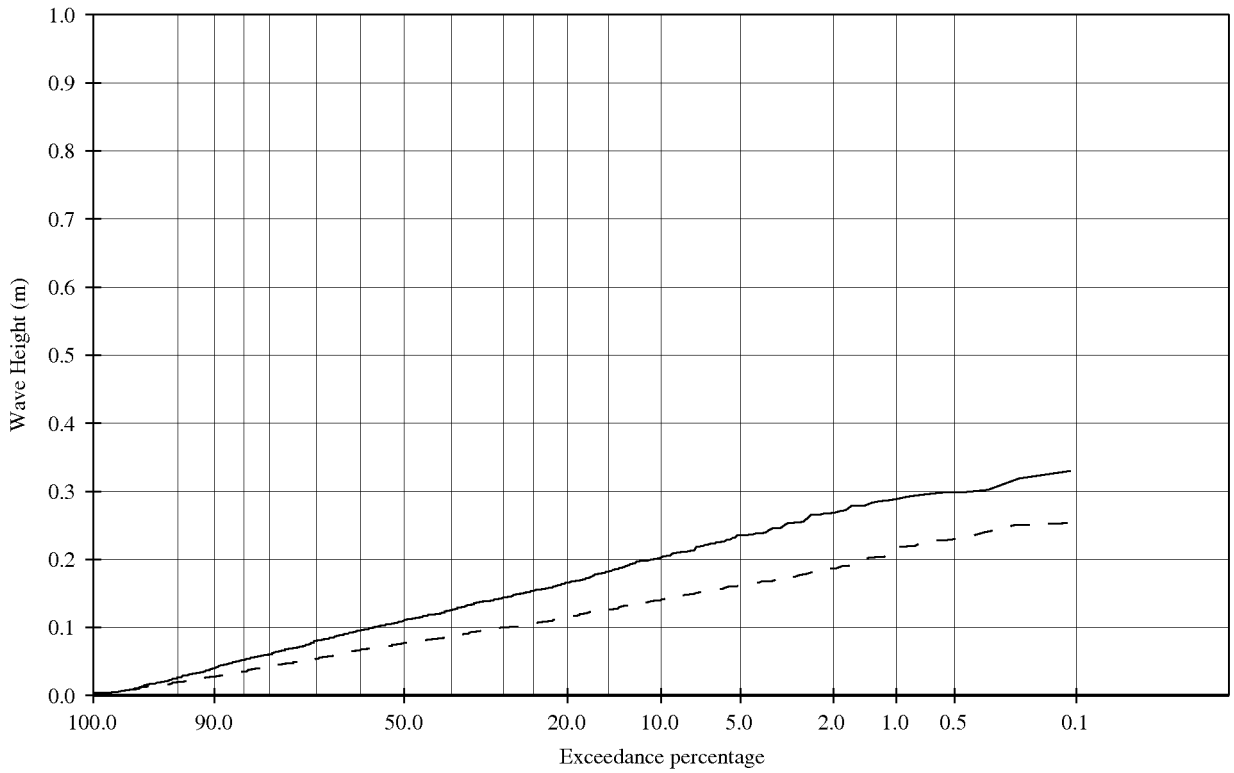
Wave height exceedance curves and
 energy spectra.

t408

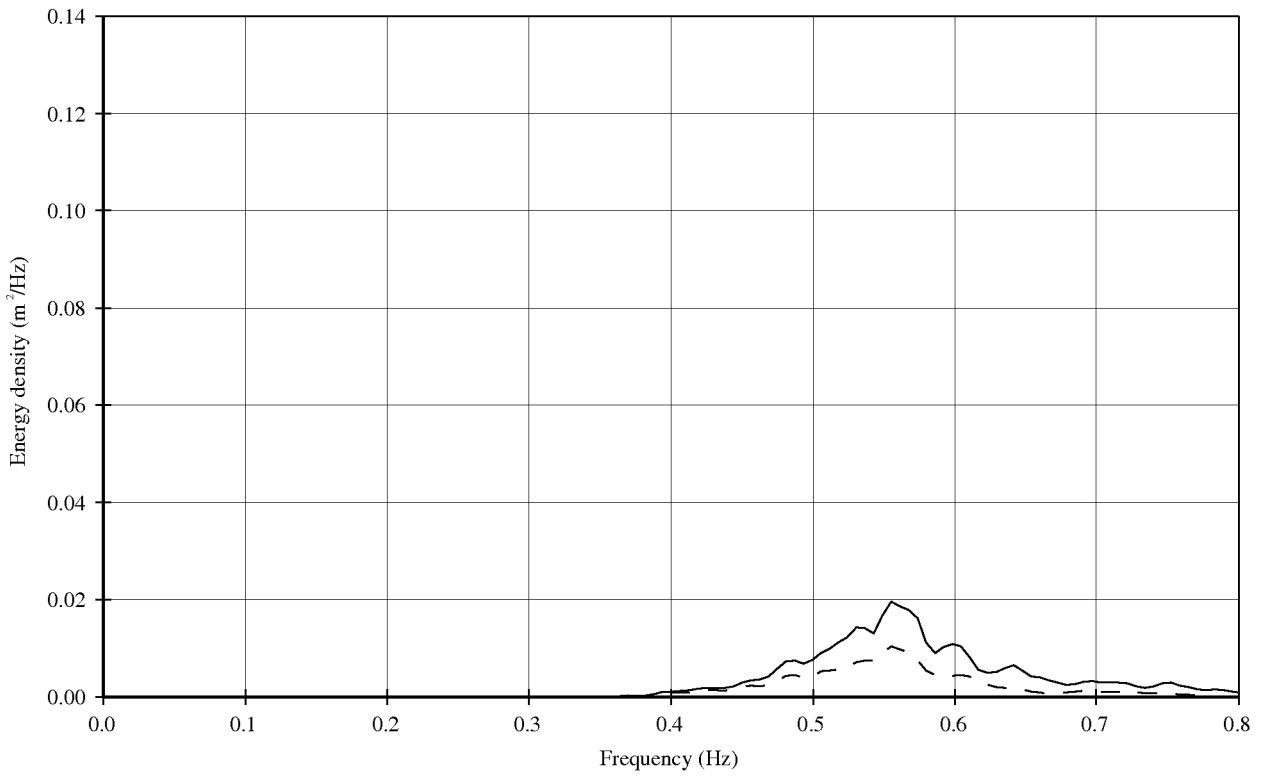
Deltares

1202393.005

FIG. D.4



— Incoming GHM 11;12;13 (Seaside of mussels)
 - - - Incoming WHM 1;2;3 (Landside of mussels)



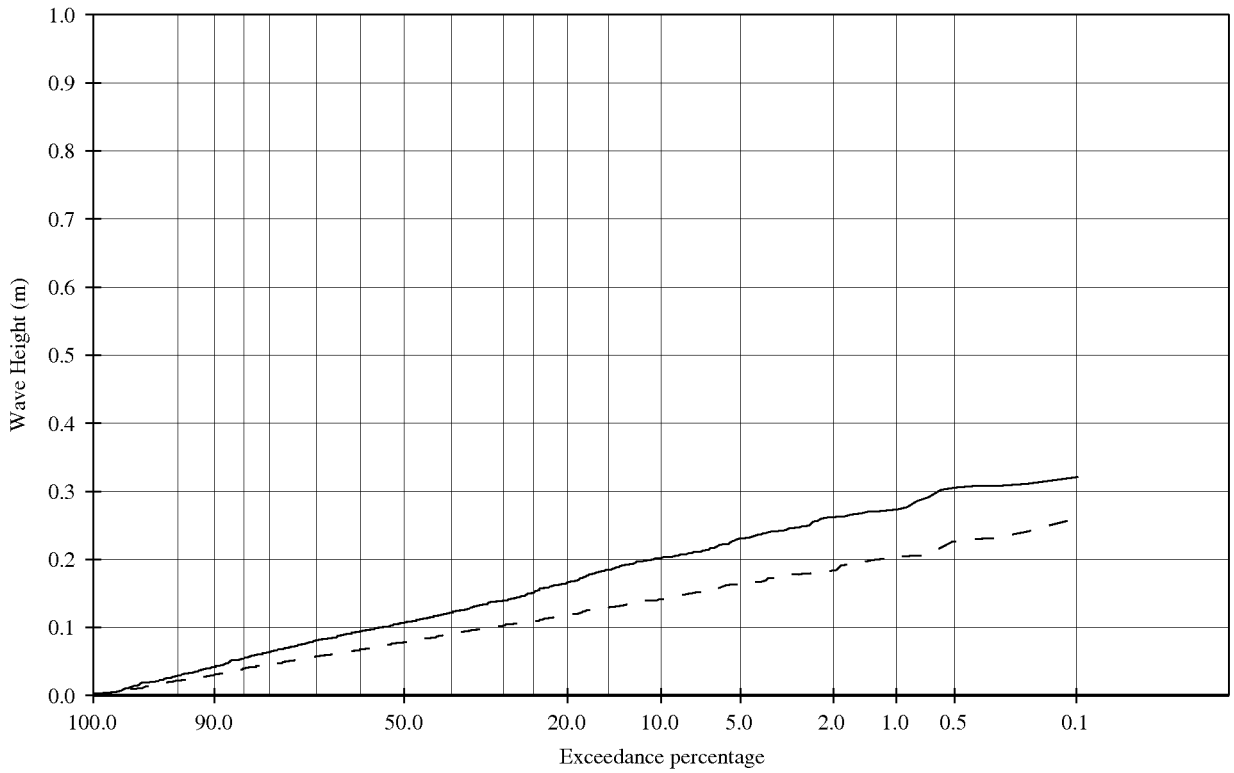
Wave height exceedance curves and
 energy spectra.

t401

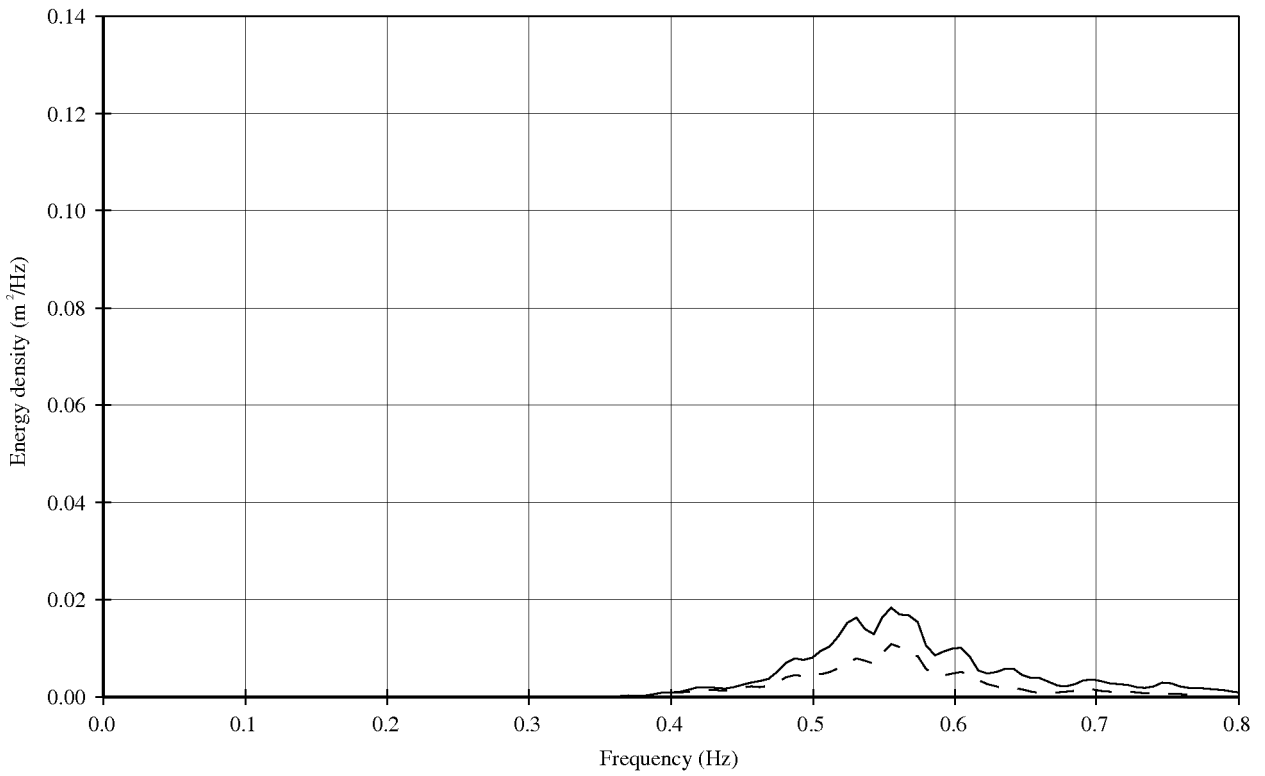
Deltares

1202393.005

FIG. D.5



———— Incoming GHM 11;12;13 (Seaside of mussels)
 - - - - Incoming WHM 1;2;3 (Landside of mussels)



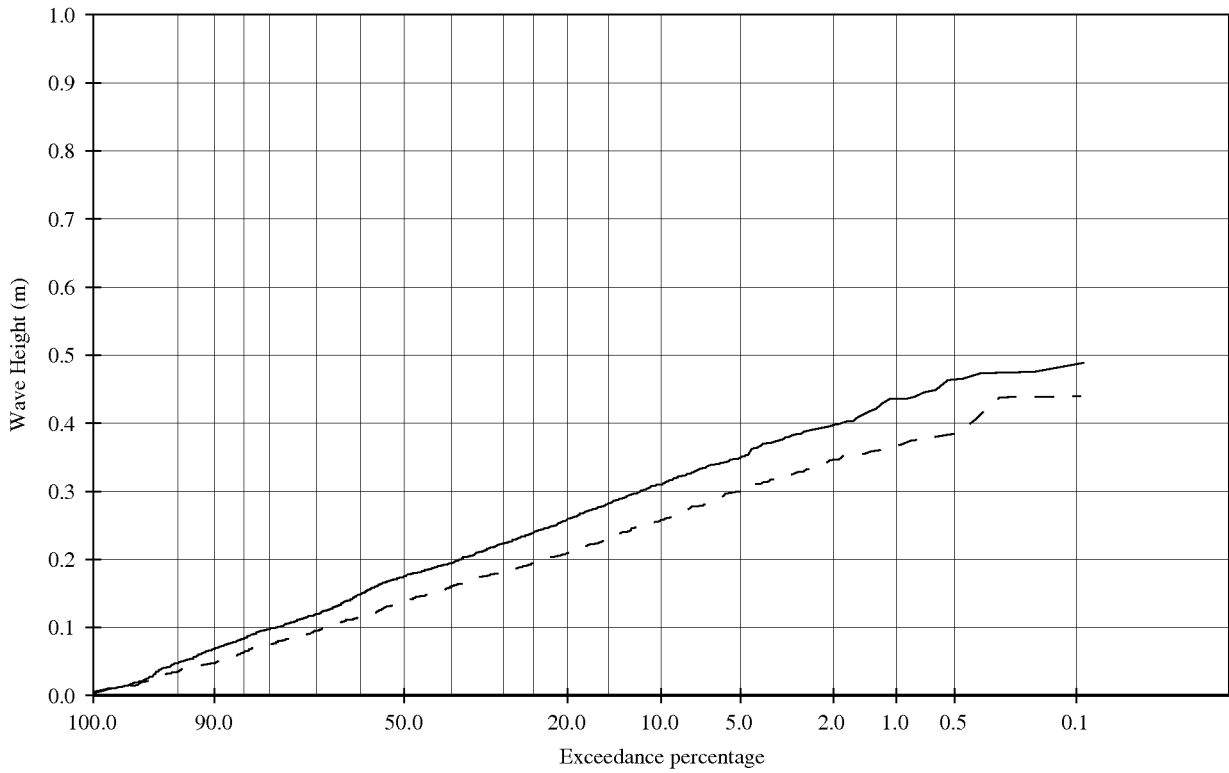
Wave height exceedance curves and
 energy spectra.

t4011

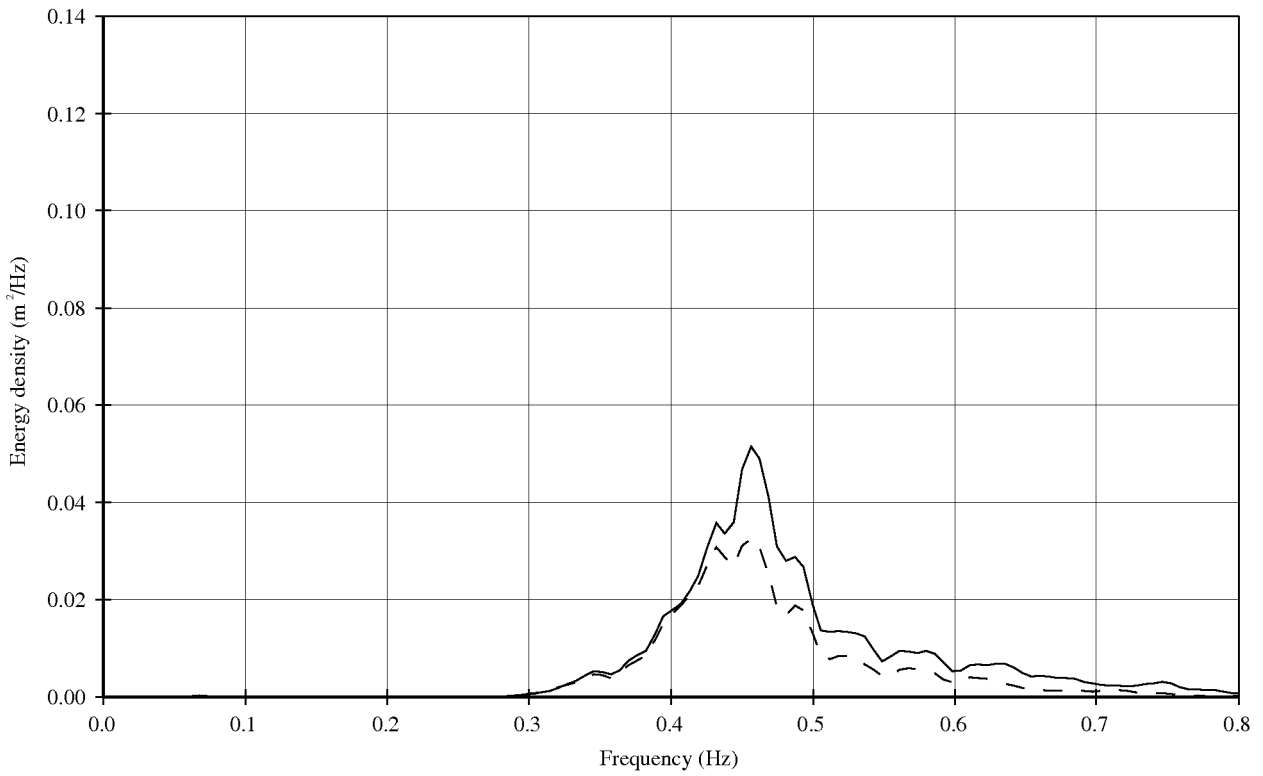
Deltares

1202393.005

FIG. D.6



— Incoming GHM 11;12;13 (Seaside of mussels)
 - - - Incoming WHM 1;2;3 (Landside of mussels)



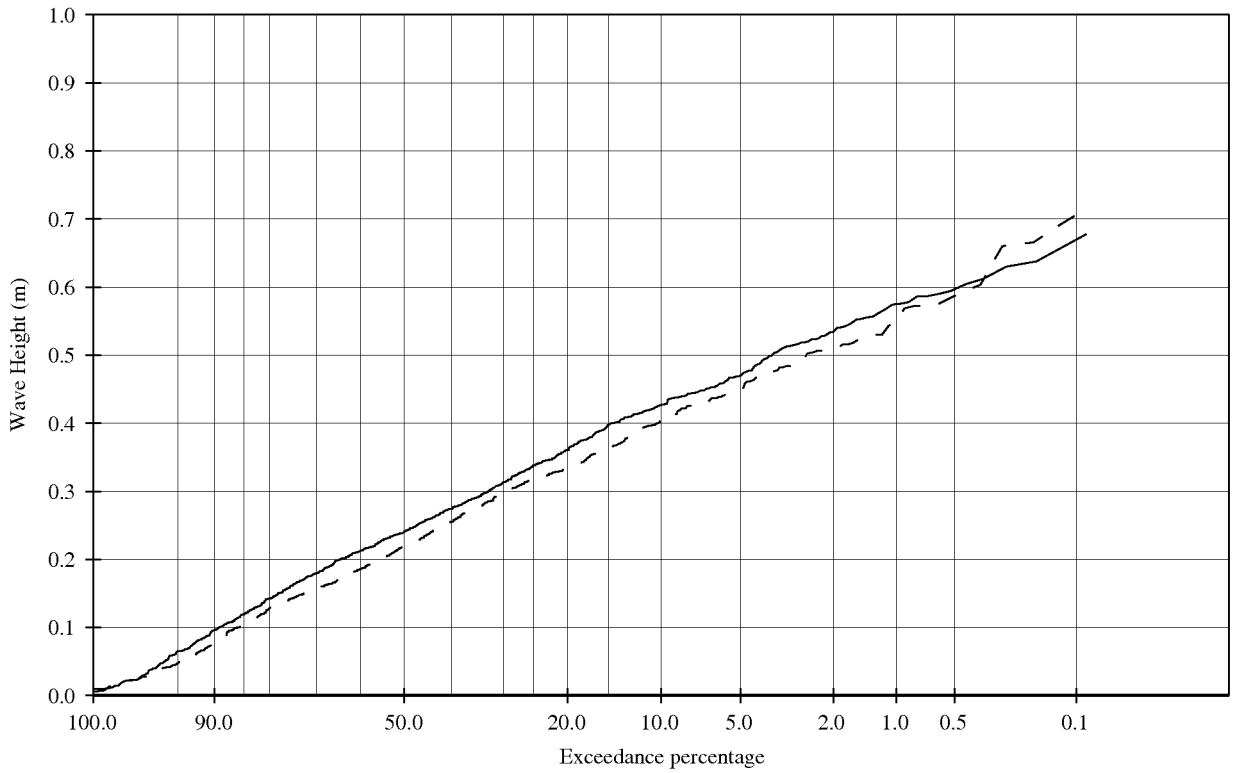
Wave height exceedance curves and
 energy spectra.

t412

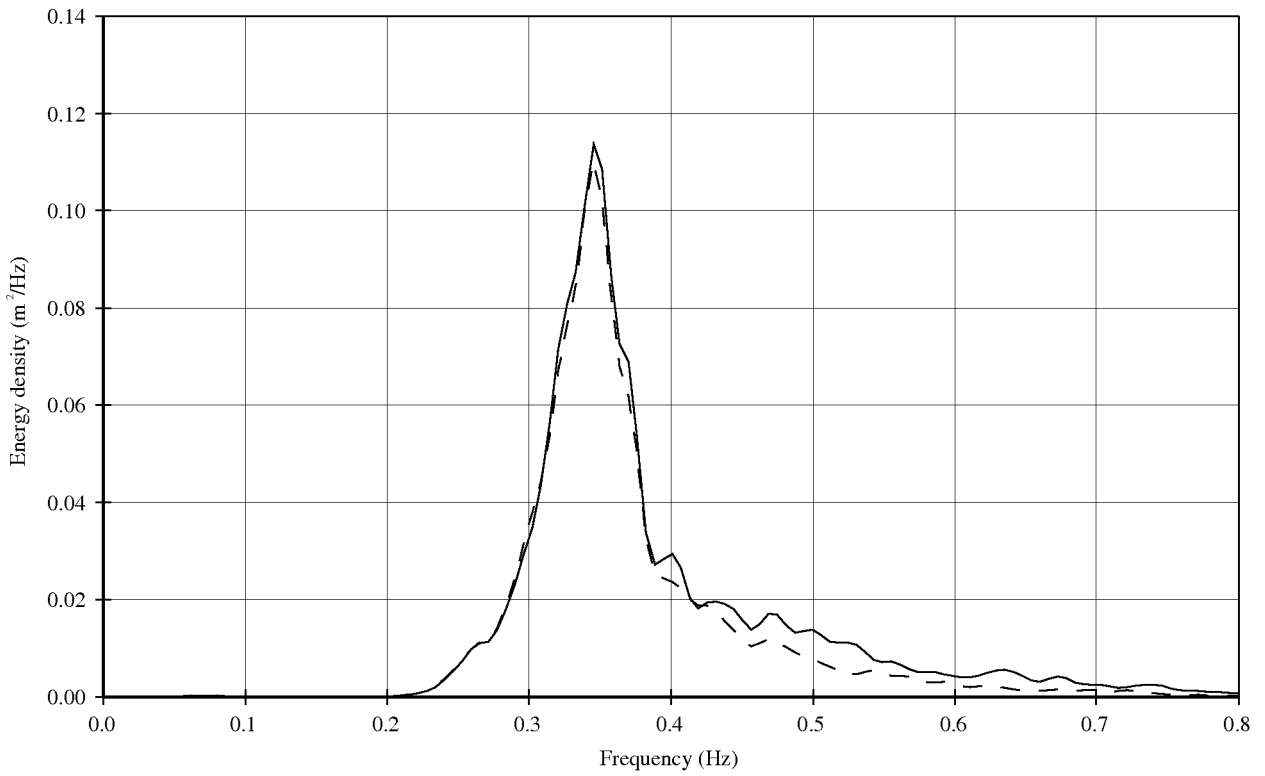
Deltares

1202393.005

FIG. D.7



———— Incoming GHM 11;12;13 (Seaside of mussels)
 - - - - Incoming WHM 1;2;3 (Landside of mussels)



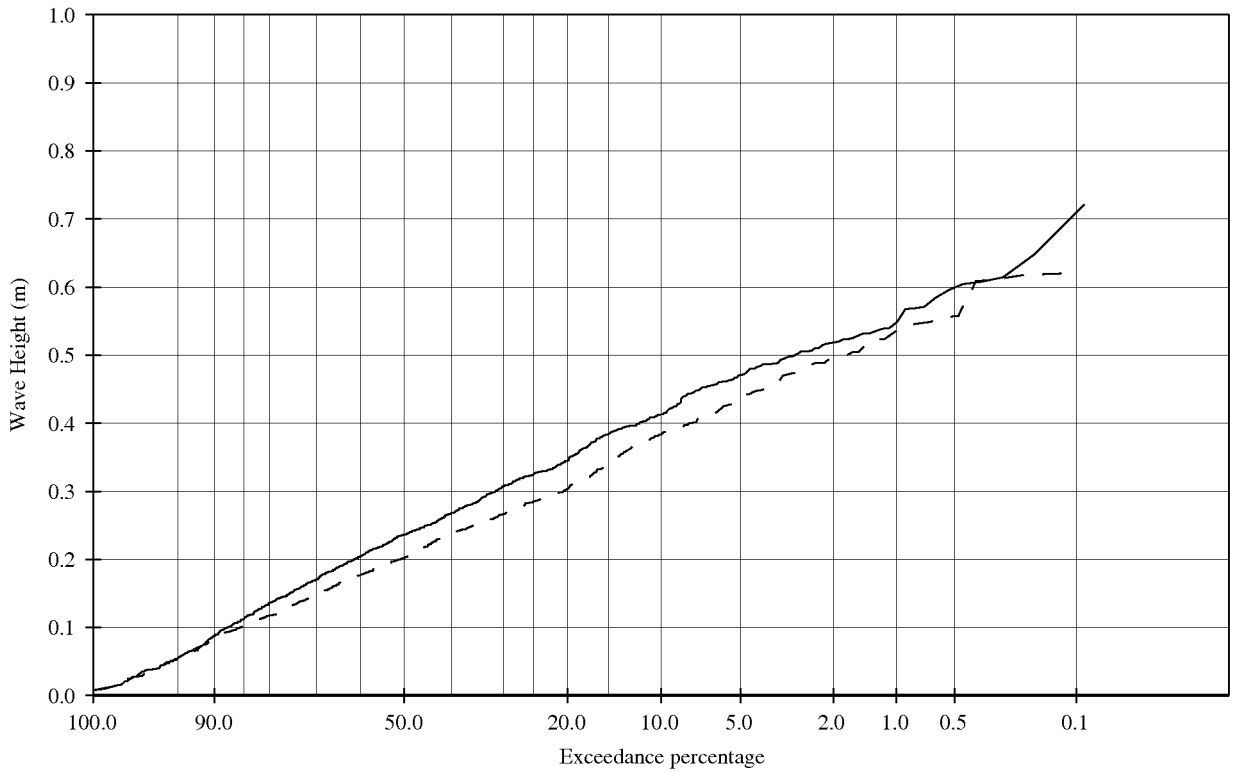
Wave height exceedance curves and
 energy spectra.

t405

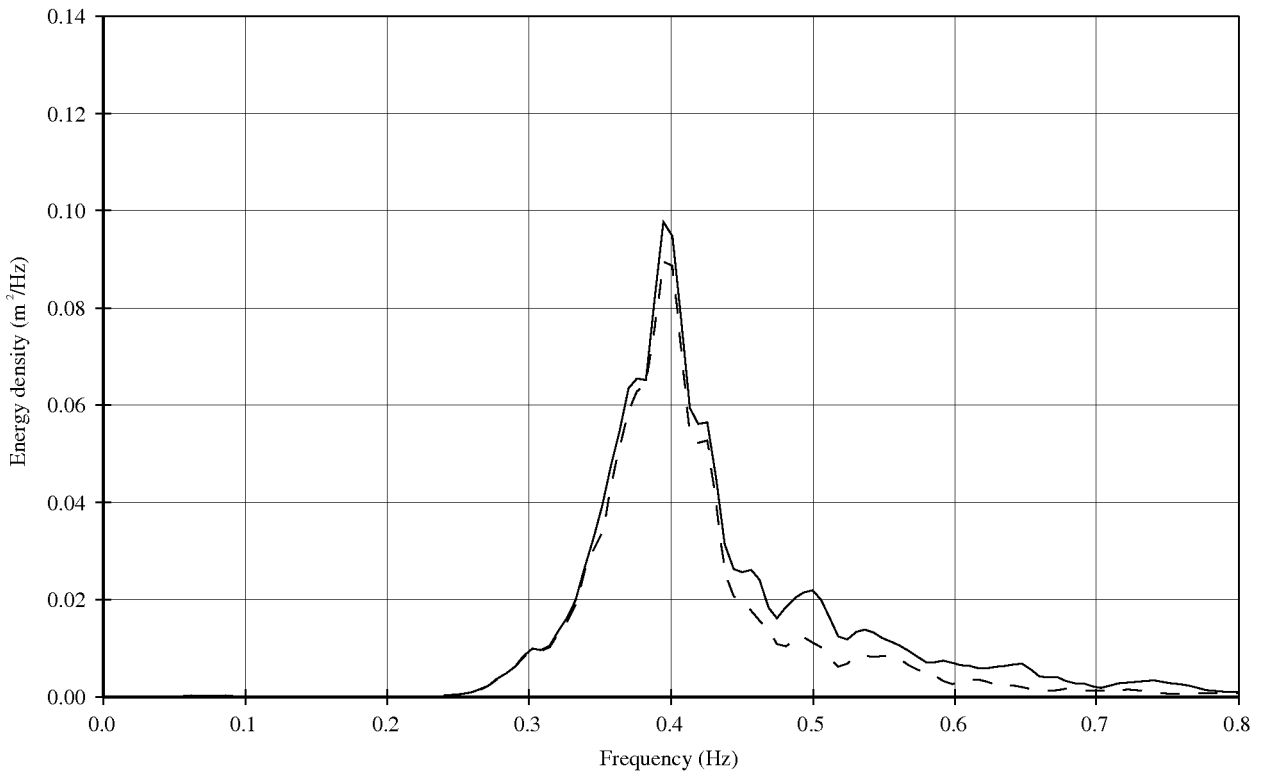
Deltares

1202393.005

FIG. D.8



———— Incoming GHM 11;12;13 (Seaside of mussels)
 - - - - - Incoming WHM 1;2;3 (Landside of mussels)



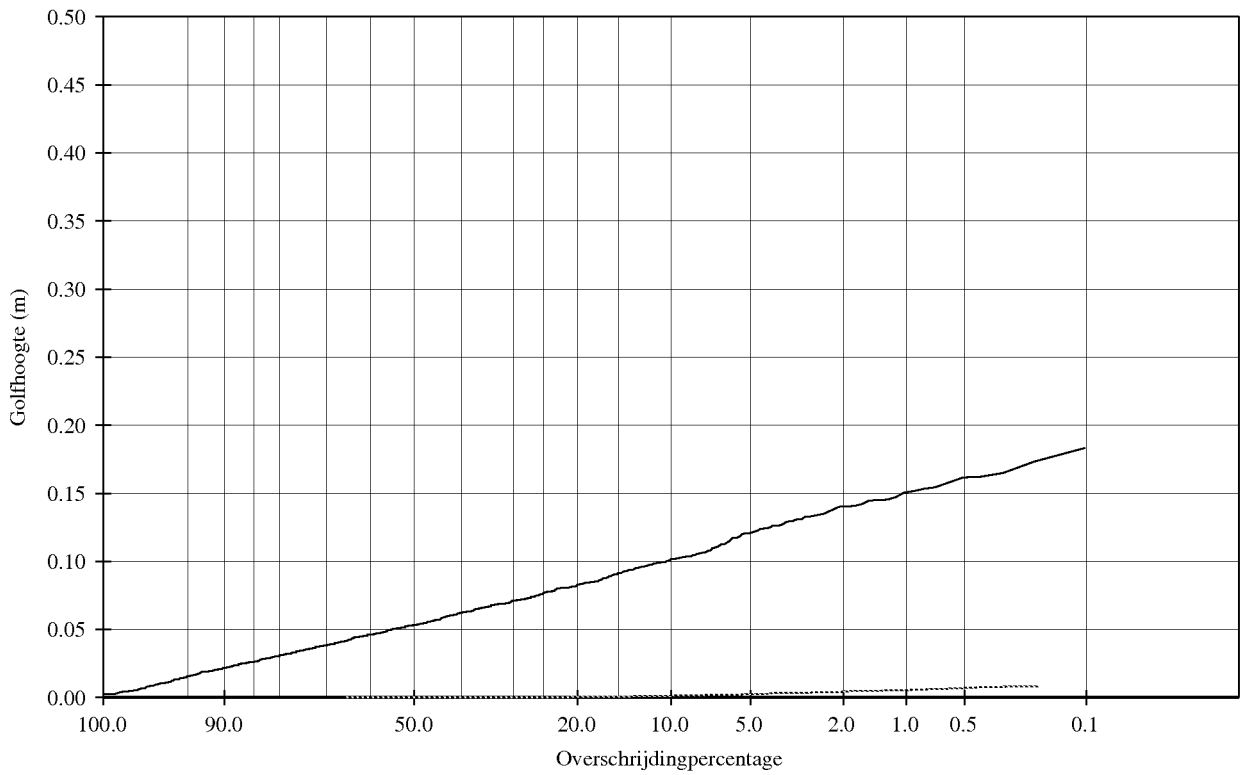
Wave height exceedance curves and
 energy spectra.

t402

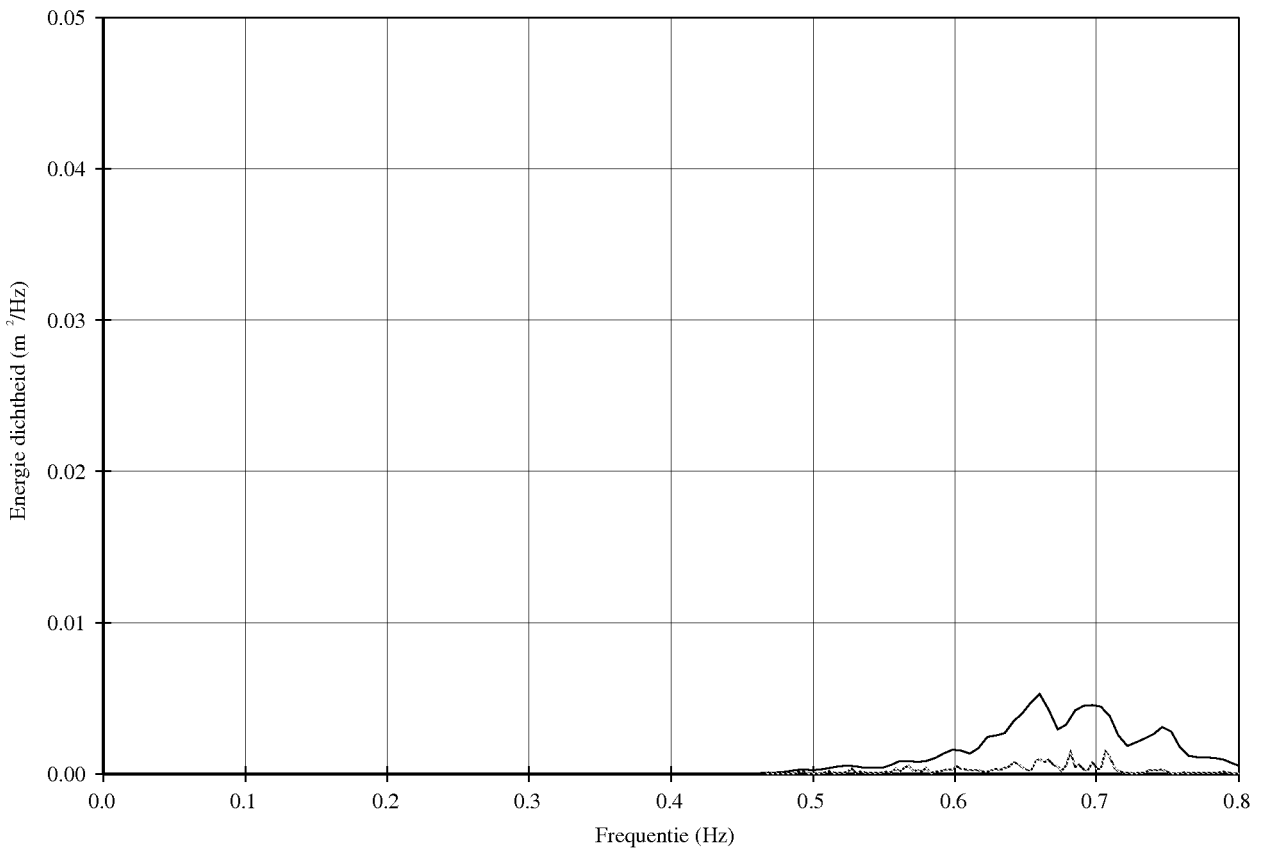
Deltares

1202393.005

FIG. D.9



— Inkomend
 Gereflecteerd



golfhoogte overschrijdingskrommen en
 energie dichtheidsspectra

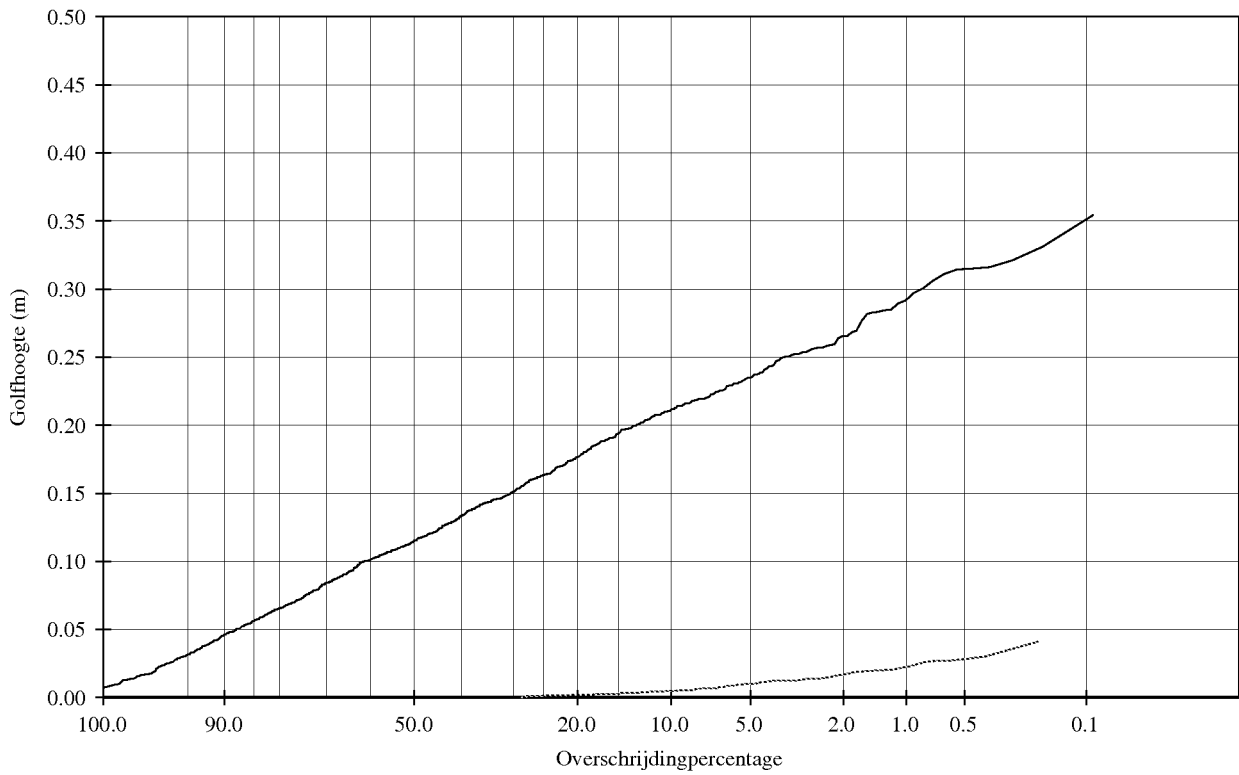
#t514

Inkomend

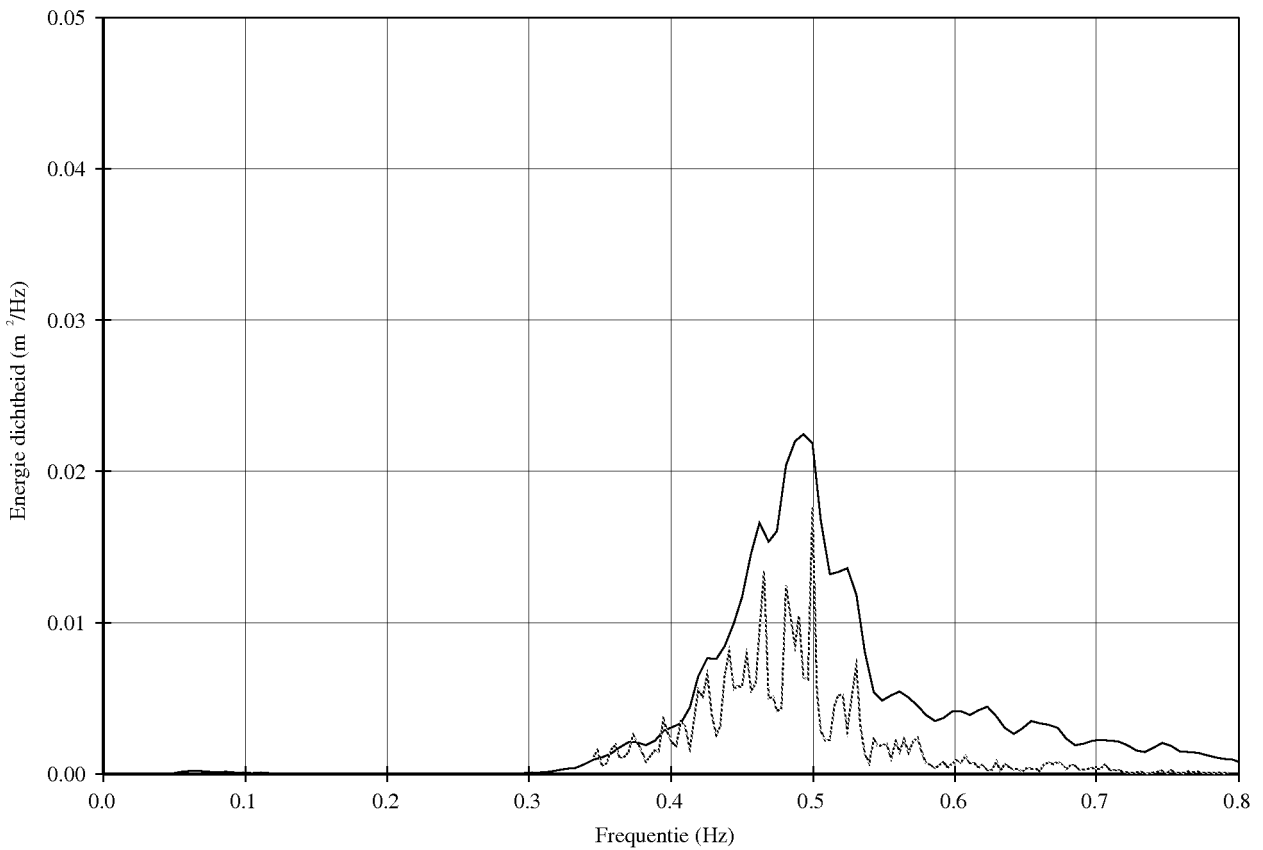
Deltares | Delft Hydraulics

1202393

FIG. D.10



— Inkomend
 Gereflecteerd



golfhoogte overschrijdingskrommen en
 energie dichtheidsspectra

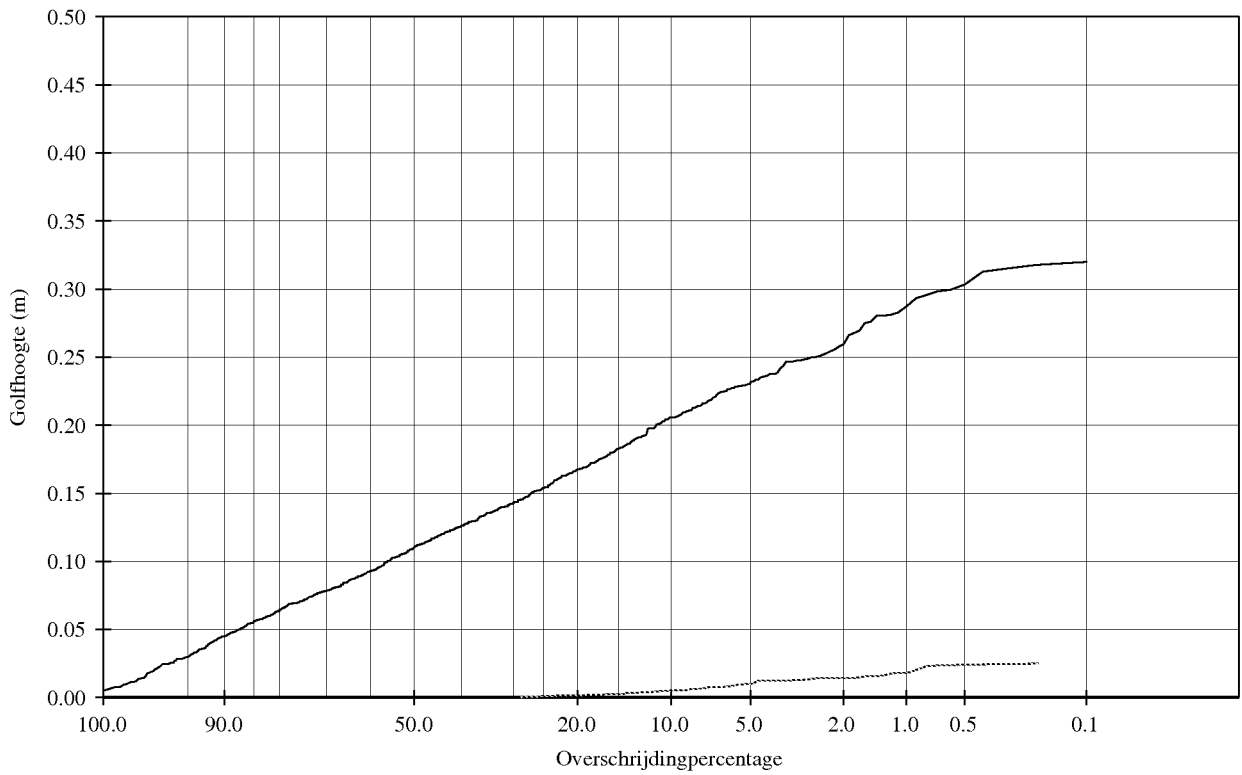
#t508

Inkomend

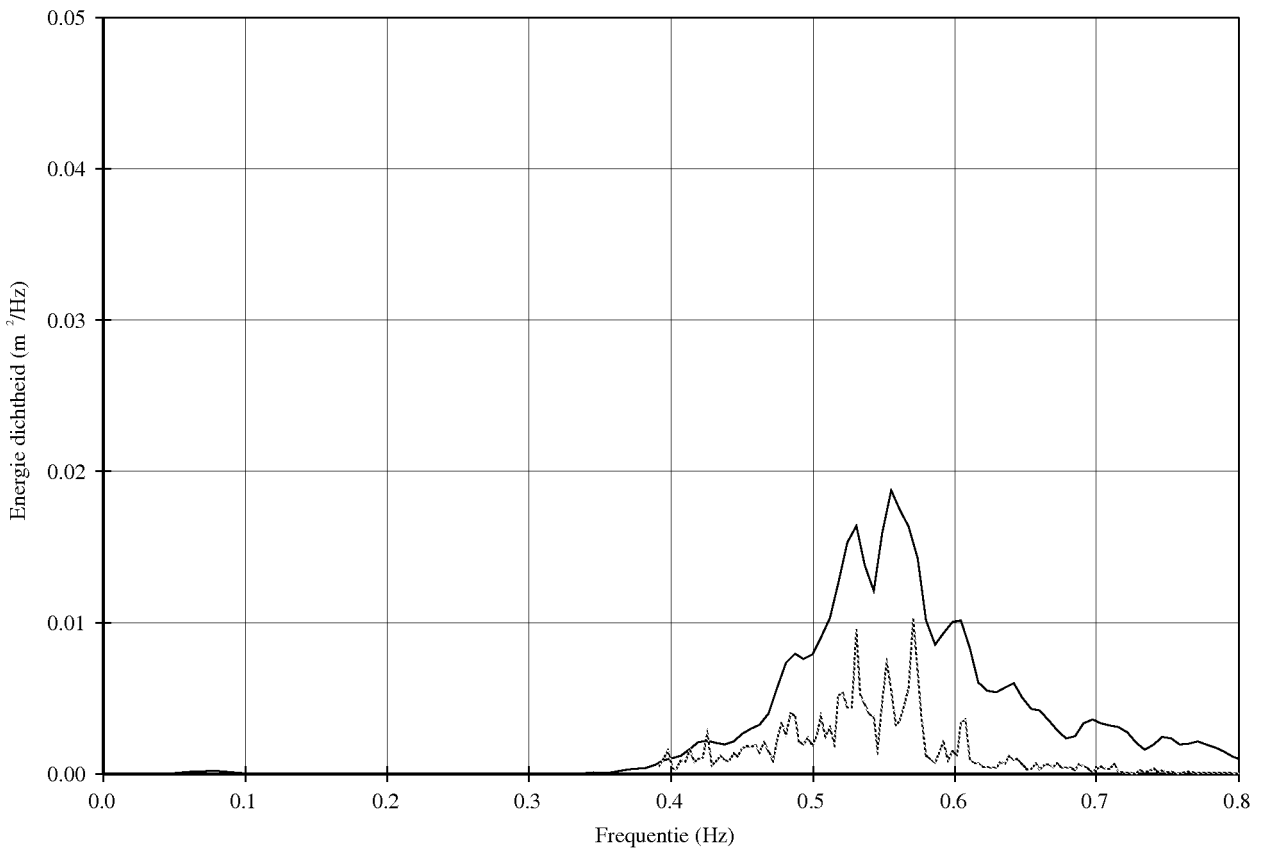
Deltares | Delft Hydraulics

1202393

FIG. D.11



— Inkomend
 Gereflecteerd



golfhoogte overschrijdingskrommen en
 energie dichtheidsspectra

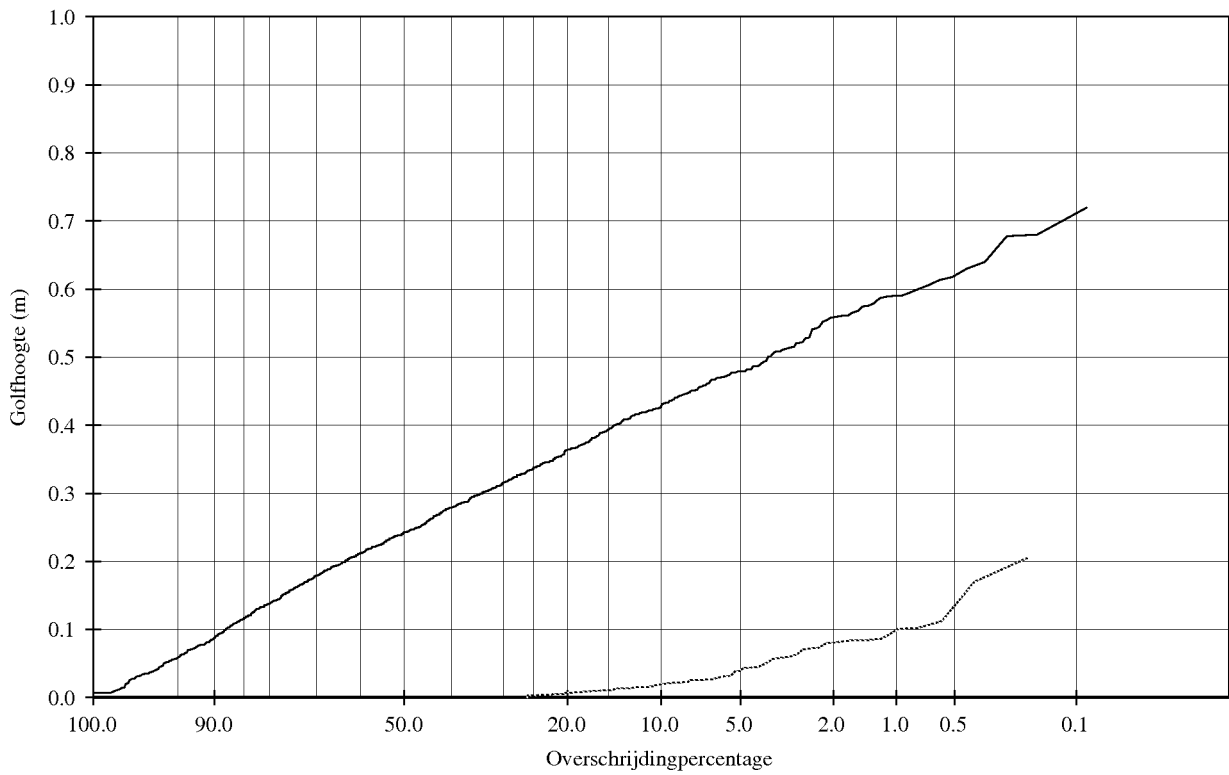
#t501

Inkomend

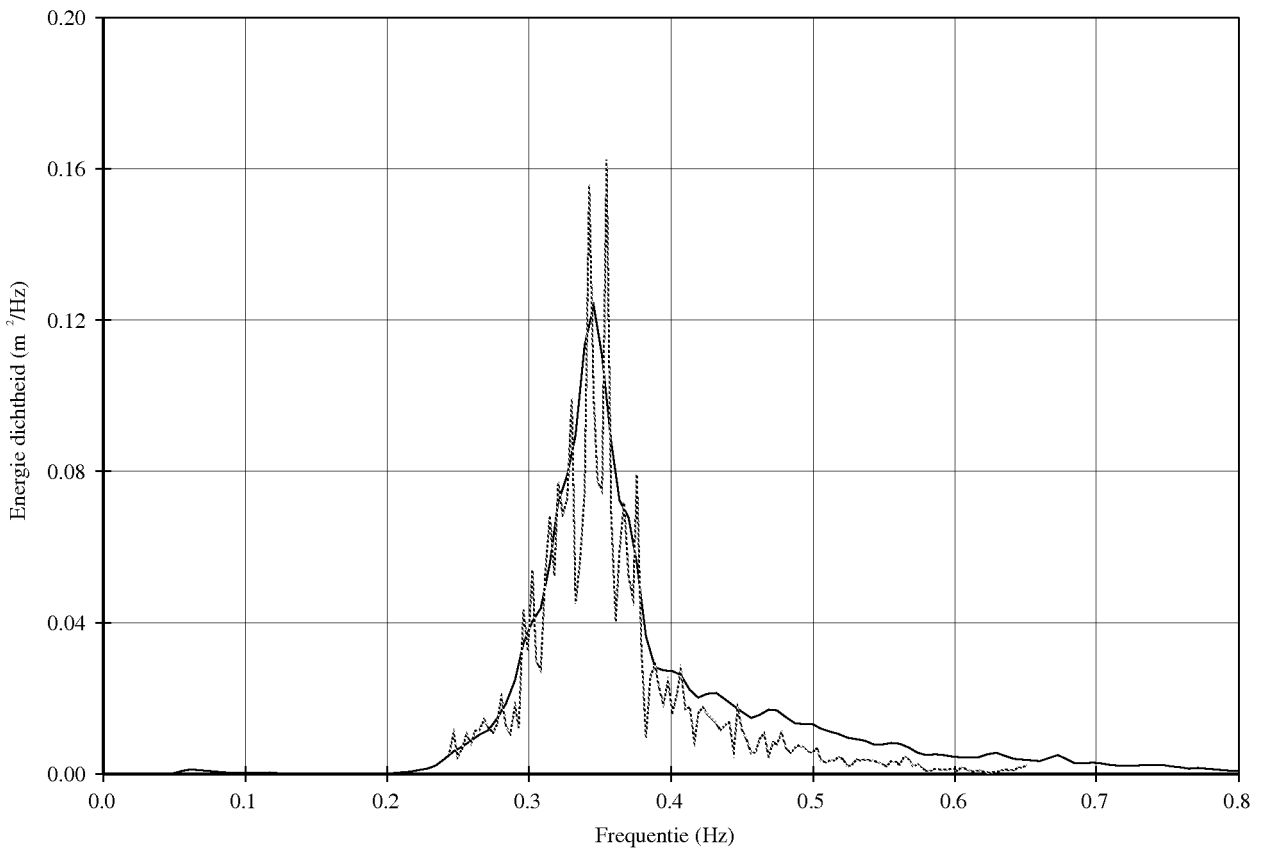
Deltares | Delft Hydraulics

1202393

FIG. D.12



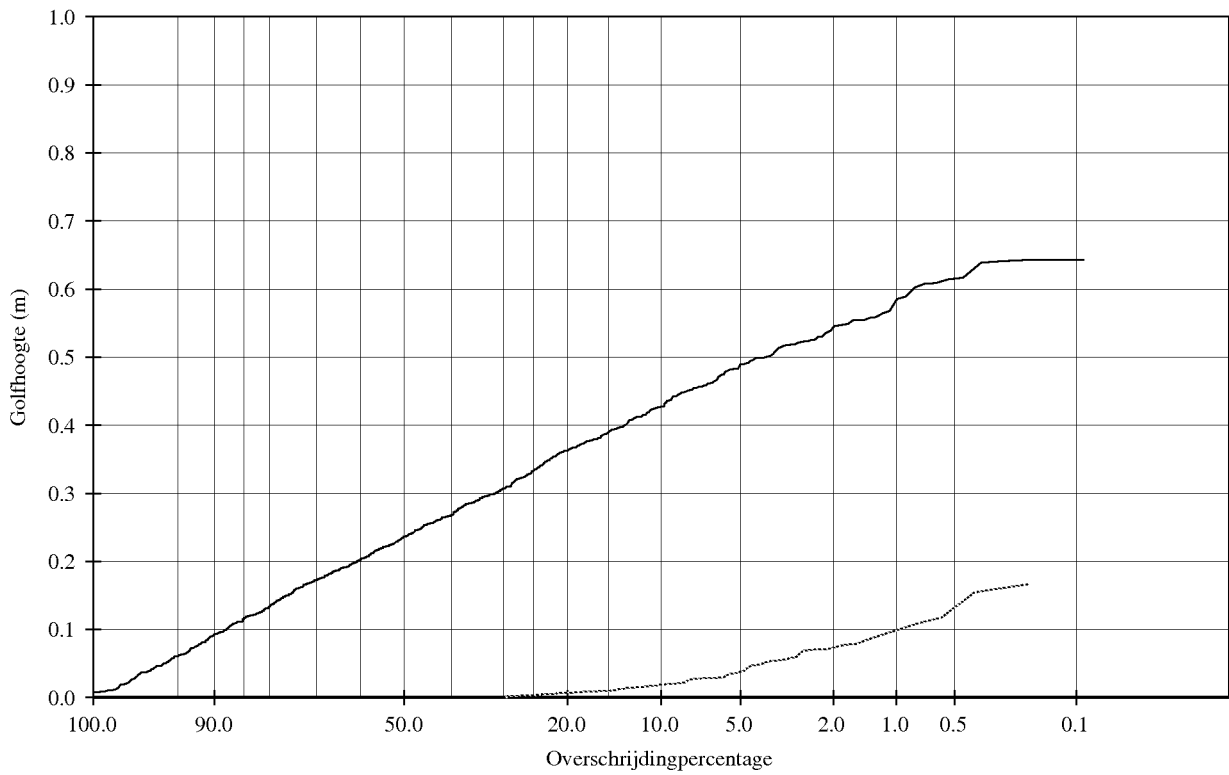
— Inkomend
 Gereflecteerd



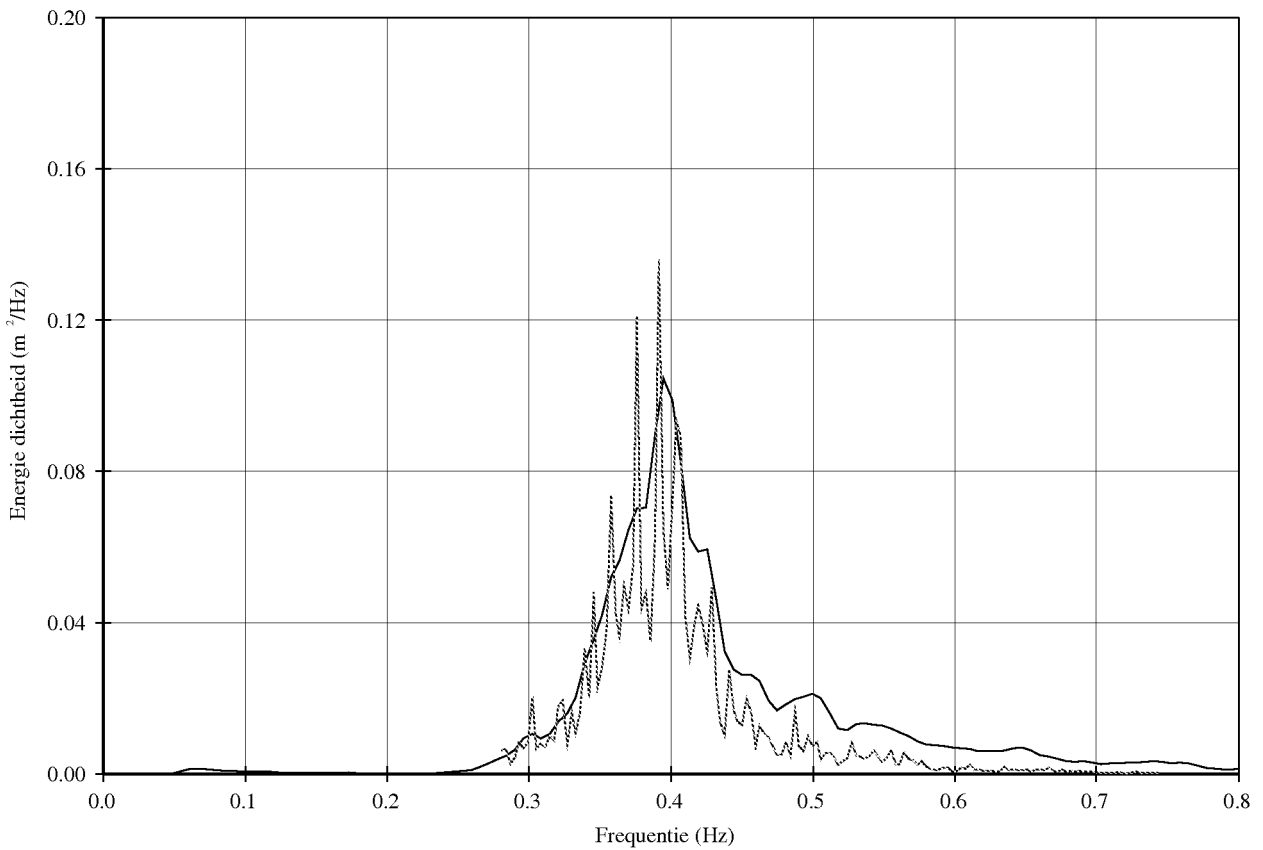
golfhoogte overschrijdingskrommen en
 energie dichtheidsspectra

#t505

Inkomend



— Inkomend
 Gereflecteerd



golfhoogte overschrijdingskrommen en
 energie dichtheidsspectra

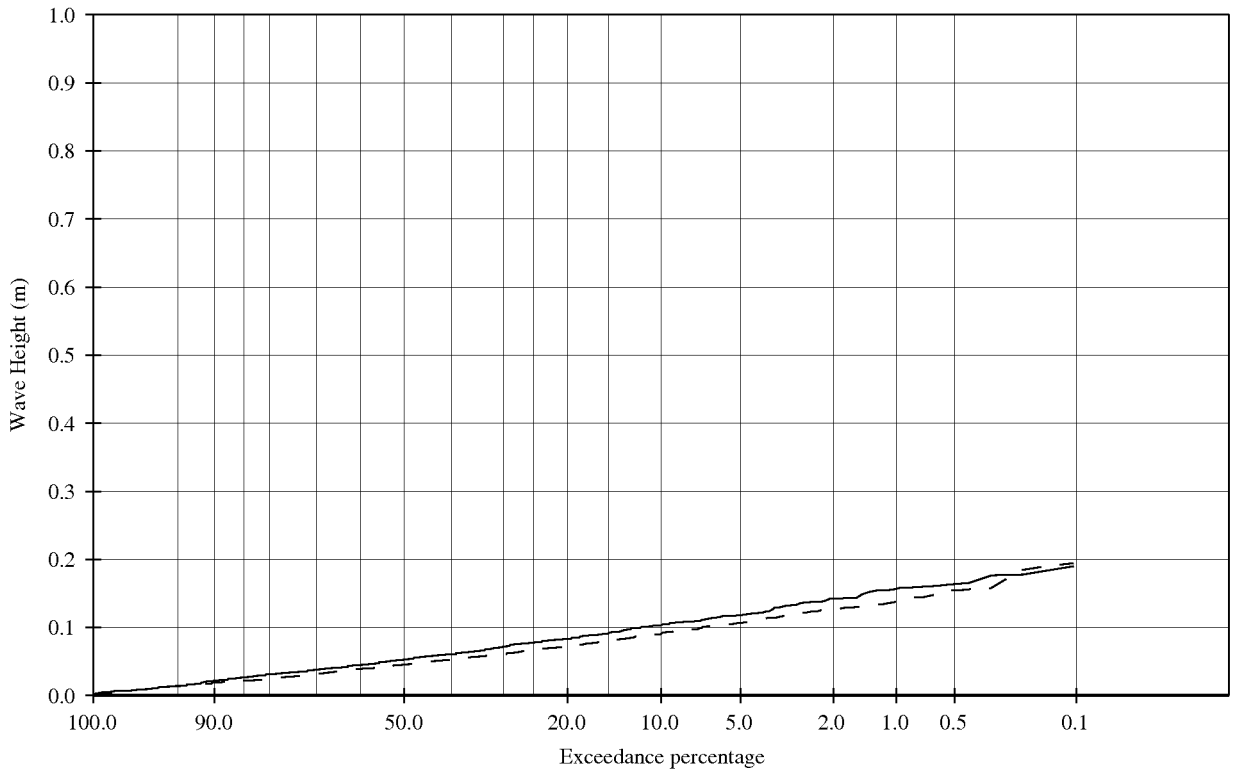
#t502

Inkomend

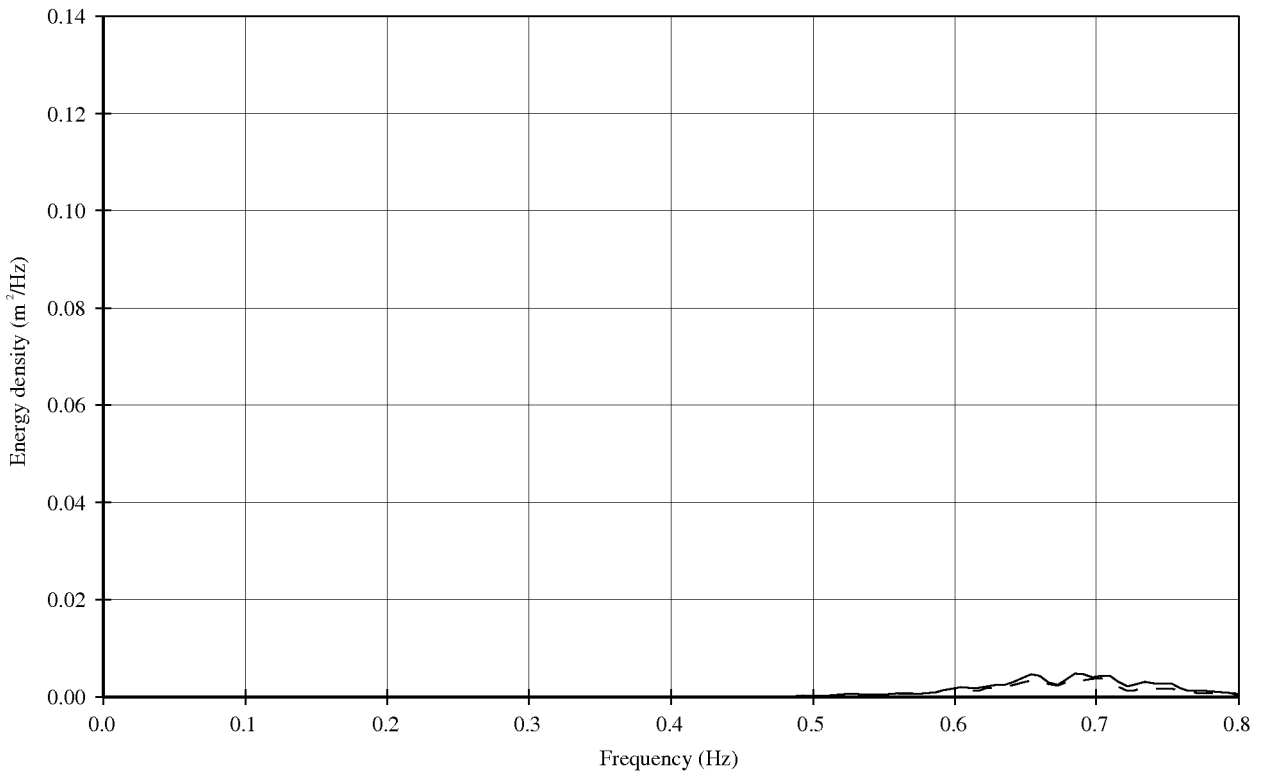
Deltares | Delft Hydraulics

1202393

FIG.D.14



— Incoming GHM 11;12;13 (Seaside of mussels)
 - - - Incoming WHM 1;2;3 (Landside of mussels)



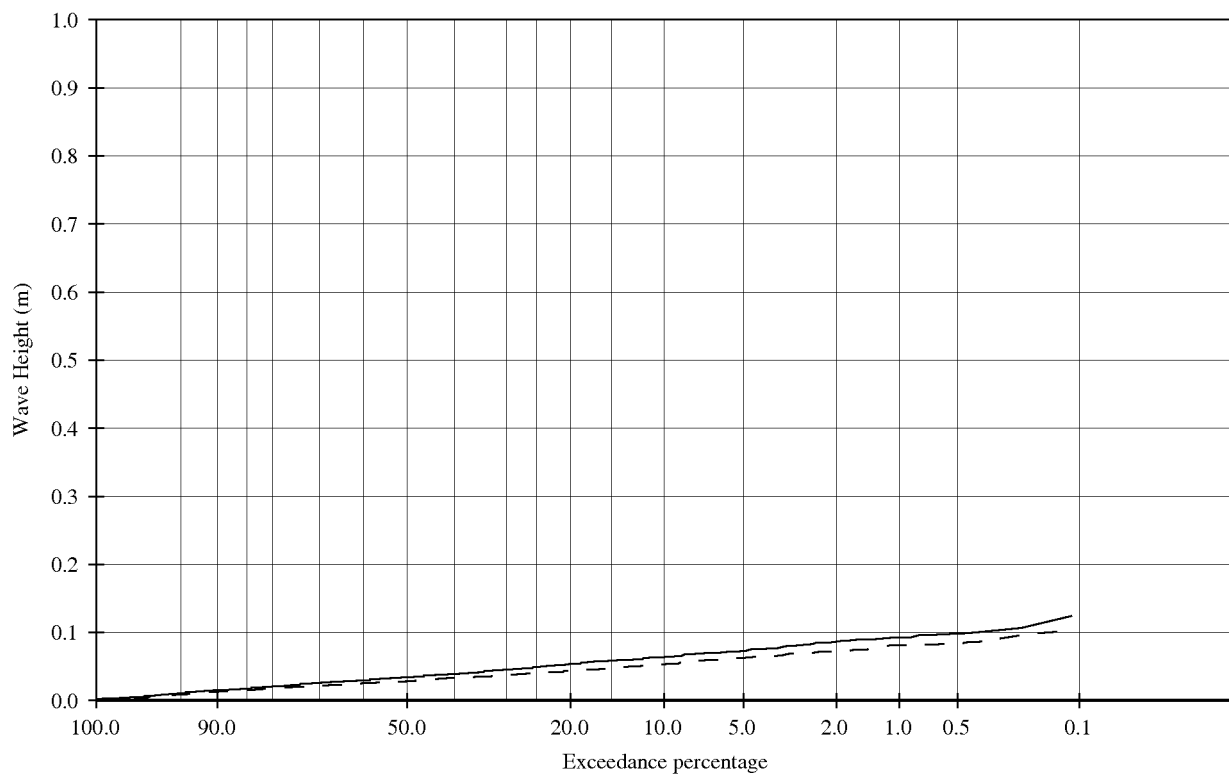
Wave height exceedance curves and
 energy spectra.

t714

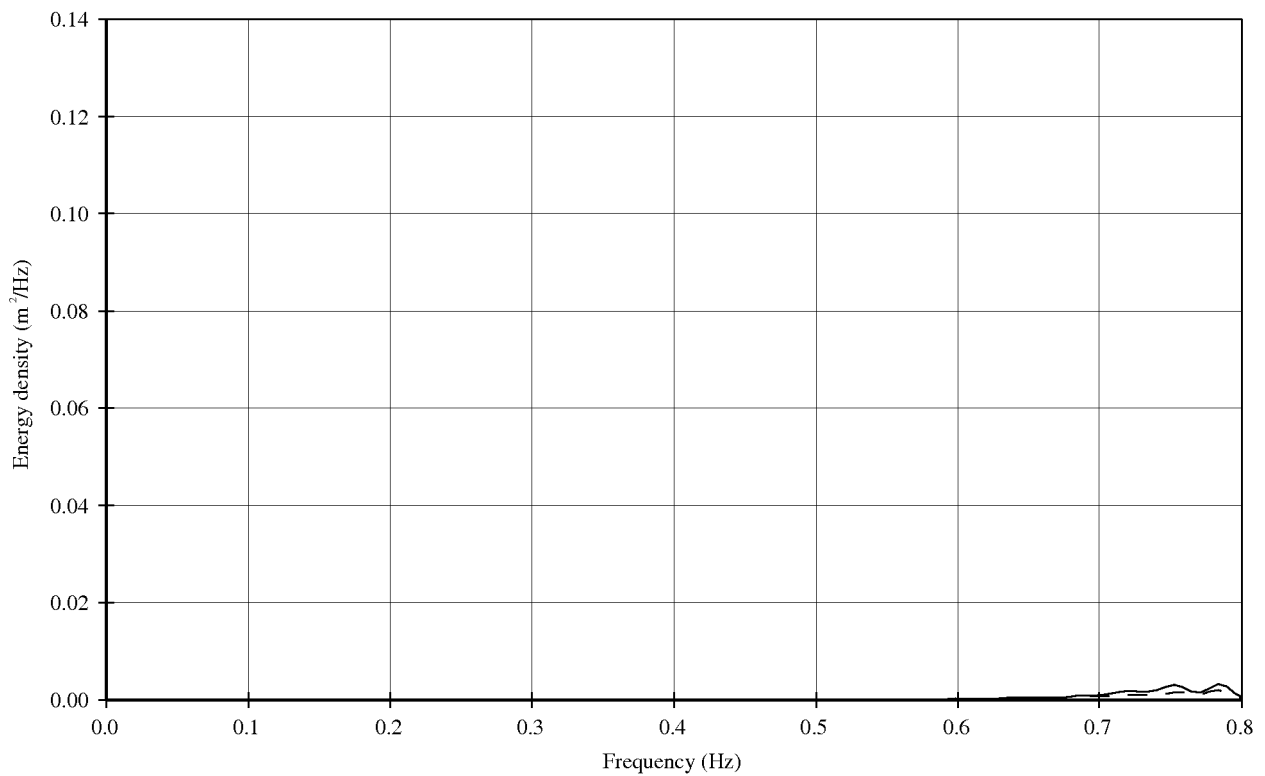
Deltares

1202393.005

FIG. D.15



— Incoming GHM 11;12;13 (Seaside of mussels)
 - - - Incoming WHM 1;2;3 (Landside of mussels)

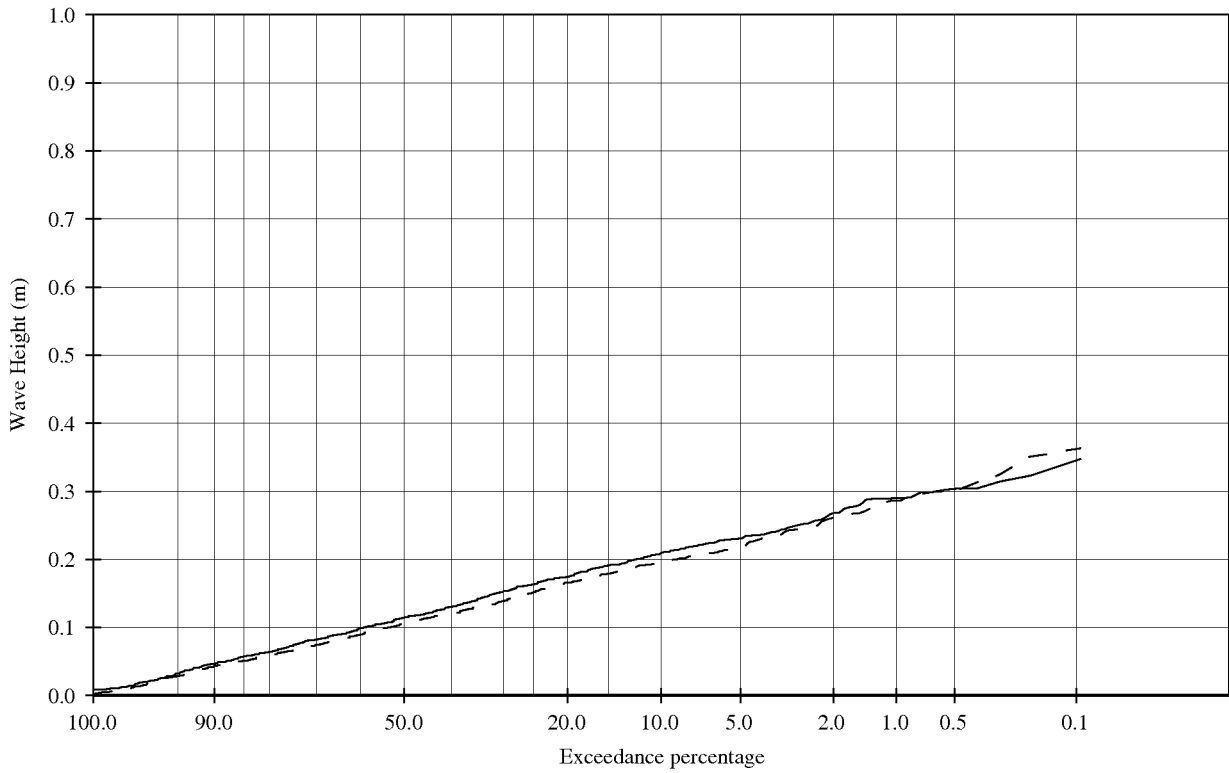


Wave height exceedance curves and
 energy spectra.

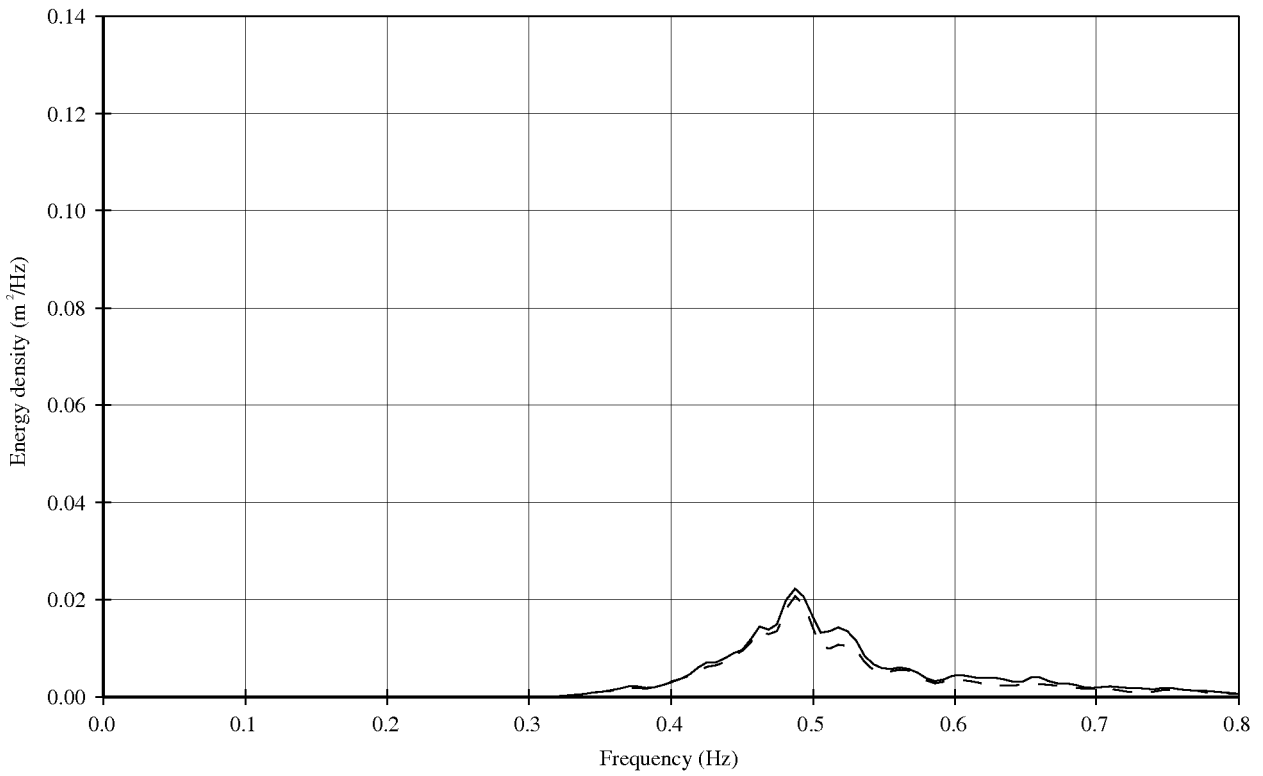
t713

Deltares

1202393.005 FIG. D.16



———— Incoming GHM 11;12;13 (Seaside of mussels)
 - - - - Incoming WHM 1;2;3 (Landside of mussels)



Wave height exceedance curves and
 energy spectra.

t708

Deltares

1202393.005

FIG. D.17

E Theoretical background: determination of reflected, transmitted and dissipated wave energy

This section describes an approach to determine the ratio between the reflected energy (E_r) and the dissipated energy (E_{diss}).

It is assumed that wave measurements with three wave gauges are performed before and after the floating structure. By using three wave gauges, the incident and reflected wave (energy) can be measured using the technique as described in Mansard and Funke (1980). Wave measurements were performed at two locations: one location in front of the structure (Location 1) and one location behind the structure (Location 2). In total four parameters were measured: the incident wave energy at Location 1 ($E_{i,WHM1}$) and Location 2 ($E_{i,WHM2}$) and the reflected wave energy at Location 1 ($E_{r,WHM1}$) and Location 2 ($E_{r,WHM2}$).

When the wave approaches the floating structure, the energy is partly reflected (E_r) partly dissipated (E_{diss}) and partly transmitted (E_t). This is illustrated in Figure E.1. How the wave measurements ($E_{i,WHM1}$, $E_{i,WHM2}$, $E_{r,WHM1}$ and $E_{r,WHM2}$) leads to individual values for reflected wave energy ($E_{r,A}$, $E_{r,B}$), transmitted wave energy ($E_{t,A}$, $E_{t,B}$) and dissipated wave energy ($E_{diss,A}$, $E_{diss,B}$) is explained below.

The relation between energy and wave heights is the following:

$$C_t = \sqrt{\frac{E_t}{E_i}} = \frac{H_t}{H_i} \quad (4.1)$$

$$C_r = \sqrt{\frac{E_r}{E_i}} = \frac{H_r}{H_i} \quad (4.2)$$

$$C_{diss} = \sqrt{\frac{E_{diss}}{E_i}} \quad (4.3)$$

It is assumed that the waves are fully absorbed by the wave paddle. Besides this, it is assumed that the waves that reflect from the wall are not re-reflected at the floating structure ($E_{r,C} = 0$).

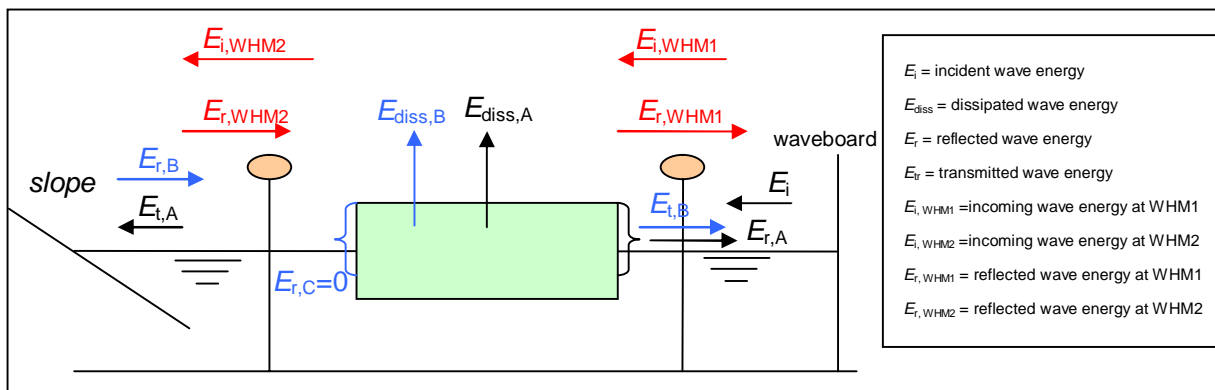


Figure E.1 Schematisation of the model set-up for an irregular wave field

Based on Figure E.1, the following equations are derived:

$$E_i = E_{i,WHM1} \quad (4.4)$$

$$E_{t,A} + E_{r,C} = E_{i,WHM2} \quad (4.5)$$

$$E_{r,A} + E_{t,B} = E_{r,WHM1} \quad (4.6)$$

$$E_i = E_{r,A} + E_{diss,A} + E_{t,A} \quad (4.7)$$

$$E_{r,B} = E_{r,WHM2} \quad (4.8)$$

$$E_{r,B} = E_{r,C} + E_{diss,B} + E_{t,B} \quad (4.9)$$

$$E_{r,C} = 0 \text{ (assumption)} \quad (4.10)$$

Unfortunately, it is not possible to solve these equations. An additional equation is required based on the assumption that the transmission coefficient C_t is in both directions the same:

$$C_{t,A} = C_{t,B} \quad (4.11)$$

$$C_{t,A} = \sqrt{\frac{E_{t,A}}{E_i}} \quad (4.12)$$

$$C_{t,B} = \sqrt{\frac{E_{t,B}}{E_{r,B}}} \quad (4.13)$$

Combining Equation (4.11) until Equation (4.13) gives:

$$E_{t,A} E_{r,B} = E_{t,B} \cdot E_i \quad (4.14)$$

Now it is possible to solve the equations:

$$\text{(based on Eq. (4.14))}: E_{t,B} = \frac{E_{t,A} E_{r,B}}{E_i} = \frac{E_{i,WHM2} E_{r,WHM2}}{E_{i,WHM1}} \quad (4.15)$$

(based on Eq. (4.9):
$$E_{diss,B} = E_{r,B} - E_{r,C} - E_{t,B} = E_{r,WHM2} - \frac{E_{i,WHM2}E_{rWHM2}}{E_{i,WHM1}} \quad (4.16)$$

(based on Eq.(4.6):
$$E_{r,A} = E_{r,WHM1} - E_{t,B} = E_{r,WHM1} - \frac{E_{i,WHM2}E_{rWHM2}}{E_{i,WHM1}} \quad (4.17)$$

(based on Eq.(4.7):
$$E_{diss,A} = E_i - E_{r,A} - E_{t,A} = E_{i,WHM1} - E_{r,WHM1} + \frac{E_{i,WHM2}E_{rWHM2}}{E_{i,WHM1}} - E_{i,WHM2} \quad (4.18)$$

$$\alpha = \frac{E_{diss,A}}{E_{r,A}} \quad (4.19)$$

All relevant parameters are now expressed as a function of measurable parameters. An overview of the resulting formulae is given in Table E.1.

Table E.1 Overview determination incident, transmitted and reflected wave energy for an irregular wave field

$E_i = E_{i,WHM1}$
$E_{t,A} = E_{i,WHM2}$
$E_{t,B} = \frac{E_{i,WHM2}E_{rWHM2}}{E_{i,WHM1}}$
$E_{r,A} = E_{r,WHM1} - \frac{E_{i,WHM2}E_{rWHM2}}{E_{i,WHM1}}$
$E_{r,B} = E_{r,WHM2}$
$E_{r,C} = 0$
$E_{diss,A} = E_{i,WHM1} - E_{r,WHM1} + \frac{E_{i,WHM2}E_{rWHM2}}{E_{i,WHM1}} - E_{i,WHM2}$
$E_{diss,B} = E_{r,WHM2} - \frac{E_{i,WHM2}E_{rWHM2}}{E_{i,WHM1}}$
$\alpha = \frac{E_{diss,A}}{E_{r,A}}$

F Theoretical derivation of χ

Ratio of non blocked energy χ_{TR} is defined by:

$$\chi_{tr} = \frac{E_{transmitted}}{E_{incident}} = 1 - \frac{E_{blocked}}{E_{incident}} \quad (5.1)$$

Kinetic energy is assumed to be proportional with maximum horizontal velocity in orbital motion:

$$E \propto u_{hor,max}^2 \quad (5.2)$$

With, according to linear wave theory

$$u_{hor,max} = \omega a \frac{\cosh k(h+z)}{\sinh kh} \quad \text{or} \quad u_{hor,max}^2 \propto \cosh^2 k(h+z) \quad (5.3)$$

Eq. (5.3) is rewritten as

$$E(z) \propto u_{hor,max}^2 \propto \cosh 2k(h+z) + 1 \quad (5.4)$$

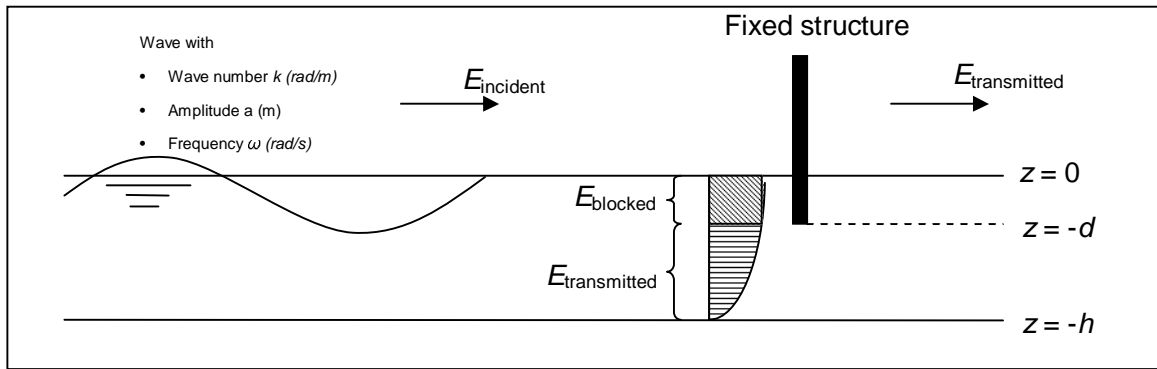


Figure F.1 Schematisation of fixed structure blocking wave energy

Combining Eq. (5.1) and Eq. (5.4) gives:

$$\chi_{tr} = 1 - \frac{\int_{-d}^0 Edz}{\int_{-h}^0 Edz} = 1 - \frac{\int_{-d}^0 (\cosh 2k(h+z) + 1) dz}{\int_{-h}^0 (\cosh 2k(h+z) + 1) dz} = 1 - \frac{\left[\frac{1}{2k} \sinh 2k(h+z) + z \right]_{-d}^0}{\left[\frac{1}{2k} \sinh 2k(h+z) + z \right]_{-h}^0} \quad (5.5)$$

or

$$\chi_{tr} = 1 - \frac{\left[\frac{1}{2k} \sinh 2k(h+0) + 0 \right] - \left[\frac{1}{2k} \sinh 2k(h-d) - d \right]}{\left[\frac{1}{2k} \sinh 2k(h+0) + 0 \right] - \left[\frac{1}{2k} \sinh 2k(h-h) - h \right]} \quad (5.6)$$

or

$$\chi_{tr} = 1 - \frac{\sinh 2kh - \sinh 2k(h-d) + 2kd}{\sinh 2kh + 2kh} \quad (5.7)$$

or

$$\chi_{tr} = \frac{\sinh 2k(h-d) - 2kd + 2kh}{\sinh 2kh + 2kh} \quad (5.8)$$

Eq. (5.8) is also found with Eq. (5.9) as starting point:

$$\chi_{tr} = \frac{\int_0^{-d} Edz}{\int_{-h}^{-d} Edz} \quad (5.9)$$

The ratio of blocked energy is determined by:

$$\chi_{bl} = 1 - \chi_{tr} \quad (5.10)$$

With Eq. (5.6), the energy transmission ratio parameter χ_{tr} is written as a function of wave number k , depth h and structure depth d :

$$\chi_{tr} = f(k, d, h) \quad (5.11)$$

Energy component	Ratio
Blocked energy by structure	$\chi_{bl} = \frac{\sinh 2kh - \sinh 2k(h-d) + 2kd}{\sinh 2kh + 2kh}$
Transmitted energy	$\chi_{tr} = \frac{\sinh 2k(h-d) - 2kd + 2kh}{\sinh 2kh + 2kh}$

With

$$\text{wave number} \quad k \text{ (rad/m)} \quad k = \frac{2\pi}{L} \quad (5.12)$$

$$\text{wave length} \quad L \text{ (m)} \quad L = L_o \tanh\left(\frac{2\pi h}{L}\right) \quad (5.13)$$

$$\text{deep water wave length} \quad L_o \text{ (m)} \quad L_o = \frac{gT^2}{2\pi} \quad (5.14)$$

$$\text{water depth} \quad h \text{ (m)}$$

$$\text{structure depth} \quad d \text{ (m)}$$

G Theoretical determination of dissipation coefficient C_{diss}

To include length effect of a porous structure into the dissipation coefficient C_{diss} a porous medium with a length w is assumed to have n segments with length Δx as illustrated in Figure G.1.

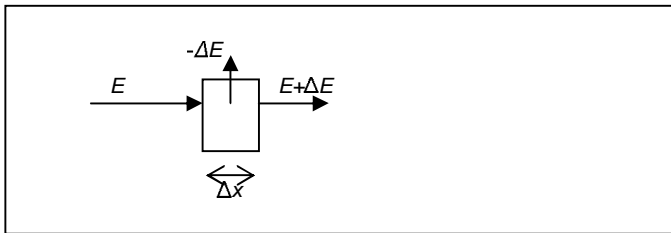


Figure G.1 Dissipation of energy on a porous segment

Dissipated energy is described by:

$$\Delta E = -D\Delta x \quad (6.1)$$

Where D is dissipated energy per unit of length. Dissipated energy is assumed to be proportional with incoming energy E :

$$D = f \cdot E \quad (6.2)$$

Combining Eq. (6.1) and Eq. (6.2) gives

$$\Delta E = -f \cdot E \cdot \Delta x \quad (6.3)$$

Rewriting gives:

$$\frac{\Delta E}{\Delta x} = -f \cdot E \quad (6.4)$$

With infinitesimal small Δx this is rewritten as:

$$\frac{\partial E}{\partial x} = -f \cdot E \quad (6.5)$$

General solution of Eq (6.5) is given by:

$$E = E_0 \cdot e^{-f \cdot x} \quad (6.6)$$

or

$$\frac{E}{E_0} = e^{-f \cdot x} \quad (6.7)$$

Dissipation coefficient C_{diss} is defined as:

$$C_{diss} = \sqrt{\frac{E_{diss}}{E_0}} = \sqrt{\frac{E_0 - E}{E_0}} = \sqrt{1 - \frac{E}{E_0}} \quad (6.8)$$

Combining Eq. (6.7) and Eq. (6.8) gives

$$C_{diss} = \sqrt{1 - e^{-fx}} \quad (6.9)$$

Eq. (6.9) is graphical presented in Figure G.2.

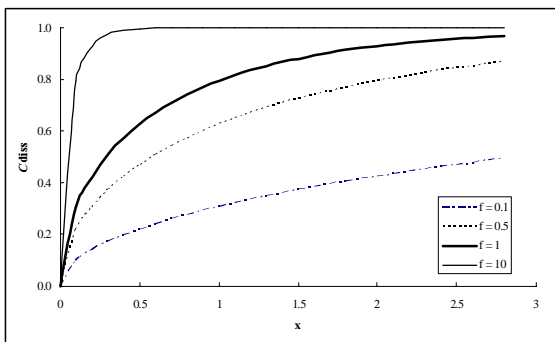


Figure G.2 Graphical presentation of dissipation coefficient based on Eq. (6.9)

H Calculation tool

Determination of wave transmission coefficients of floating mussel structures

- This sheet can be used for a first estimate of wave transmission of a floating mussel structure. Used formulas in this sheet are based on empirical data obtained with large scale physical modelling in Deltares Deltaflume. The amount of empirical data obtained in this flume is limited. Therefore, care should be taken when using this sheet for situations which are different than tested. For detailed modelling it is strongly recommended to perform additional analysis or physical model tests.

- A description of the physical model tests and foundation of the formulas used in this sheet is given in Deltares report "Large scale physical modelling of wave damping floating mussel structures", 1202393, P. van Steeg, B.K. van Wesenbeeck, August 2011

Case A: floating mussel structure without reflecting component behind structure

Input

structural conditions			
length of mussel structure	<i>w</i>	19.4 m	WARNING: outside range of tested conditions
depth of structure in water	<i>d</i>	0.5 m	
coefficient	<i>f_{r1}</i>	0.13 -	
coefficient	<i>f_{diss}</i>	1.5 -	
Hydraulic conditions			
water depth at mattress	<i>h</i>	4 m	
significant wave height	<i>H_{m0}</i>	0.3 m	
local wave length	<i>L_p</i>	9 m	

version 1 augustus 2011
P. van Steeg, Deltares

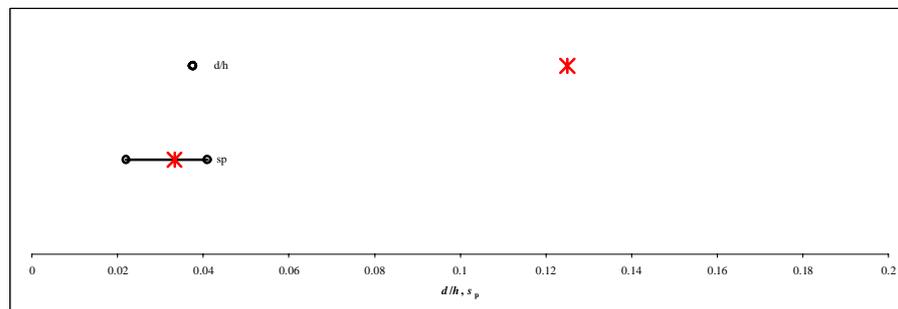
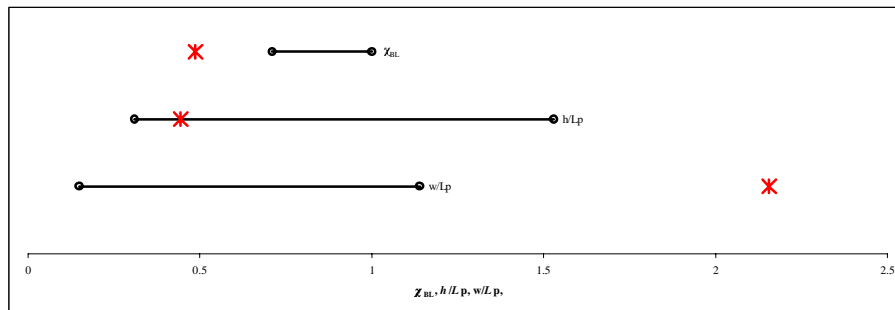
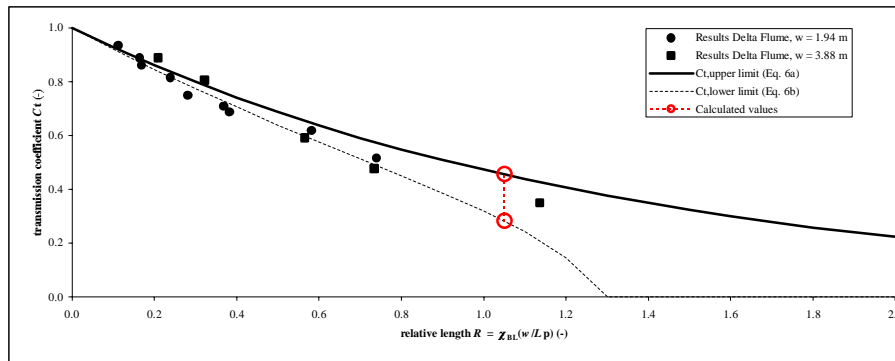
Output		Formula	
wave number	<i>k</i>	0.70 rad/m	Eq. 1 $k = \frac{2\pi}{L_p}$
energy blocking ratio	χ_{BL}	0.487 -	Eq. 2 $\chi_{BL} = \frac{\sinh 2kh - \sinh 2k(h-d) + 2kd}{\sinh 2kh + 2kh}$
dim. parameter	<i>R</i>	1.05 -	Eq. 3 $R = \chi_{BL} \frac{w}{L_p}$
reflection coefficient	<i>C_r</i>	0.36 -	Eq. 4 $C_r = \sqrt{1 - e^{-f_{r1} \chi_{BL} \frac{w}{L_p}}}$
dissipation coefficient	<i>C_{diss}</i>	0.89 -	Eq. 5 $C_{diss} = \sqrt{1 - e^{-f_{diss} \chi_{BL} \frac{w}{L_p}}}$
transmission coefficient (upper limit)	<i>C_{t,LL}</i>	0.45	Eq. 6a $C_{t,LL} = \sqrt{e^{-f_{diss} \chi_{BL} \frac{w}{L_p}}}$
transmission coefficient (lower limit)	<i>C_{t,UL}</i>	0.28 -	Eq. 6b $C_{t,UL} = \sqrt{e^{-f_{diss} \chi_{BL} \frac{w}{L_p}} + e^{-f_r \chi_{BL} \frac{w}{L_p}} - 1}$
minimum transmitted wave height	<i>H_{mo,tr,min}</i>	0.14 m	Eq. 7a $H_{mo,tr} = C_{t,LL} H_{mo,i}$
transmitted wave height	<i>H_{mo,tr,max}</i>	0.08 m	Eq. 7b $H_{mo,tr} = C_{t,UL} H_{mo,i}$

Output (Dimensionless parameter)			
ratio structure length and wave length	<i>w/L_p</i>	2.2 -	WARNING: outside range of tested conditions
ratio structure depth and water depth	<i>d/h</i>	0.1250 -	
ratio water depth and wave length	<i>h/L_p</i>	0.44 -	
wave steepness based on local water peak period	<i>s_p</i>	0.03 -	
ratio blocked wave energy	χ_{BL}	0.49 -	WARNING: outside range of tested conditions

Page 1/2

www.deltares.nl

Figure H.1 Impression of calculation tool (page 1/2)



Black line indicates test range conditions of flume test on which the prediction model is based.

Red marker indicates calculated parameter based on input prediction model